UDK 621.3:(53+54+621+66)(05)(497.1)=00 ISSN 0352-9045

INFORMACIJE MIDEM 2 • 1997

Strokovno društvo za mikroelektroniko elektronske sestavne dele in materiale

Strokovna revija za mikroelektroniko, elektronske sestavne dele in materiale
Journal of Microelectronics, Electronic Components and Materials

INFORMACIJE MIDEM, LETNIK 27, ŠT. 2(82), LJUBLJANA, junij 1997

44. SEJEM SODOBNA ELEKTRONIKA

THE 44th MODERN ELECTRONICS FAIR

Ljubljana, 6. - 10.oktober 1997

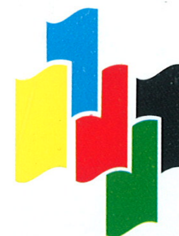

INFORMACIJE MIDEM 2 ◦ 1997

INFORMACIJE MIDEM LETNIK 27, ŠT. 2(82), LJUBLJANA, JUNIJ 1997

INFORMACIJE MIDEM VOLUME 27, NO. 2(82), LJUBLJANA, JUNE 1997

Izdaja trimesečno (marec, junij, september, december) Strokovno društvo za mikroelektroniko, elektronske sestavne dele in materiale.

Published quarterly (march, june, september, december) by Society for Microelectronics, Electronic Components and Materials - MIDEM.

Glavni in odgovorni urednik
Editor in Chief

Mag. Iztok Šorli, dipl.ing.,
MIKROIKS d.o.o., Ljubljana

Tehnični urednik
Executive Editor

Mag. Iztok Šorli, dipl.ing.,

Uredniški odbor
Editorial Board

Doc. dr. Rudi Babič, dipl.ing., Fakulteta za elektrotehniko, računalništvo in informatiko Maribor
Dr.Rudi Ročak, dipl.ing., MIKROIKS d.o.o., Ljubljana
mag.Milan Slokan, dipl.ing., MIDEM, Ljubljana
Zlatko Bele, dipl.ing., MIKROIKS d.o.o., Ljubljana
Dr. Wolfgang Pribyl, SIEMENS EZM, Villach
mag. Meta Limpel, dipl.ing., MIDEM, Ljubljana
Miloš Kogovšek, dipl.ing., Ljubljana
Dr. Marija Kosec, dipl. ing., Inštitut Jožef Stefan, Ljubljana

Časopisni svet
International Advisory Board

Prof. dr. Slavko Amon, dipl.ing., Fakulteta za elektrotehniko, Ljubljana, PREDSEDNIK - PRESIDENT
Prof. dr. Cor Claeys, IMEC, Leuven
Dr. Jean-Marie Haussonne, EIC-LUSAC, Octeville
Dr. Marko Hrovat, dipl.ing., Inštitut Jožef Stefan, Ljubljana
Prof. dr. Zvonko Fazarinc, dipl.ing., CIS, Stanford University, Stanford
Prof. dr. Drago Kolar, dipl.ing., Inštitut Jožef Stefan, Ljubljana
Dr. Giorgio Randone, ITALTEL S.I.T. spa, Milano
Prof. dr. Stane Pejovnik, dipl.ing., Kemijski inštitut, Ljubljana
Dr. Giovanni Soncini, University of Trento, Trento
Prof.dr. Janez Trontelj, dipl.ing., Fakulteta za elektrotehniko, Ljubljana
Dr. Anton Zalar, dipl.ing., ITPO, Ljubljana
Dr. Peter Weissglas, Swedish Institute of Microelectronics, Stockholm

Naslov uredništva
Headquarters

Uredništvo Informacije MIDEM
Elektrotehniška zveza Slovenije
Dunajska 10, 1000 Ljubljana, Slovenija
tel.: +386(0)61 31 28 98
fax: +386(0)61 31 91 70
Iztok.Sorli@guest.arnes.si
http://pollux.fer.uni-lj.si/midem/journal.htm

Letna naročnina znaša 12.000,00 SIT, cena posamezne številke je 3000,00 SIT. Člani in sponzorji MIDEM prejemajo Informacije MIDEM brezplačno.
Annual subscription rate is DEM 200, separate issue is DEM 50. MIDEM members and Society sponsors receive Informacije MIDEM for free.

Znanstveni svet za tehnične vede I je podal pozitivno mnenje o reviji kot znanstveno strokovni reviji za mikroelektroniko, elektronske sestavne dele in materiale. Izdajo revije sofinanci rajo Ministrstvo za znanost in tehnologijo in sponzorji društva.
Scientific Council for Technical Sciences of Slovene Ministry of Science and Technology has recognized Informacije MIDEM as scientific Journal for microelectronics, electronic components and materials.
Publishing of the Journal is financed by Slovene Ministry of Science and Technology and by Society sponsors.

Znanstveno strokovne prispevke objavljene v Informacijah MIDEM zajemamo v:
* domačo bazo podatkov ISKRA SAIDC-el, kakor tudi
* v tujo bazo podatkov INSPEC

Prispevke iz revije zajema ISI® v naslednje svoje produkte: Sci Search®, Research Alert® in Materials Science Citation Index™

Scientific and professional papers published in Informacije MIDEM are assessed into:
* domestic data base ISKRA SAIDC-el and
* foreign data base INSPEC

The Journal is indexed by ISI® for Sci Search®, Research Alert® and Material Science Citation Index™

Po mnenju Ministrstva za informiranje št.23/300-92 šteje glasilo Informacije MIDEM med proizvode informativnega značaja, za katere se plačuje davek od prometa proizvodov po stopnji 5 %.

Grafična priprava in tisk / Printed by: BIRO M, Ljubljana

Naklada / Circulation: 1000 izvodov / 1000 issues

Poštnina plačana pri pošti 1102 Ljubljana
Slovenia Taxe Percue

UDK621.3:(53+54+621+66), ISSN0352-9045 Informacije MIDEM 27(1997)2,Ljubljana

ZNANSTVENO STROKOVNI PRISPEVKI		PROFESSIONAL SCIENTIFIC PAPERS
T.A. Dzhekov: Optimizacija votline bistabilnega fotorefraktivnega etalona	79	T.A. Dzhekov: On the Cavity Optimization of the Photorefractive Bistable Etalon
De. Đonlagić, M. Završnik, Da. Đonlagić: Uporaba akustične resonance v meritvah in detekciji nivoja fluidov	86	De. Đonlagić, M. Završnik, Da. Đonlagić: Application of Acoustic Resonance for Fluid Level Measurements and Detection
A. Babnik, A. Kobe, I. Bajsić, J. Možina: Kondenzacijski vlagomer z optičnimi vlakni	97	A. Babnik, A. Kobe, I. Bajsić, J. Možina: Fiber -Optic Condensation Hygrometer
D. Kuščer, J. Holc, M. Hrovat, S. Bernik, D. Kolar: Karakterizacija $LaMnO_3$ modificiranega z Al_2O_3 in SrO, za katodni material za SOFC	104	D. Kuščer, J. Holc, M. Hrovat, S. Bernik, D. Kolar: Characterization of Al_2O_3 and SrO Modified $LaMnO_3$ for SOFC Cathode Material
A. Žemva, B. Zajc: Logične perturbacije: Osnova za optimizacijo digitalnih vezij	112	A. Žemva, B. Zajc: Logic Perturbations: A Basis for Digital Circuits Optimization
M.K. Gunde: Uporaba infrardeče spektroskopije pri analizi materialov za mikroelektronsko industrijo, 2. Tanke plasti	120	M.K. Gunde: Infrared Spectroscopy as Analysing Tool for Materials Used in Microelectronics, 2. Thin Films
APLIKACIJSKI ČLANKI		**APPLICATION ARTICLES**
I. Šorli: TOC v vodi, II. del: Uporaba v farmaciji in polprevodništvu	131	I. Šorli: Total Organic Carbon - TOC in Water, part II.: Pharmaceutical and Semiconductor Applications
PREDSTAVLJAMO PODJETJE Z NASLOVNICE		**PRESENTATION OF COMPANY FROM FRONT PAGE**
44. Sejem Sodobna eletkronika v organizaciji Ljubljanskega sejma	141	The 44th Modern Electronics Fair Organized by Ljubljana Fair
MIDEM IN NJEGOVI ČLANI, NOVICE IZ DRUGIH SREDIN		**MIDEM SOCIETY AND ITS MEMBERS, NEWS FROM OTHER INSTITUTIONS**
W. Pribyl: Siemensova mikroelektronska tovarna v Dresdenu	144	W. Pribyl: Siemens Dreseden Semiconductor Plant
KONFERENCE, POSVETOVANJA, SEMINARJI, POROČILA		**CONFERENCES, COLLOQUYUMS, SEMINARS, REPORTS**
D. Belavič: IMAPS/NATO ARW'97 na Bledu	146	D. Belavič: IMAPS/NATO Advance Research Workshop'97 and Exhibition, Bled
D. Ročak: 11. Evropska mikroelektronska konferenca, Benetke	148	D. Ročak: 11th European Microelectronics Conference, Venezia
V SPOMIN		**IN MEMORIAM**
M. Slokan: Pavle Tepina in memoriam	150	M. Slokan: Pavle Tepina in memoriam
VESTI	151	**NEWS**
KOLEDAR PRIREDITEV	154	**CALENDAR OF EVENTS**
MIDEM prijavnica		MIDEM Registration Form
Slika na naslovnici: 44. Sejem Sodobna elektronika je pred durmi		Front page: The 44th Modern Electronics Fair will be held at the beginning of October in Ljubljana

VSEBINA CONTENT

DRUŠTVO MIDEM IN KONFERENCA MIDEM NA INTERNETU

Dragi člani društva in bralci revije!

Predstavitev društva MIDEM in predstavitev letošnje konference MIDEM'97 lahko poiščete na INTERNETU in sicer:

1. Predstavitev društva MIDEM in revije "Informacije MIDEM" na naslovu
   http://pollux.fer.uni-lj.si/midem/society.htm
   http://pollux.fer.uni-lj.si/midem/journal.htm

2. Predstavitev konference MIDEM'97 na naslovu
   http://pollux.fer.uni-lj.si/midem/conf97.htm

3. Elektronsko pošto lahko pošiljate na naslov:
   Iztok.Sorli@guest.arnes.si

Pri vpisu pazite na velike in male črke!!

Vse člane vljudno prosimo, da poravnajo članarino za leto 1997.

MIDEM SOCIETY AND MIDEM CONFERENCE ON INTERNET

Dear readers and Society members!

Presentation of MIDEM Society and the information on the next MIDEM'97 Conference can be found on INTERNET as follows:

1. Presentation of MIDEM Society and Journal "Informacije MIDEM", address
   http://pollux.fer.uni-lj.si/midem/society.htm
   http://pollux.fer.uni-lj.si/midem/journal.htm

2. Presentation of the MIDEM'97Conference, address
   http://pollux.fer.uni-lj.si/midem/conf97.htm

3. Email can be sent to:
   Iztok.Sorli@guest.arnes.si

Please, use exact lower and upper case letters as indicated.

We kindly ask all our members to pay the membership fee for 1997.

UDK621.3:(53+54+621+66), ISSN0352-9045 Informacije MIDEM 27(1997)2, Ljubljana

ON THE CAVITY OPTIMIZATION OF THE PHOTOREFRACTIVE BISTABLE ETALON

Tomislav A. Dzhekov
Faculty of Electrical Engineering, Skopje, R. of Macedonia

Keywords: optical devices, resonator cavities, Fabry-Perot interferometer, photorefractive bistability, photorefractive bistable etalons, intrinsic bistable devices, bistable cavities, cavity optimization, cavity optimization on transmission, cavity optimization on reflection, cavity optimization for given absorption per pass, high fineness cavities

Abstract: The analytical and numerical results of a study on the problem of bistable cavity optimization (on transmission and on reflection) for plane-wave excitation and equal end-face reflectivities, are presented. Three different optimization conditions have been considered (fixed finesse, fixed end-face reflectivity and fixed absorption per pass). Special attention has been given to the case of high finesse cavity.

Optimizacija votline bistabilnega fotorefraktivnega etalona

Ključne besede: naprave optične, votline resonatorske, Fabry-Perot interferometri, bistabilnost fotorefraktivna, etaloni fotorefraktivni bistabilni, naprave bistabilne notranje, votline bistabilne, optimizacija votlin, optimizacija votlin za prenos, optimizacija votlin za refleksijo, optimizacija votlin za dano absorpcijo optično, votline z visoko finostjo površine

Povzetek: V prispevku so predstavljeni analitični in numerični rezultati študije problema optimizacije votline fotorefraktivnega bistabilnega etalona (za transmisijo in refleksijo) za primer vzbujanja z ravnim valom pri enaki odbojnosti končnih zrcal.
Prispevek obravnava tri različne optimizacijske pogoje: fiksno finost votline, fiksno reflektivnost zrcal in fiksno absorpcijo na prehod. Posebna pozornost je posvečena votlini z visoko finostjo.

1. INTRODUCTION

Optical bistability has attracted a continuous interest over the past two decades /1-18/. This is especially true for the intrinsic photorefractive bistability (the nonlinearity of the medium of the photorefractive Fabry-Perot etalon is of the Kerr-type, i.e. the refractive index is given by:

$$n = n_0 + n_2 I = n_0 + \frac{n_2 n_0}{2\eta_0}|\mathbf{E}|^2 \quad ,$$

where n_0 and n_2 are the linear and nonlinear refractive indexes of the medium, I is the optical intensity, $\mathbf{E}$ is the optical electric field vector and η_0 is the wave impedance in the vacuum), owing to its potential application to all optical signal processing /10, 11, 18/.

The critical intensity I_C /6/ is certainly a parameter of central importance concerning the potential applications of the intrinsic photorefractive bistable etalons. Since lower critical intensity means switching at lower powers, it is desirable, of course, for this parameter to be as small as possible. Therefore, cavity optimization of the photorefractive bistable etalon implies such a choice of the final parameters used for fabrication (i.e., the end-face reflectivities and the absorption per pass), which leads to the smallest possible critical intensity for given conditions. Other important parameters are the transmission difference T_D (for the case when the transmitted wave is used as an output) and the reflection difference R_D (for the case when the reflected wave is used as an output) /9/. It is necessary for these parameters to be as large as possible, because larger T_D (or R_D) means in, principle, larger output signal.

In /6/, which is the first paper to treat this question, Miller reduces the problem of cavity optimization to minimization of I_C for fixed finesse. He concentrates on transmission, but does not include explicitly the transmission difference in his analysis. One could hardly say, however, that the cavity is optimally designed if I_C was minimized at the expense of T_D (for the case of transmission) or at the expense of R_D (for the case of reflection). Wherrett /9/ gives emphasis on reflectivity and is concerned with the dependence of the critical intensity and the reflection difference on the values of end-face reflectivities for specific absorption per pass conditions. No attempt is made, however, to obtain explicit expressions for the optimal values of the end-face reflectivities and of the absorption per pass for given conditions.

Normally, one expects from a cavity to have small I_C, but, at the same time, large T_D (or R_D). Thus, it seems more meaningful if by cavity optimization is understood minimization of I_C/T_D (or I_C/R_D), rather than minimization of I_C. As can be easily seen, the former insures, effectively, maximization of the efficacy by which the input power is used. Therefore, in this paper we pay special attention to the minimizations of I_C/T_D and I_C/R_D. This is done for three different conditions, i.e. for given finesse Φ, for given end-face reflectivity R (we assume equal end-face reflectivities), and for given absorption per pass A.

2. THEORETICAL OUTLINE

The following parameters characterize the analyzed bistable cavity:

R	Intensity reflectivity of the faces
α	Linear absorption coefficient
d	Cavity length
A	$1 - e^{-\alpha d}$ (absorption per pass)
B	$e^{-\alpha d} \equiv 1\text{-}A$ (absorption per pass complement)
R_a	$Re^{-\alpha d} \equiv RB$ (effective intensity reflectivity)
F	$4R_a / (1\text{-}R_a)^2 = 4RB / (1\text{-}RB)^2$
Φ	$\pi F^{1/2} / 2 \equiv \pi R_\alpha^{1/2} / (1\text{-}R_a)$ (cavity finesse)

In terms of these parameters, the critical intensity (I_c), the transmission difference (T_D) and the reflection difference (R_D) are given by /6, 9/:

$$I_c = \frac{1}{\beta\mu} \quad , \tag{1}$$

where $\beta = 3n_2 / \lambda\alpha$ is a constant which contains all the relevant material properties, and

$$\mu = \frac{16\pi}{\sqrt{2}} \frac{(1-R)(1-e^{-da})(1+R_\alpha)}{(1-R_a)^2} \frac{H(F)}{G^2(F)} \tag{2}$$

with

$$H(F) = \left\{(F+2)\left[(F+2)^2 + 8F^2\right]^{1/2} - (F+2)^2 - 2F^2\right\}$$

$$G(F) = 3(F+2) - \left[(F+2)^2 + 8F^2\right]^{1/2}$$

is a figure of merit for the cavity design,

$$T_D = \frac{4R\left(e^{-\alpha d}\right)^2(1-R)^2}{\left[1-R^2\left(e^{-\alpha d}\right)^2\right]^2} \tag{3}$$

$$R_D = \frac{4Re^{-\alpha d}(1-R)\left[1-R\left(e^{-\alpha d}\right)^2\right]}{\left[1-R^2\left(e^{-\alpha d}\right)^2\right]^2} \tag{4}$$

As can be seen, μ, T_D and R_D can be considered as functions of two variables - the mirrors' reflectivity R and the absorption per pass complement $B=1\text{-}A=e^{-\alpha d}$. These functions are physically meaningful only within the domain $0 \le R \le 1$, $0 \le B \le 1$, Fig. 1. Note that m is a symmetrical function with respect to the line R=B, i.e. $\mu|_{B=X,R=Y} = \mu|_{B=Y,R=X}$. It increases monotonically along the diagonal OP, from zero at point O to infinity at point P, being equal to zero along the lines B=0, R=0, B=1 and R=1, except at the point P at which it becomes unlimited. On the other hand, T_D and R_D are asymmetrical functions with respect to R=B. They are both equal to zero along B=0, R=0 and R=1 and equal to $4R / (1+R)^2$ at B =1. Along the diagonal OP, T_D increases from zero to 1/4, whereas R_D - from zero to 3/4. The point P is a singular point for these functions.

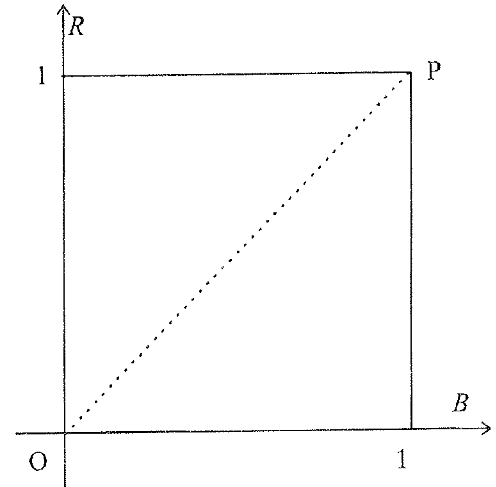

Fig. 1. Domain of definition of μ, T_D and R_D

In the limit of high finesse (i.e., small A=1-B and small 1-R) is:

$$F \cong \frac{4}{(1-R+1-B)^2} >> 1 \tag{5}$$

and expressions (2), (3) and (4) reduce to:

$$\mu \cong \frac{3\sqrt{3}\pi}{2} \frac{(1-R)(1-B)}{(1-R+1-B)^3} \tag{6}$$

$$T_D = \frac{(1-R)^2}{(1-R+1-B)^2} \tag{7}$$

$$R_D = \frac{(1-R)[1-R+2(1-B)]}{(1-R+1-B)^2} \tag{8}$$

3. RESULTS AND DISCUSSION

A. Cavity optimization for given finesse

As was shown in /6/, the pairs of values of R and B which for given finesse F minimize the critical intensity Ic, are given by:

Table 1. Optimal values of R and B for given finesse Φ. / Ra= RB = {[1+(π / 2Φ)²]½ - π / 2Φ }² /

Minimized parameter	*Location of the minimum*
I_c	$R_{op} = B_{op} = R_\alpha^{1/2}$
I_c/T_D *(optimization on transmission)*	$R_{op(t)} = \frac{1}{4}\left\{-(1-R_\alpha)+\left[(1-R_\alpha)^2+16R_\alpha\right]^{1/2}\right\}$; $B_{op(t)} = \frac{R_\alpha}{R_{op(t)}}$
I_c/R_D *(optimization on reflection)*	$R_{op(r)} = \begin{cases} -2\frac{q}{\lvert q\rvert}\lvert p\rvert^{1/2}\cos\left(\frac{1}{3}\arccos\frac{\lvert q\rvert}{\lvert p\rvert^{3/2}}\right)+\frac{R_\alpha(1+R_\alpha)}{6}, & \text{for } q<0 \\ 2\frac{q}{\lvert q\rvert}\lvert p\rvert^{1/2}\cos\left(\frac{\pi}{3}-\arccos\frac{\lvert q\rvert}{\lvert p\rvert^{3/2}}\right)+\frac{R_\alpha(1+R_\alpha)}{6}, & \text{for } q>0 \end{cases}$ $B_{op(r)} = \frac{R_\alpha}{R_{op(r)}}$ where: $q = -\frac{R_\alpha^3(1+R_\alpha)^3}{216} - \frac{R_\alpha^2(1+R_\alpha)^2}{24} + \frac{R_\alpha^3}{2}$ and $p = -\frac{R_\alpha(1+R_\alpha)[6+R_\alpha(1+R_\alpha)]}{36}$

$$R_{op} = B_{op} = R_\alpha^{1/2}$$

In accordance with (1), (2), (3) and (4), minimizations of I_c/T_D and I_c/R_D for given finesse Φ are equivalent to location of the maxima of the functions $f_t = (1-R)^3 B(1-B)$ and $f_r = (1-R)^2 (1-B)(1-R_\alpha B)$ along the curve $RB = R_\alpha =$ *const.*, respectively. Table 1 presents the required solutions. For completeness, the case of minimization of I_c is also included. Graphical presentations of these solutions are given in Fig. 2. $R_o = R_\alpha$ and $B_o = 1$ are the pairs of values of R and B which for given finesse maximize T_D and R_D (the maximal value of T_D and R_D for given finesse is $4R_\alpha / (1+R_\alpha)^2$). As one can see, cavity optimization on transmission requires considerably smaller values for R, and, therefore, larger values for B (thinner etalon), than are the values that minimize the critical intensity. The values of R for cavity optimization on reflection are larger then for cavity optimization on transmission, but, still smaller than the ones that minimize the critical intensity. For the special case of high finesse cavity, relations given in Table 1 reduce to those in Table 2.

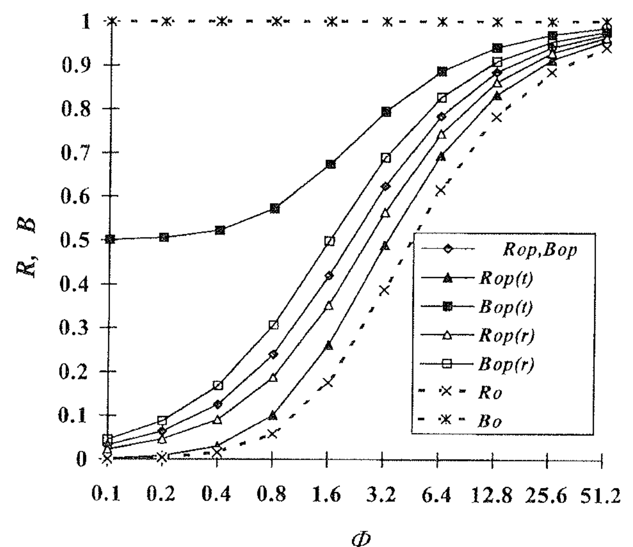

Fig. 2. Pairs of optimal values of R and B, for given finesse Φ. R_{op} and B_{op}, $R_{op(t)}$ and $B_{op(t)}$, and $R_{op(r)}$ and $B_{op(r)}$ correspond to minimization of I_c, I_c/T_D and I_c/R_D, respectively.

Table 2. (high finesse cavity) Optimal values of R and B for given finesse Φ.

Minimized parameter	*Location of the minimum*
I_c	$R_{op} = B_{op} = R_\alpha^{1/2} \approx 1 - \frac{1-R_\alpha}{2}$
I_c/T_D	$R_{op(t)} = \sqrt{1+3R_\alpha} - 1 \approx 1 - \frac{3(1-R_\alpha)}{4}$, $B_{op(t)} = \frac{R_\alpha}{R_{op(t)}} \approx 1 - \frac{1-R_\alpha}{4}$
I_c/R_D	$R_{op(r)} = \frac{\sqrt{(7-\sqrt{17})^2 + 32(1+\sqrt{17})R_\alpha} - (7-\sqrt{17})}{2(1+\sqrt{17})} \approx 1 - \frac{8}{9+\sqrt{17}}(1-R_\alpha)$, $B_{op(r)} = \frac{R_\alpha}{R_{op(r)}} \approx 1 - \frac{1+\sqrt{17}}{9+\sqrt{17}}(1-R_\alpha)$

To show that cavity optimization based on minimization of I_C/T_D or on minimization of I_C/R_D could be advantageous or more acceptable than cavity optimization based on minimization of I_C, it is useful to calculate the values of I_C, T_D and R_D for each of the three cases. Such calculations have been done for a high finesse cavity, Table 3. Comparing the presented values, we note that a cavity optimized for a minimum I_C/T_D is characterized by a 2.25 times larger transmission difference than a cavity optimized for a minimum I_C, and that this is paid by an 33% increase in the required holding power (critical intensity). Also, the optimization for a minimum I_C/R_D offers a 13% larger reflection difference for a 5% increase in the holding power, as compared to cavity optimization for minimum I_C. We also note that in each case R_D is considerably larger than T_D. This clearly indicates that the reflection mode of operation can prove to be better suited for device purposes.

*Table 3. Critical intensity, transmission difference and reflection difference of an optimized high finesse cavity (optimization for given finesse)**

Optimization criteria	I_c	T_D	R_D	I_c/T_D	I_c/R_D
minimum I_c	$4.000(1-R_\alpha)C_o$	1/4	3/4	$16.000\,(1-R_\alpha)C_o$	$\approx 5.333(1-R_\alpha)C_o$
minimum I_c/T_D	$\approx 5.333(1-R_\alpha)C_o$	9/16	15/16	$\approx 9.481(1-R_\alpha)C_o$	$\approx 5.688(1-R_\alpha)C_o$
minimum I_c/R_D	$\approx 4.202(1-R_\alpha)C_o$	≈0.372	≈0.848	$\approx 11.296(1-R_\alpha)C_o$	$\approx 4.955(1-R_\alpha)C_o$

*) $C_o = 2/3\sqrt{3\pi\beta}$ is a constant which depends on the properties of the medium.

B. Cavity optimization for given absorption per pass

In accordance with (1), (2), (3) and (4), minimizations of I_c, I_c/T_D and I_c/R_D for given absorption per pass A = 1-B are equivalent to solving the equations $\partial\mu / \partial R = 0$ and $\partial(\mu R_D) / \partial R = 0$, respectively. The results will be of the form $R'_{op} = R'_{op}(B)$, $R'_{op(t)} = R'_{op(t)}(B)$, and $R'_{op(r)} = R'_{op(r)}(B)$, respectively, where R'_{op}, $R'_{op(t)}$ and $R'_{op(r)}$ are the required optimal values of R. Because of the very complex dependence of μ on R and B (note that H(F) and G(F) are functions of R and B!), it is clear that analytical solutions of these equations are not possible. In Fig. 3, we present the solutions obtained by numerical methods. R'_{to} and R'_{ro} are the of values of R which for given finesse maximize T_D and R_D, respectively. As expected, cavity optimization on transmission for given absorption per pass will lead to smaller values for R than cavity optimization on reflection. For $B \Rightarrow 0$, R'_{op}, $R'_{op(t)}$ and $R'_{op(r)}$ assume the values 1/2, 2/5 and 1/2, respectively, as obtained theoretically. For $B \Rightarrow 0$, R'_{op}, $R'_{op(t)}$ and $R'_{op(r)}$ approach unity.

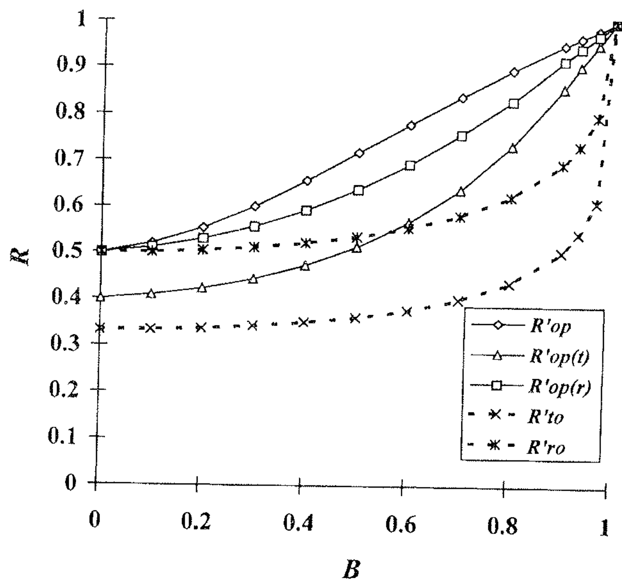

Fig. 3. Optimal values of R for given B. R'_{op}, $R'_{op(t)}$ and $R'_{op(r)}$ correspond to minimizations of I_c, I_c/T_D and I_c/R_D, respectively.

The case of high finesse cavity allows analytical treatment. The corresponding expressions of R'_{op}, $R'_{op(t)}$ and $R'_{op(r)}$, obtained by using (6), (7) and (8), are given in Table 4.

Table 5 presents the calculated values of I_c, T_D and R_D for high finesse cavities, optimized for minimum I_c, for minimum I_c/T_D or for minimum I_c/R_D.

Table 4. (high finesse cavity) Optimal values of R for given B.

minimized parameter	Location of the minimum
I_c	$R'_{op} = 1 - \frac{1-B}{2}$
I_c/T_D	$R'_{op(t)} = 1 - \frac{3(1-B)}{2}$
I_c/R_D	$R'_{op(r)} = 1 - \frac{\sqrt{41}-3}{4}(1-B)$

C. Cavity optimization for given end-face reflectivity

Minimizations of I_c, I_c/T_D and I_c/R_D for given end-face reflectivity R are equivalent to solving the equations $\partial\mu/\partial B=0$, $\partial(\mu T_D)/\partial B=0$ and $\partial(\mu R_D)/\partial B=0$, respectively. The results are of the form $B'_{op}=B'_{op}(R)$, $B'_{op(t)}=B'_{op(t)}(R)$, and $B'_{op(r)}=B'_{op(r)}(R)$, respectively, where B'_{op}, $B'_{op(t)}$ and $B'_{op(r)}$ are the required optimal values of B. As in the previous case, analytical solutions

Table 5. Critical intensity, transmission difference and reflection difference of an optimized high finesse cavity (optimization for given B=1-A)

Optimization criteria	I_c	T_D	R_D	I_c/T_D	I_c/R_D
minimum I_c	$6.750(1-B)C_o$	≈0.111	≈0.555	$\approx 60.756\ (1-B)C_o$	$\approx 12.151(1-B)C_o$
minimum I_c/T_D	$\approx 10.420(1-B)C_o$	0.360	0.840	$\approx 28.444(1-B)C_o$	$\approx 12.405\ (1-B)C_o$
minimum I_c/R_D	$\approx 7.452(1-B)C_o$	≈0.211	0.740	$\approx 35.318(1-B)C_o$	$\approx 10.070(1-B)C_o$

of these equations are not possible. In Fig. 4, we present the results obtained by numerical methods. $B'_o=1$ presents the values of B which, for given R, maximize T_D and R_D. As expected, for given end-face reflectivity R, the optimal values of B for minimum I_c/T_D are larger (thinner cavity is required) than are the optimum values B for minimum I_c or for minimum I_c/R_D. One can show analytically, that for $R \Rightarrow 0$, B'_{op}, $B'_{op(t)}$ and $B'_{op(r)}$ approach 1/2, 3/4 and 2/3, respectively.

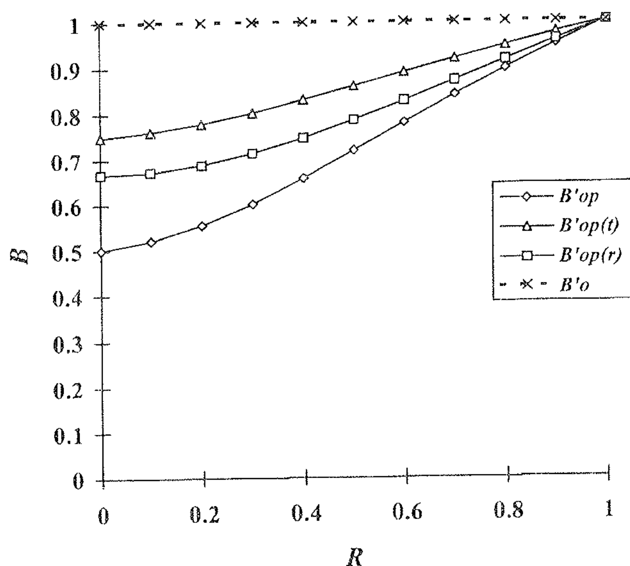

Fig. 4. *Optimal values of B for given R, B'_{op}, $B'_{op(t)}$ and $B'_{op(r)}$ correspond to minimizations of I_c, I_c/T_D and I_c/R_D, respectively.*

It is easy to show, by using (6), (7) and (8), that for the case of high finesse cavity $B'_{op}=B'_{op}(R)$, $B'_{op(t)}=B'_{op(t)}(R)$, and $B'_{op(r)}=B'_{op(r)}(R)$ reduce to the simple expressions given in Table 6.

Table 7 presents the calculated values of I_c, T_D and R_D for a high finesse cavity, optimized for minimum I_c, for minimum I_c/T_D or for minimum I_c/R_D.

Table 6. *(high finesse cavity) Optimal values of B for given R.*

Minimized parameter	*Location of the minimum*
I_c	$B'_{op} = 1 - \frac{1-R}{2}$
I_c/T_D	$B'_{op(t)} = 1 - \frac{1-R}{4}$
I_c/R_D	$B'_{op(r)} = 1 - \frac{1-R}{\sqrt{6}}$

4. CONCLUSIONS

We have been able within the limitations of the plane-wave approximation to give criteria for optimizing the design of a refractive nonlinear Fabry-Perot etalon in the presence of linear absorption for minimum critical intensity, minimum critical intensity - transmission difference ratio or minimum critical intensity - reflection difference ratio. Three optimization conditions have been considered: fixed finesse, fixed absorption per pass and fixed end-face reflectivity.

5. REFERENCES

/1/ H. M. Gibbs, S. L. McCall and T. N. C. Vencatesan, "Differential gain and bistability using a sodium-filled Fabry-Perot interferometer", Physical Review Letters, 36, 1135-1138 (1976).

/2/ J. H. Marburger and F. S. Felber, "Theory of lossless nonlinear Fabry-Perot interferometer", Physical Review, A-17, 335-342 (1978)

/3/ H. M. Gibbs, S. L. McCall , T. N. C. Vencatesan, A. C. Gossard, A. Passner and W. Wiegmann, "Optical bistability in semiconductors", Applied Physics Letters, 35, 451-453 (1979).

Table 7. *Critical intensity, transmission difference and reflection difference of an optimized high finesse cavity (optimization for given end-face reflectivity R)*

Optimization criteria	I_c	T_D	R_D	I_c/T_D	I_c/R_D
minimum I_c	$6.750(1-R)C_o$	≈ 0.444	≈ 0.888	$\approx 15.803\ (1-R)C_o$	$\approx 7.601(1-R)C_o$
minimum I_c/T_D	$\approx 7.812(1-R)C_o$	0.640	0.960	$\approx 12.207(1-R)C_o$	$\approx 8138\ (1-R)C_o$
minimum I_c/R_D	$\approx 6.8461(1-R)C_o$	≈ 0.504	≈ 0.916	$\approx 13.573(1-R)C_o$	$\approx 7.468(1-R)C_o$

/4/ T. Bischolberger and Y. R. Shen, "Theoretical and experimental study of the dynamic behavior of a non-linear Fabry-Perot interferometer", Physics Review, A-19, 1169-1176 (1979).

/5/ P. W. Smith, "Hybrid bistable optical devices", Optical Engineering, 19(4), 456-462 (1980).

/6/ D. A. B. Miller, "Refractive Fabry-Perot bistability with linear absorption: Theory of operation and cavity optimization", IEEE Journal of Quantum Electronics,Vol. 17(3), 306-311 (1981).

/7/ D. A. B. Miller, S. D. Smith and C. T. Seaton, "Optical bistability in semiconductors", IEEE Journal of Quantum Electronics, Vol. 17(3), 312-317 (1981).

/8/ W. J. Firth and E. M. Wright, "Theory of Gaussian-beam optical bistability", Optical communications, Vol. 40, 233 (1982).

/9/ B. S. Wherrett, "Fabry-Perot bistable cavity optimization on reflection", IEEE Journal of Quantum Electronics, Vol. 20, 646-651 (1984).

/10/ S. D. Smith, A. C. Walker, B. S. Wherrett, F. A. P. Tooley, J. G. H. Mathew, M. R. Taghizadeh and I. Janossy, "Cascadable digital optical logic circuit elements in the visible and infrared: demonstrations of some first all-optical circuits", Applied Optics, 25, 1586-1593 (1986).

/11/ M. E. Warren, S. W. Koch and H. M. Gibbs, "Optical bistability, logic gating and waveguide operation in semiconductor etalons", Computer, University of Arizona, 68-81, December, 1987.

/12/ M. Haelterman, M. D. Tolley and G. Vitrant, "Transverse effects in optical bistability with nonlinear Fabry-Perot etalon: a new theoretical approach", Journal of Applied Physics, 67(6), 2725-2730 (1990).

/13/ R. Reinish and G. Vitrant, "Transferse effects and enhanced dispersive optical bistability in a nonlinear Fabry-Perot filled with self-focusing medium", Journal of Applied Physics, 67(11), 6671-6674 (1990).

/14/ F. J. Fraile-Pelaez, J Capmany and M. A. Muriel, "Transmission bistability in a double-coupler fiber ring rezonator", Optical Letters, Vol. 16, 907-909 (1991)

/15/ K. Ogusu and S. Yamamoto, "Nonlinear fiber Fabry-Perot resonator using termooptic effect", Journal of Lightwave Technology, Vol. 11, 1774-1781 (1993)

/16/ J. Capmany, F. J. Fraile-Pelaez and M. A. Muriel, "Optical bistability and differential amplification in nonlinear fiber resonators", IEEE Journal of Quantum Electronics,Vol. 30, 2578-2588 (1994).

/17/ K. Ogustu, H. Shigekuni and Y. Yokota, "Dynamic transmission properties of a nonlinear ring resonator", "Optical Letters, Vol. 20, 2288-2290 (1995).

/18/ K. Ogustu, "Dynamic behavior of reflection optical bistability in a nonlinear ring resonator", IEEE Journal of Quantum Electronics, Vol. 32, 1537-1543 (1996).

dr. Tomislav A. Dzhekov
Faculty of Electrical Engineering
Cyril and Methody University
Orce Nikolov bb., Skopje
Republic of Macedonia
Tel.: (+389 91) 363566
Fax.: (+389 91) 364 262,
E-mail: tdzhekov @cerera.etf.ukim.edu.mk

Prispelo (Arrived):17.01.1997 *Sprejeto (Accepted):06.05.1997*

 UDK621.3:(53+54+621+66), ISSN0352-9045

UPORABA AKUSTIČNE RESONANCE V MERITVAH IN DETEKCIJI NIVOJA FLUIDOV

Denis Đonlagić, Miha Završnik, Dali Đonlagić
Fakulteta za elektrotehniko, računalništvo in informatiko, Laboratorij za elektrooptične in senzorske sisteme, Univerza v Mariboru, Slovenija

Ključne besede: merjenje nivoja fluidov, detekcija nivoja fluidov, valovodi akustični, resonanca valovoda akustična, resonatorji akustični odprti, resonatorji akustični zaprti, materiali sipki, materiali fluidni, merilniki akustični resonančni, mreže nevronske, ločljivost velika

Povzetek: Predstavljamo novi metodi za zvezno merjenje in detekcijo nivoja fluidov, ki temeljita na pojavu akustične resonance valovoda. Metodi se odlikujeta po veliki robustnosti, ki se odraža v neobčutljivosti na obloge, usedline, delne zamašitve, pene, površinsko stanje fluida, itd. Eksperimentalno sta bila realizirana detektor in zvezni merilnik nivoja fluidov. Eksperimentalni rezultati nakazujejo na veliko robustnost obeh sistemov in s tem na možnost uporabe detektorja in merilnika v ekstremnih industrijskih razmerah.

Application of Acoustic Resonance for Fluid Level Measurements and Detection

Keywords: fluid level measurement, fluid level detection acoustic waveguides, acoustic waveguide resonance, open acoustic resonators, closed acoustic resonators, granular materials, fluid materials, acoustic resonance meters, neural networks, high resolution

Abstract: A new level measurement and level detection methods are presented. They are based on the acoustic resonance of a waveguide and can be successfully implemented for fluid level measurements and fluid level detection in industrial plants, where problems of residues, deposits, foams, etc. can be expected. An experimental level gauge and level detector have been built and tested under artificially induced residues, foams, deposits, etc. The resonance methodes prove to be insensitive under extreme operating conditions. The proposed method represents an alternative to ultrasonic as well to some other level measurement and detection methods.

1. Uvod

V mnogih vejah industrije, posebej procesne industrije, je potrebno meriti in zaznavati nivo fluidov. Merilniki nivoja in nivojski detektorji (stikala) so tako nepogrešljivi členi zelo raznolikih tehnoloških procesov. Zelo pogosto imamo opraviti z visoko viskoznimi fluidi, fluidi katerih viskoznost je odvisna od tehnološkega procesa, fluidi z nedefiniranimi lastnostmi (npr. odpadne vode), itd. Značilen problem, ki ga srečamo pri procesnih merilnikih nivoja so raznovrstne zamašitve, obloge, pene, itd. Tovrstnih problemov ni možno prebroditi s klasičnimi merilnimi postopki, ki temeljijo na mehanskih, prevodnostnih, ultrazvočnih ali mikrovalovnih principih. Tako je večina današnjih merilnikov in detektorjev nivoja omejena le na določene vrste fluidov in specifične delovne pogoje.

V procesni industriji danes pogosto srečujemo ultrazvočne merilnike, ki temeljijo na uporabi ultrazvočnih akustičnih valov. Tovrstni merilniki so relativno preprosti in učinkoviti v primeru dobro definiranih delovnih pogojev. Uporaba ultrazvoka je močno omejena s parazitnimi odboji, ki jih povzročajo npr.: pene, obloge, površinska valovitost fluida, objekti v notranjosti posode, usedline, itd. Delno rešitev tovrstnih problemov zasledimo v literaturi /4,5,6,7,8,9/.

Probleme s parazitnimi odboji je možno odpraviti s povečanjem valovne dolžine akustičnih valov, kar pa povzroči zmanjšanje ločljivosti in razreda točnosti merilnika.

V članku predstavljamo rešitev, ki sloni na uporabi pojava akustične resonance akustičnega valovoda. Akustična resonanca omogoča uporabo relativno dolgih akustičnih valov. Valovna dolžina je lahko tako celo večja od razdalje med pokrovom merilnika in nivojem fluida. Tovrstni valovi se ne odbijajo od ovir, ki so (precej) manjše od njihove valovne dolžine. Dodaten pojav, ki prispeva k zmanjšanju občutljivosti na obloge in ovire znotraj resonančnega prostora, je značilna porazdelitev tlačne in hitrostne amplitude znotraj resonatorja.

V obstoječi literaturi zasledimo uporabo akustične resonance le v primeru uporabe Helmholtzovega resonatorja, ki ga je možno uporabiti za neposredno merjenje prostornine posod in rezervoarjev /10/. Uporaba Helholtzovega resonatorja je omejena z lastnostmi, kot so relativno nizke akustične frekvence (zlasti, ko je prostornina rezervoarja večja od 1 m^3) in korenske odvisnosti med prostornino ter resonančno frekvenco, kar močno omejuje uporabnost tovrstnih merilnikov. Poleg omenjenih problemov se pogosto pojavijo še problemi z obliko in linearnostjo merilnika.

V nadaljevanju bomo podali teoretične osnove delovanja akustičnega resonančnega merilnika in detektorja nivoja fluidov, ki temeljita na resonanci valovoda. Sledita opisa realizacije zveznega merilnika ter detektorja nivoja fluidov. Eksperimentalni rezultati podajajo nekatere pomembne lastnosti in prednosti akustičnega resonančnega merilnika in detektorja pred klasičnimi pristopi.

2. Teorija

Opis akustičnih valovodov in resonatorjev najdemo v mnogih referencah /1,2,3,11/, sledi kratek povzetek:

2.1 Odprt akustični resonator

Odprt akustični resonator je valovod, ki je odprt na eni strani in zaprt na drugi (Slika 1).

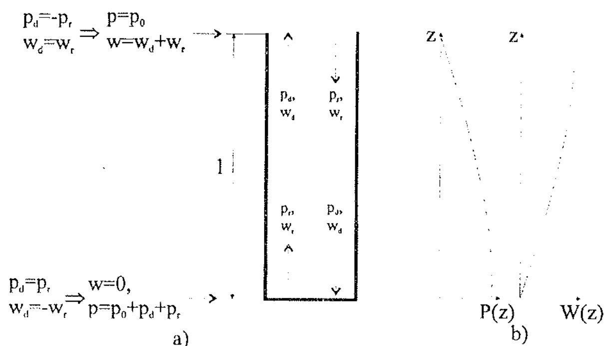

Slika 1. a) Princip odprtega resonatorja z robnimi pogoji; w_d=direktni hitrostni val, w_r-odbiti hitrostni val, p_d=direktni tlačni val, p_r=odbiti tlačni val, p_0=tlak okolice.
b) P(z) tlačna amplituda v odvisnost od osne koordinate; W(z) hitrostna amplituda v odvisnosti od osne koordinate

Za odprt konec valovoda lahko zapišemo naslednje ugotovitve:
(1) Odbiti tlačni val ima obratno fazo kakor prvotni val (prvotni in odbiti val se drug od drugega odštevata).
(2) Odbiti hitrostni val ima enako fazo kakor prvotni val (odbiti in prvotni val se seštevata)

Za zaprt konec valovoda velja:
(1) odbiti tlačni val ima enako fazo kakor prvotni val (odbiti in prvotni val se seštevata)
(2) odbiti hitrostni val ima nasprotno fazo kakor prvotni val (prvotni in odbiti val se drug od drugega odštevata).

Resonančna frekvenca odprtega resonatorja je določena z zgoraj omenjenimi robnimi pogoji. V primeru, ko nastopi resonančni pojav, mora biti tlačna amplituda enaka nič na zaprtem koncu resonatorja ter maksimalna na odprtem koncu resonatorja. Do podobnega sklepa lahko pridemo tudi za hitrostno amplitudo, ki mora biti največja na odprtem koncu in nič na zaprtem koncu resonatorja. To pomeni, da je odprti resonator četrtvalni resonator, resonančne frekvence pa so podane z:

$$f_n = (2n+1)\frac{c}{4l} \qquad n = 0,1,2,3... \qquad (1)$$

pri tem je *c* hitrost zvoka, *l* dolžina resonatorja in *n* celo število (*n*=0,1,...). V primer ko je *n*=0, govorimo o osnovni resonančni frekvenci, za n>0 pa govorimo o višjih harmoničnih frekvencah. Slika 1b predstavlja porazdelitev tlaka in hitrosti delcev za primer osnovne resonančne frekvence v odprtem resonatorju.

V realnosti nihajo zvočni delci nekoliko v prostor okoli odprtega konca resonatorja, tako da hitrostna amplituda na robu resonatorja ne upade povsem na nič. Zato je potrebno dolžino l v enačbi (1) podaljšati za faktor Δl. Raighlijevo priporočilo je empirični izraz in podaja Δl kot:

$$\Delta l = \pi D / 4 \qquad (2)$$

pri tem je D premer valovoda (velja za primer valovoda krožnega preseka).

2.2 Zaprt akustični resonator

Zaprt akustični resonator je valovod, ki je zaprt na obeh straneh (slika 2). Za zaprti konec resonatorja velja:
(1) odbiti tlačni val ima enako fazo kakor prvotni val (odbiti in prvotni val se seštevata)
(2) odbiti hitrostni val ima nasprotno fazo kakor prvotni val (prvotni od odbiti val se odštevata).

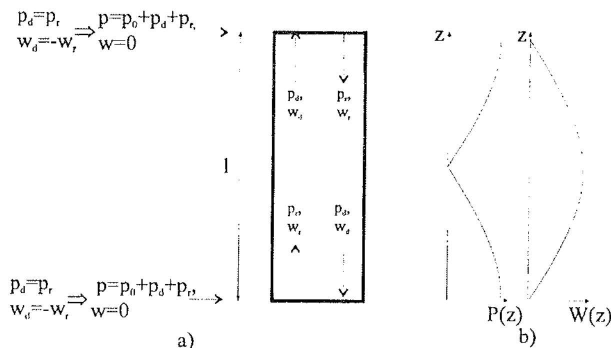

Slika 2 a) Princip zaprtega resonatorja z robnimi pogoji w_d=direktni hitrostni val, w_r-odbiti hitrostni val, p_d=direktni tlačni val, p_r=odbiti tlačni val, p_0=tlak okolice.
b) P(z) tlačna amplituda v odvisnost od osne koordinate; W(z) hitrostna amplituda v odvisnosti od osne koordinate

Ob nastopu resonance mora biti zato tlačna amplituda na koncih resonatorja nič, nasprotno pa velja za hitrostno amplitudo, ki mora biti na obeh koncih resonatorja največja. To pomeni, da je zaprti resonator polvalni resonator in resonančno frekvenco lahko zapišemo v naslednji obliki:

$$f_n = (n+1)\frac{c}{2l} \qquad n = 0,1,2,3... \qquad (3)$$

pri tem je c hitrost zvoka, l dolžina resonatorja in n celo število (n=0,1,...). V primeru ko je n=0, govorimo o osnovni resonančni frekvenci za primer n>0 pa govorimo o višjih harmoničnih frekvencah. Slika 2b pred-

stavlja porazdelitev tlaka in hitrosti delcev za primer osnovne resonančne frekvence v zaprtem resonatorju.

2.3 Odzivni čas

Odzivni čas je čas, ki je potreben, da se v resonatorju vzpostavijo stacionarne razmere. Pravilna ocena odzivnega časa je izjemno pomembna. Karakteristike, ki so zajete s prekratko zakasnitvijo med začetkom vzbujanja in zajetjem amplitude stojnega vala so slabo izražene in netočne, kar neposredno vpliva na merilno negotovost in ločljivost merilnika. V primerih, ko je zakasnitev med začetkom vzbujanja in zajetjem amplitud zelo dolga in bistveno presega odzivni čas resonatorja, po nepotrebnem poslabšamo dinamične lastnosti merilnika. Odzivni čas merilnika lahko ocenimo z izrazom /11/:

$$T = \frac{\ln 0.1}{\ln[k \exp(-Dl)]} \frac{l}{c} \qquad (4)$$

pri tem je D koeficient slabljenja akustičnega valovanja v plinu, l dolžina resonatorja in c hitrost zvočnega valovanja. Če v izraz (4) vstavimo značilne vrednosti $D=0.003\ m^{-1}$, k=0.95 (zrak-voda), l=1 m, c=340 m/s, dobimo značilen odzivni čas T=130 ms.

3. Akustični resonančni detektor nivoja fluidov in sipkih materialov

3.1 Osnovni princip delovanja

Akustični resonančni detektor nivoja je sestavljen iz: valovoda, oddajnika zvočnega valovanja (zvočnika), sprejemnika (mikrofona) in procesne enote. Položaj spodnjega roba valovoda določa nivo pri katerem detektor zazna prisotnost fluida oziroma sipkega materiala. Postavitev resonančnega detektorja ponazarja slika 3.

V odvisnosti od položaj nivoja fluida ali sipkega materiala je spodnji konec resonatorja odprt (nivo je nižji od točke detekcije) ali zaprt (nivo je enak ali višji od točke detekcije). Resonančne frekvence valovoda se v primeru, da nivo fluida preseže spodnji rob valovoda

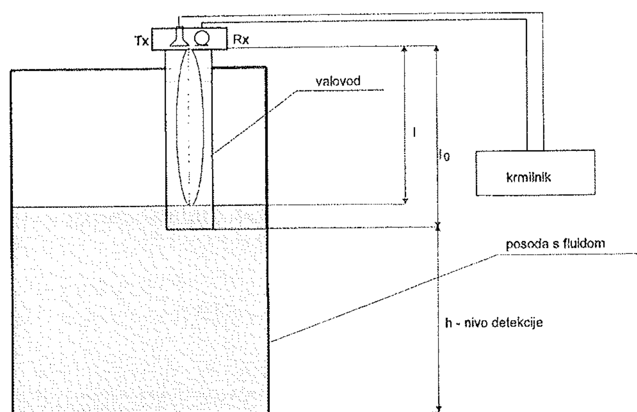

Slika 3 Akustični resonančni detektor nivoja

skokovito spremenijo. V idealnem primeru dobimo dva nabora resonančnih frekvenc:

(1) nabor resonančnih frekvenc, ki je značilen za zaprti resonator (fluid je dosegel spodnji rob resonatorja), enačba (1):

$$f_n = (2n+1)\frac{c}{4l} \qquad n = 0,1,2,3...$$

(2) nabor resonančnih frekvenc, ki je značilen za odprti resonator (fluid ni dosegel spodnji rob resonatorja), enačba (3):

$$f_n = (n+1)\frac{c}{2l} \qquad n = 0,1,2,3...$$

S pomočjo identifikacije nabora resonančnih frekvenc lahko tako sklepamo na prisotnost nivoja.

3.2 Detekcija nivoja

V eksperimentalni postavitvi smo uporabili dva pristopa za detekcijo:

3.2.1 Nadzor resonančne frekvence odprtega resonatorja

Procesna enota tvori konstantno frekvenco, ki ustreza osnovni resonančni frekvenci odprtega resonatorja (enačba (1)) in hkrati nadzoruje amplitudo akustičnega valovanja, ki se ustvari v resonatorju. V primeru, ko doseže nivo fluida spodnji rob valovoda akustična amplituda močno upade, saj pride do skokovite spremembe resonančne frekvence (enačba (3)). Tako lahko sklepamo na prisotnosti nivoja fluida neposredno iz velikost amplitude akustičnega valovanja v valovod. Postopek je izjemno preprost. Celoten detektor je možno v celoti realizirati z uporabo analognih komponent.

Resonator bi bilo možno vzbujati tudi z osnovno resonančno frekvenco zaprtega resonatorja, vendar pa je takšen postopek manj primeren oziroma bolj zapleten, saj se resonančna frekvenca zaprtega valovoda spreminja z nivojem (kadar nivo preseže spodnji rob valovoda je resonančna frekvenca odvisna od dolžine resonančnega prostora in s tem od nivoja).

3.2.2 Skaniranje frekvenčne karakteristike resonatorja in klasifikacija s pomočjo nevronske mreže

Procesna enota zajame celotno ali del frekvenčne karakteristike resonatorja in jo nato obdela. Takšen pristop je zelo primeren za obratovanje detektorja pod ekstremnimi pogoji, ko pričakujemo obloge, zamašitve, pene ter druge nepredvidljive dogodke.

V eksperimentalni izvedbi je potekalo zajemanje frekvenčne karakteristike s skaniranjem. Procesna enota vzbudi resonator, počaka odzivni čas, nato zajame in hkrati filtrira akustični signal. Postopek se ponavlja pri tem pa se frekvenca v vsakem koraku poveča za določeno vrednost, vrednosti akustične am-

plitude se sproti shranjujejo v pomnilnik. Po končanem skaniranju je potrebno frekvenčno karakteristiko ustrezno klasificirati, tj. razpoznati ali je resonator odprt ali zaprt.

V ta namen je bila uporabljena nevronska mreža, saj ima v danem primeru vrsto prednosti pred ostalimi postopki za razpoznavanje vzorcev. Najpomembnejša lastnost nevronske mreže je sposobnost učenja na primerih. Detektor je tako možno preprosto optimirati (naučiti) za specifične pogoje obratovanja, tudi za primere, ko pogoji obratovanja močno odstopajo od idealnih.

V procesu učenja je tako potrebno pripraviti dva nabora karakteristik: prvi nabor mora vsebovati čim bolj različne primere, v katerih je nivo fluida prisoten, drugi niz mora vsebovati različne primere, v katerih je nivo odsoten. Oba niza je potrebno pripraviti čim bolj raznovrstno, vključujoč mejne in neidealne primere. Kvaliteta detekcije v neidealnih primerih je močno odvisna prav od raznovrstnosti primerov s katerimi učimo nevronsko mrežo.

3.3 Eksperimentalna izvedba resonančnega detektorja

Eksperimentalna izvedba resonančnega detektorja je ponazorjena na sliki 3. Eksperimentalni resonator je dolg 70 cm in ima premer 10 cm. Izbira premera resonatorja je odvisna od lastnosti medija, katerega nivo zaznavamo. V primeru, da zaznavamo visoko viskozni medij ali medij, ki tvori obloge, je potrebno izbrati zadosten premer resonatorja tako, da preprečimo možnost popolne zamašitve. Dolžina resonatorja mora biti s stališča dinamičnih lastnosti detektorja čim manjša, saj ima daljši resonator daljši odzivni čas, vendar pa mora znašati razmerje med dolžino in premerom resonatorja vsaj tri do štiri. V nasprotnem primeru ne dobimo dobro izražene resonančne karakteristike.

V eksperimentalni izvedbi je bil uporabljen običajni audio zvočnik (moči 5W) in audio mikrofon. Pokrov resonatorja je bil ustrezno zatesnjen. Tesnjenje je pomembno, saj povzroči kakršna koli odprtina na resonatorju znaten premik resonančne frekvence, kar vpliva na kvaliteto zaznavanja nivoja.

Osrednji del procesne enote je mikrokrmilnik HITACHI H8/510. Mikrokrmilnik skrbi za tvorbo sinusnega vzbujanja, zajemanje karakteristike, filtriranje, klasifikacijo karakteristike s pomočjo nevronske mreže, logične odločitve, prikaz rezultatov ter komunikacijo s servisnim računalnikom.

Učenje nevronske mreže je potekalo na gostiteljskem računalniku (PC), uteži nevronske mreže pa so bile naknadno prenesene v pomnilnik (E^2PROM) procesne enote.

Uporabljena je bila običajna back-prop nevronska mreža z dvema aktivnima nivojema (slika 4). Vhodni vektor vsebuje frekvenčno karakteristiko (120 vrednosti, ki predstavljajo akustično amplitudo v odvisnosti od frekvence), vmesna plast je vsebovala 25 nevronov, izhodna pa dva nevrona. Nadaljnje povečanje števila

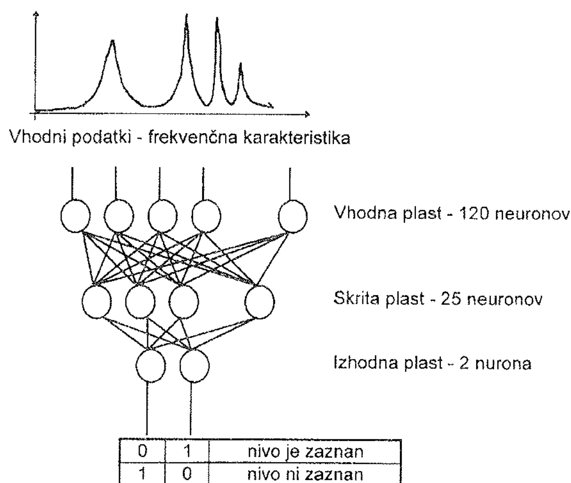

Slika 4 Klasifikacija frekvenčne karakteristike

nevronov v skriti plasti ni pokazalo bistvenega izboljšanja sposobnosti zaznavanja nivoja. Tako je poraba pomnilnika za uteži nevronske mreže relativno skromna in primerna za realizacijo z mikrokrmilnikom (uteži so zasedle približno 12 KB pomnilnika). Število učnih ciklov nevronske mreže se je gibalo med 150 in 1500, odvisno od raznolikosti vhodnih (učnih) karakteristik.

Posebej pomemben postopek v realizaciji detektorja je priprava učnih naborov karakteristik. Tako so bile umetno ustvarjene različne neidealne obratovalne razmere (zamašitve, pene, obloge), kar je omogočilo pripravo raznovrstnih učnih naborov. Poseben nabor učnih karakteristik je bil pripravljen za primer detekcije akustično redkejših snovi, kot je na primer stiroporni granulat.

3.4 Eksperimentalni rezultati

3.4.1 Značilne karakteristike

Slike 5-9 kažejo značilne karakteristike, ki so bile zajete med eksperimentalno fazo. Pri tem je na x-osi podan nihajni čas in ne frekvenca (takšen pristop je primernej-

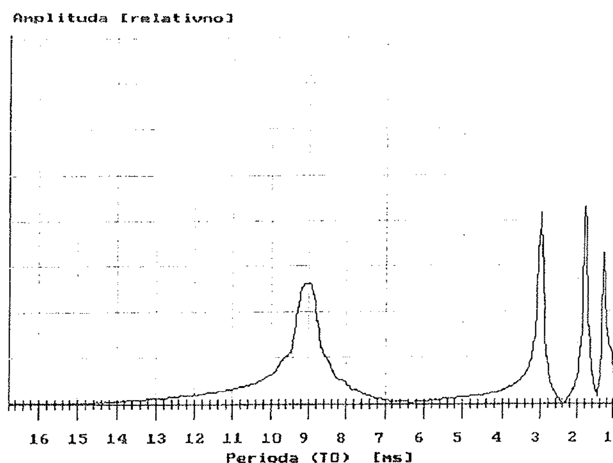

Slika 5 Frekvenčna karakteristika odprtega resonatorja, brez oblog, vsedlin in pen.

ši, saj je dejanski nivo tekočine sorazmeren z nihajnim časom, kar je pomembno pri zveznih meritvah nivoja).

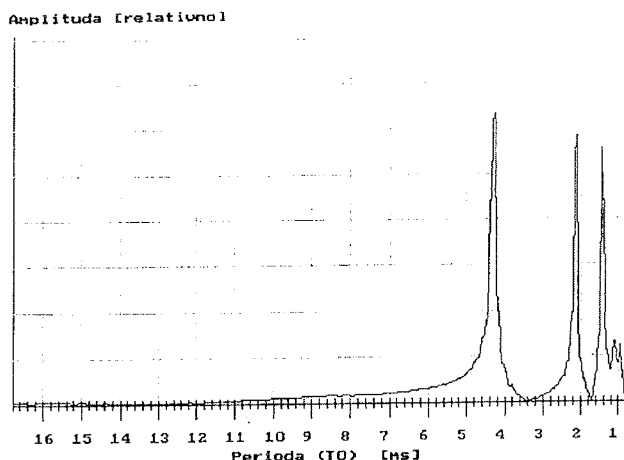

Slika 6 *Frekvenčna karakteristika zaprtega resonatorja, brez oblog, vsedlin in pen.*

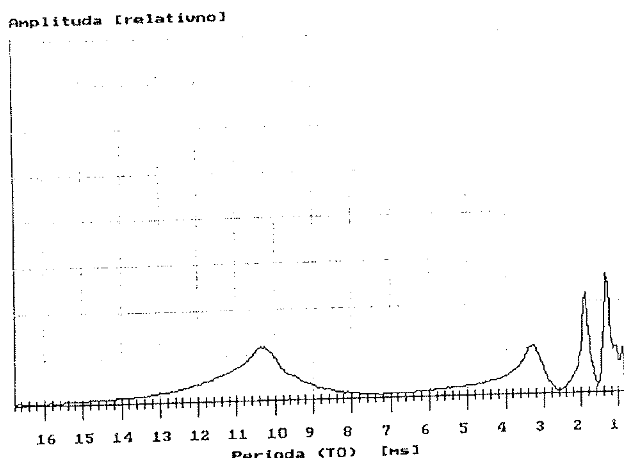

Slika 7 *Frekvenčna karakteristika resonatorja zaprtega s stiropornim granulatom*

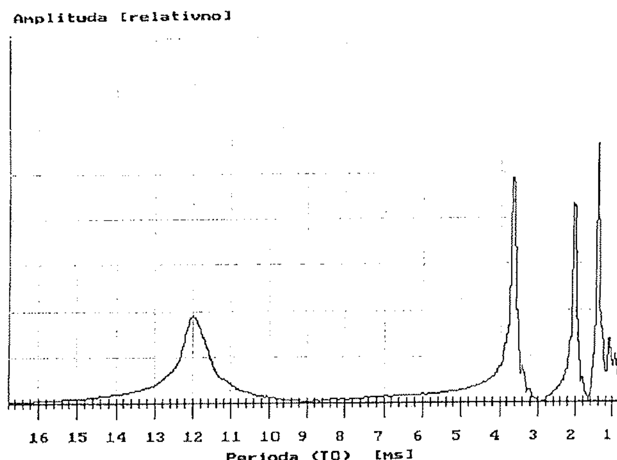

Slika 8 *Frekvenčna karakteristika zaprtega resonatorja, ob prisotnosti zmernih oblog (80% zamašitev)*

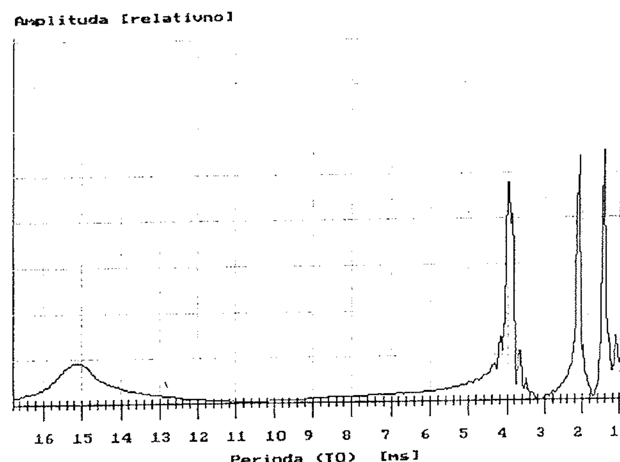

Slika 9 *Frekvenčna karakteristika zaprtega resonatorja, ob prisotnosti močnih oblog (95% zamašitev).*

Slika 5 in 6 ponazarjata značilna odziva, ki jih dobimo v primeru, da so odsotne obloge, pene, zamašitve, itd. Resonančna maksimuma v popolnosti ustrezata enačbam (1) in (3). Slika 7 ponazarja razmere, ko je resonator zaprt s stiropornim granulatom. Resonančni maksimumi so glede na enačbo 3 premaknjeni, nižji in nekoliko zabrisani. Sliki 8 in 9 ponazarjata razmere, ko je bila prisotna močna zamašitev. V primeru na sliki 8 je bilo zamašenega približno 80% celotnega preseka resonatorja, v primeru 9 pa je bilo zamašenega 95% celotnega preseka resonatorja.

3.4.2 Detekcija nivoja

Po opravljenem učenju nevronske mreže je bil detektor pripravljen na zaznavanje nivoja pod različnimi obratovalnimi pogoji. Nivo je bil uspešno zaznan tudi v primeru, ko je zamašitev znašala več kakor 96% celotnega preseka resonatorja. Z ustreznim učenjem je bil detektor sposoben zaznati nastajanje oblog med samim učenjem. Tovrsten pristop omogoča pravočasno opozorilo operaterju, da je potrebno čiščenje detektorja, kar izboljša zanesljivost celotnega sistema.

Tovrstno robustnost akustičnega resonančnega detektorja nivoja lahko razložimo z dejstvom, da imamo opraviti z relativno dolgimi akustičnimi valovi. Valovna dolžina akustičnega vala je ob nastopu resonance dva do štiri krat večja od valovne dolžine resonatorja ter mnogo večja od morebitnih ovir znotraj ali v neposredni okolici resonatorja. Tako se akustično valovanje od morebitnih ovir ne odbije.

Pogrešek zaznavanja znaša v primeru akustično gostejših fluidov in snovi ter manjših zamašitev resonatorja približno $\Delta h \approx +2$ mm (Slika 10). V primeru, ko je bil resonator močno zamašen (90% in več), se je pogrešek zaznavanja povečal na $\Delta h \approx +1$-3 cm. Detektor je tako zaznal nivo še preden je le ta dosegel nominalno točko zaznavanja (spodnji rob resonatorja). Pogrešek zaznavanja je odvisen od raznovrstnosti učnih karakteristik, velikosti, položaja in oblike zamašitev oziroma obloge. V našem primeru je prišlo do največjega odstopanja $\Delta h = +3$ cm.

V primeru stiropornega granulata so bili pogreški večji in so znašali od Δh=-3 cm do Δh=-15 cm. Tako je prišlo do zaznavanja šele, ko je bil nominalni nivo (spodnji rob resonatorja) presežen. Pogrešek zaznavanja je bil odvisen od učnih karakteristik in velikosti stiropornih zrnc in je v povprečju znašal Δh=-7cm.

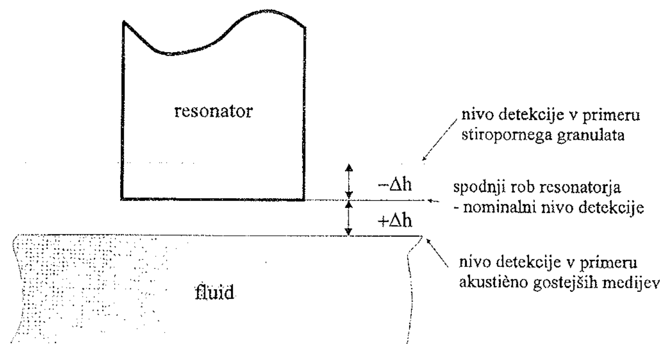

Slika 10 Nivoji detekcije

3.4.3 Dinamika detektorja

Osrednja pomanjkljivost resonančnega detektorja je dinamika. Odzivni časi resonatorja so lahko relativno dolgi (npr. okoli 130 ms za 1 m dolg resonator), tako da lahko traja skaniranje karakteristike tudi 10 ali več sekund. Obstaja več možnosti za zmanjšanje časa skaniranja: odzivni čas lahko prilagodimo frekvenci vzbujanja, skaniramo le del ali dele karakteristike, ločljivost karakteristike je možno zmanjšati v celotnem ali v delu frekvenčnega območja, itd., vendar je učinkovitost tovrstnih pristopov odvisna od specifičnih obratovalnih pogojev.

3.4.4 Primerjava resonančnega detektorja nivoja fluidov z nekaterimi drugimi detektorji

V primerjavi z ultrazvočnimi in mikrovalovnimi detektorji, resonančni detektor ni občutljiv na obloge, površinsko stanje fluida, odboje povzročene z oblogami, penami ter drugimi dejavniki. Kapacitivni, induktivni, konduktivni ter optični detektorji so mnogo bolj občutljivi na obloge, usedline in korozijo. V primerjavi s transverzalnim vibracijskim detektorjem resonančni detektor ni občutljiv na spremembe v gostoti in viskoznosti fluida.

4. Akustični resonančni merilnik nivoja fluidov

Poleg detekcije nivoja fluidov in sipkih materialov omogoča uporaba akustične resonance konstrukcijo učin-kovitega merilnika nivoja fluidov.

4.1 Osnovni princip delovanja

Nivo fluida določa spodnji rob in s tem dolžino resonatorja. Resonančna frekvenca resonatorja je tako odvisna od nivoja fluida in jo lahko izrazimo s pomočjo enačbe (3).

Podobno, kakor akustični resonančni detektor, je zvezni merilnik nivoja sestavljen iz: valovoda (resonatorja), oddajnika zvočnega valovanja (zvočnika), sprejemnika (mikrofona) in procesne enote. Resonančni merilnik nivoja ponazarja slika 11.

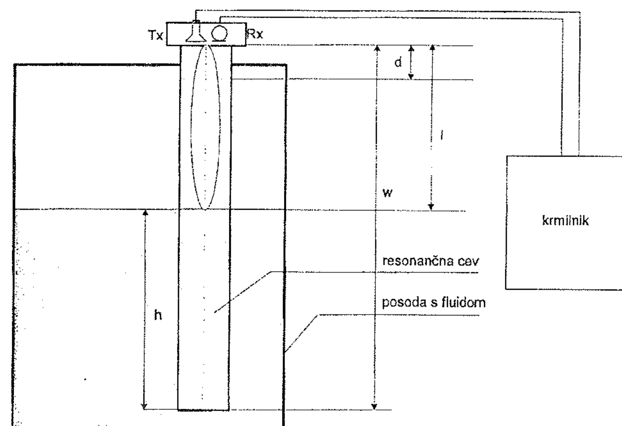

Slika 11 Akustični resonančni merilnik nivoja - princip delovanja

Valovod je na eni strani omejen s fluidom, katerega nivo merimo, na drugi strani pa s pokrovom valovoda v katerem sta nameščena oddajnik in sprejemnik. Oddajnik in sprejemnik sta lahko postavljena kjerkoli znotraj valovoda; zaradi merilnega območja je najugodnejša namestitev v pokrovu merilnika. Stoječe valovanje se vzpostavi med pokrovom in nivojem fluida. Resonančna frekvenca za tako konstruiran valovod, je funkcija razdalje med pokrovom valovoda in gladino fluida. Uporabimo lahko tudi odprt resonator, vendar so eksperimentalni rezultati pokazali, da je resonančni pojav pri zaprtem resonatorju bistveno bolj izrazit, kar ugodno vpliva na ločljivost. Zato smo obravnaval le zaprt resonator.

Poleg osnovne resonančne frekvence ima takšen tip resonatorja tudi izrazite višje harmonične frekvence.

Za meritve nivoja so zanimivi tako osnovni, kakor tudi višji harmoniki. V skladu z enačbo (3) obstoja med dolžino resonančnega prostora l in resonančnimi frekvencami f_n naslednja povezava:

$$l=(n+1)\frac{c}{2f_n} \qquad n=0,1,2,3... \tag{5}$$

V skladu s sliko 11 velja:

$$h=w-l\frac{c}{2f_0} \tag{6}$$

Merilno območje merilnika:

Merilno območje merilnika je omejeno z dolžino in premerom resonančne cevi ter izvedbo krmilnika. Premer cevi namreč določa do kod sme seči nivo; maksimalni nivo mora biti za premer cevi manjši od dolžine valovoda (h_{max}=w-d, slika 11). Kadar pogoj ni izpolnjen, ne vemo, ali se resonanca vzpostavi med pokro-

vom merilnika in gladino fluida, ali pa kar med bočnima stenama resonatorja. Zato je merilno območje za premer resonatorja manjše od dolžine celotne cevi. Druga omejitev je delovno območje krmilnika. Resonančna frekvenca narašča obratno sorazmerno z dolžino resonančnega prostora, zato je smiselno zagotoviti mrtvo območje med vrhom resonatorja in maksimalnim nivojem, saj lahko na tak način bistveno omejimo zahteve po frekvenčnem razponu v katerem mora delovati krmilnik.

Podobno, kakor drugi akustični merilnik nivoja, potrebuje tudi resonančni merilnik sistem za kompenzacijo spremenljive hitrosti zvoka v plinu nad gladino merjenega fluida. V primeru, da imamo opraviti s plini, ki imajo podobne lastnosti kakor idealni plini (npr. zrak), lahko spremembe hitrosti zvoka kompenziramo z merjenjem temperature ter ustrezno korekcijo hitrosti zvoka v enačbi (6). V primerih ko imamo opraviti z neidealnimi plini je najprimernejša uporaba referenčnega resonatorja.

4.2 Eksperimentalna izvedba resonančnega merilnika

4.2.1 Fizična izvedba merilnika

Resonančni merilnik nivoja na temelju osnovne resonančne frekvence je sestavljen iz naslednjih komponent

- valovod - resonator glava merilnika z oddajnikom in sprejemnikom mehanskega valovanja (zvočnik, mikrofon)
- krmilnik (generator z nastavljivo frekvenco, filter, logična enota)
- temperaturni senzor

Valovod (resonator) je lahko narejen iz različnih materialov. V eksperimentalni izvedbi je bila uporabljena polietilenska cev. Maksimalna dolžina cevi in s tem merilni doseg, je omejen s frekvenčnim območjem oddajnika in sprejemnika. Drugi pomemben parameter je premer resonančne cevi. S premerom cevi je določeno minimalno mrtvo področje resonančnega merilnika. Resonančna cev mora segati najmanj za lastni premer čez maksimalni nivo fluida. Minimalno mrtvo področje je mnogokrat odvisno tudi od zmogljivosti krmilnika, saj se resonančna frekvenca nelinearno povečuje s krajšanjem resonatorja.

Poseben problem predstavlja odzračevanje. Vsaka odprtina na valovodu namreč povzroči premik resonančne frekvence. Zato je potrebno odprtine za odzračevanje zmanjšati kolikor je le to mogoče. Problem odzračevanja je podrobneje opisan v eksperimentalnem delu.

Primer konstrukcijske izvedbe glave resonančnega merilnika je prikazan na sliki 12.

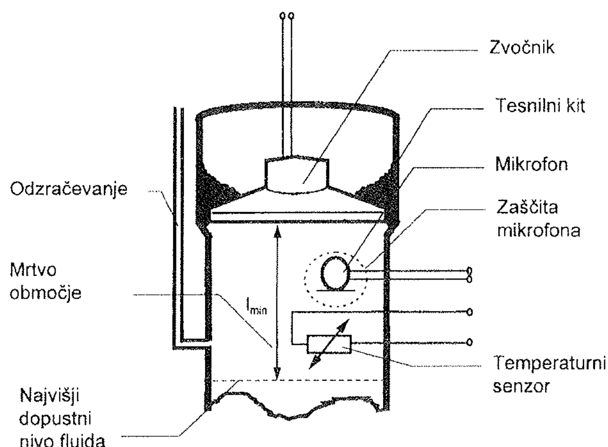

Slika 12 Primer izvedbe glave merilnika

4.3 Merilni algoritem

Postopkov, po katerih lahko določimo resonanco valovoda je več. V eksperimentalni izvedbi je bil uporabljen postopek skaniranja, s katerim pregledujemo frekvenčno območje in iščemo maksimum. Prisotnost višjih harmonikov zahteva ustrezno, dodatno obravnavo. Realizacijo dodatno zaplete primer, ko se posoda popolnoma izprazni in se resonator obnaša kot odprt resonator.

4.3.1 Skaniranje celotnega frekvenčnega območja

Resonator vzbujamo od minimalne frekvence (ta je določena z minimalnim nivojem oz. maksimalno dolžino resonatorja) do maksimalne frekvence, ki je omejena z minimalno dolžino resonančnega prostora (premer cevi) ali pa z zgornjim frekvenčnim območjem krmilnika. V primeru realizacije na H8 mikrokrmilniku (program je napisan izključno v C jeziku) je zgornje frekvenčno območje vzbujanja 1.2 KHz, kar ustreza približno 15 cm.

Merilni algoritem povečuje nihajni čas znotraj celotnega frekvenčnega območja in hkrati beleži dobljene vrednosti akustičnih amplitud. Sledi ustrezna obdelava dobljenih vrednosti:

- iskanje maksimumov v skanirani karakteristiki
- primerjava in obdelava harmonikov.

Prvi najdeni maksimum (maksimum, kateremu ustreza najdaljši nihajni čas oz. najmanjša frekvenca) predstavlja osnovno resonančno frekvenco, ki je osnova za izračun nivoja. Ostali maksimumi predstavljajo višje harmonike.

Iz razmerja med prvim harmonikom in osnovno resonančno frekvenco lahko ugotovimo, če je posoda prazna in se resonator obnaša kot odprt resonator. Prisotnost prvega harmonika (pri $T_0/2$ oz. $2f_0$) je zanesljiv znak, da prvi najden maksimum zagotovo ustreza osnovni resonančni frekvenci in zato lahko preidemo na skaniranje delnega območja.

Skaniranje celotnega frekvenčnega območja je relativno počasno. To neugodno vpliva na dinamiko merilnika. Da bi izboljšali dinamiko je bil dodan dodaten sledilni algoritem za skaniranje delnega območja.

4.3.2 Sledilni algoritem (skaniranje delnega območja)

Algoritem sledi maksimumu, ki ga poiščemo s skaniranjem celotnega območja. Algoritem skanira okolico najdenega maksimuma in stari maksimum nadomesti z novim. Tako lahko za počasne spremembe nivoja zagotovimo sledenje maksimumu (nivoju). Da se zavarujemo pred morebitnimi hitrimi spremembami nivoja, je zelo pomembna obravnava harmoničnih frekvenc:

- če maksimum pri dvakratni osnovni frekvenci ne obstaja in če frekvenca vsaj približno ustreza resonančni frekvenci odprtega resonatorja pomeni, da je posoda popolnoma prazna in se resonator obnaša kot odprt resonator; dobljena frekvenca ne predstavlja realnega nivoja.
- če maksimum pri dvakratniku osnovne frekvence obstaja pomeni, da izmerjena osnovna frekvenca ustreza realnemu nivoju.
- če obstaja maksimum pri polovici ali tretjini osnovne frekvence pomeni, da se je sledilni algoritem ujel, namesto na osnovno, na višjo harmonično frekvenco (1. ali 2.). Do tega pojava lahko pride pri naglem padcu nivoja.

4.3.3 Ukrepi za izboljšanje dinamičnih lastnosti merilnika

Algoritem vsebuje naslednje ukrepe za izboljšanje dinamike:

- Skaniranje celotnega območja ne poteka z največjo možno resolucijo. Tako s skaniranjem celotnega frekvenčnega območja ugotovimo le približno lego resonančne frekvence.
- Dokončna določitev maksimuma poteka z delnim skaniranjem (sledilni algoritem). Tudi delno skaniranje je sestavljeno iz grobega skaniranja in finega skaniranja. Grobo skaniranje zagotavlja sledenje nivoja, fino skaniranje pa omogoča doseganje maksimalne resolucije. Algoritem za delno skaniranje, realiziranega merilnika, zajema območje ±5 cm glede na zadnji izmerjeni nivo.

4.4 Blokovni diagram resonančnega merilnika nivoja

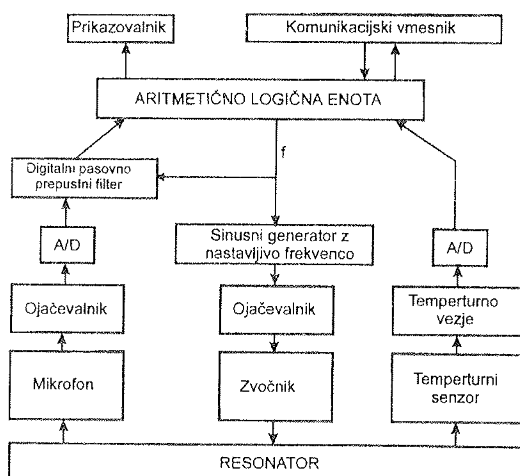

Slika 13 Blokovni diagram

Blokovni diagram celotnega merilnika ponazarja slika 13.

4.5 Eksperimentalni rezultati

4.5.1 Nekatere tipične karakteristike zaprtega resonatorja ter lastnosti realiziranega merilnika

Slike 14 do 18 prikazujejo tipične karakteristike realiziranega eksperimentalnega resonančnega merilnika, ki jih dobimo s skaniranjem celotnega merilnega območja. Iz priloženih slik je razvidno, da je resonančni vrh manj izrazit pri nižjih frekvencah, kar je posledica manjše občutljivosti audio komponent.

Realiziran resonančni akustični merilnik ima naslednje lastnosti:

- merilno območje: 1.8 m (2.06 m - resonator); sprememba nazivnega merilnega območja je enostavna, saj zahteva le spremembo dolžine resonatorja ter spremembo ustreznih programsko določenih konstant
- ločljivost: 2.1 mm (= 0.116%)
- merilna negotovost: 6.3 mm (= 0.35%)
- histereza <0.116%
- nelinearnost: 2.1 mm (=0.116%)

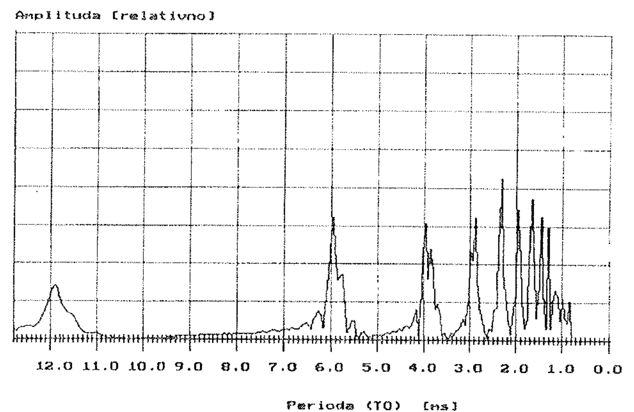

Slika 14 Resonančna karakteristika pri h =0 m. Dolžina resonatorja l =2.05 m.

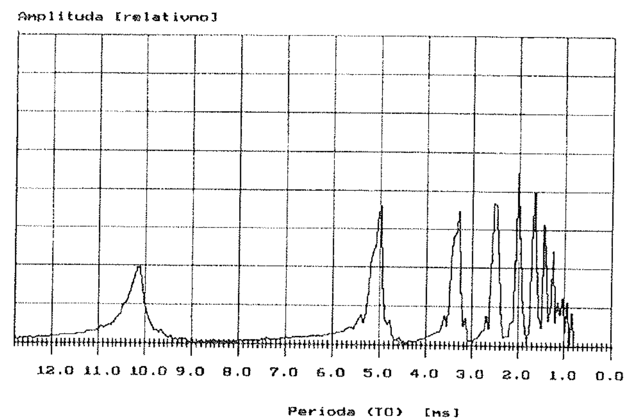

Slika 15 Resonančna karakteristika pri h=0.3 m. Dolžina resonatorja l =1.75 m.

- dinamika: skaniranje celotnega območja: 25 s
  skaniranje delnega območja (najslabši primer): 12 s

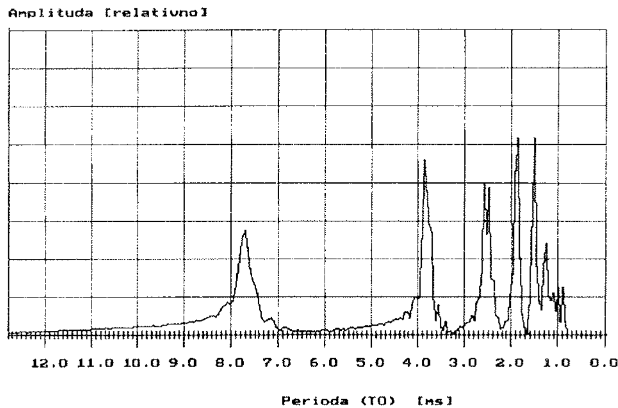

Slika 16 Resonančna karakteristika pri h=0.705 m. Dolžina resonatorja l=1.3 m

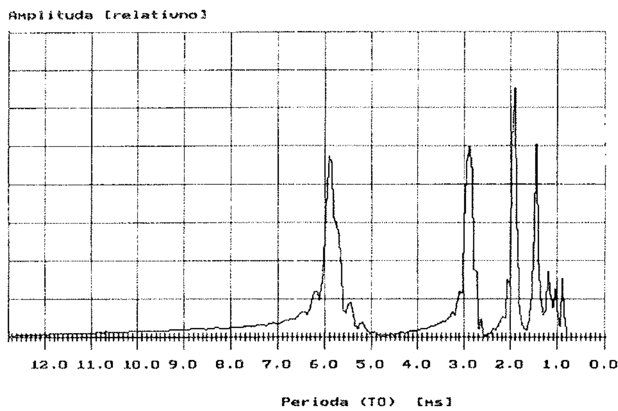

Slika 17 Resonančna karakteristika pri h=1.05 m. Dolžina resonatorja l=1.0 m.

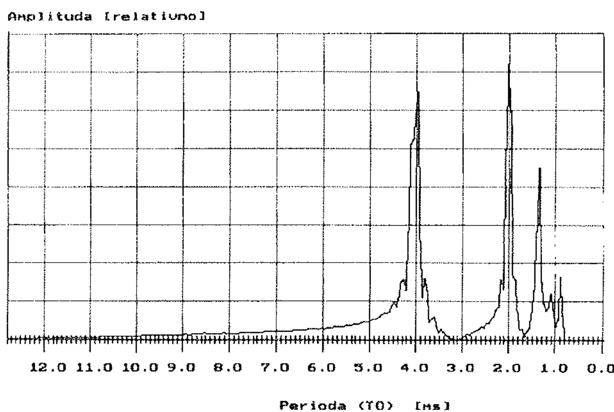

Slika 18 Resonančna karakteristika pri h=1.55 m. Dolžina resonatorja l=0.5 m.

4.5.2 Vpliv odprtin na obnašanje resonatorja

Zanimiva lastnost akustičnega resonatorja je premik resonančne frekvence zaradi dodatne odprtine na resonatorju. Frekvenčni premik resonance je opazen pri relativno majhni odprtini, hkrati pa je odvisen tudi od položaja odprtine. Velikost in položaj odprtine vplivata tudi na kvaliteto resonatorja (površino in velikost resonančnega vrha). Zato moramo paziti, da morebitna odprtina za odzračevanje ni prevelika, oziroma, da ji dodatno povečamo akustično impedanco (npr. odzračevanje izvedemo preko dolge in tanke cevke).

Da bi ugotovil vsaj približno odvisnost premika resonančne frekvence resonatorja od položaja in velikosti odprtine, smo opravili dva niza poizkusov:

- odprtino z d=10 mm smo premikal vzdolž resonatorja in opazoval odziv
- na razdalji 4 cm od glave merilnika smo postopoma večali odprtino in opazoval odziv

Rezultati poizkusov so podani na sliki 19 in 20.

Dobljene karakteristike ponazarjajo odvisnost resonančne frekvence od položaja in velikosti odprtine. Vidimo lahko, da je postavitev odzračevalne odprtine zelo pomembna.

Razlago za takšno obnašanje resonatorja je možno najti v robnih pogojih. Dodatna odprtina na steni resonatorja podre tlačno ravnovesje v resonatorju. Posledica je zamik resonančne frekvence. Tako odprtina na sredini

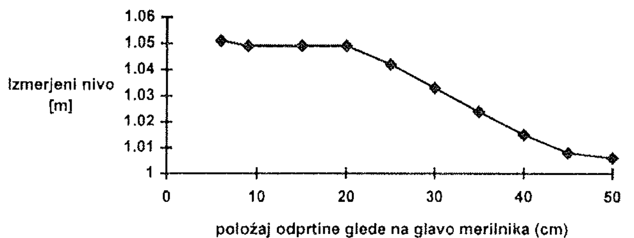

Slika 19 Izmerjeni nivo v odvisnosti od položaja odprtine (dejanski nivo je stalen)

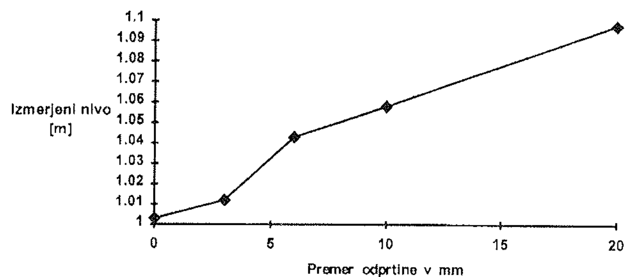

Slika 20 Izmerjeni nivo glede na velikost odprtine (dejanski nivo je stalen)

resonatorja ne vpliva bistveno na resonanco (tlačna amplituda je na sredini resonatorja nič), odprtina v glavi merilnika, pa najmočneje spremeni prvotno karakteristiko.

4.5.3 Vpliv oblog na merilno negotovost merilnika

Izvedel je bil niz poizkusov, s katerimi smo skušali ovrednotiti vpliv oblog na merilno negotovost merilnika.

Resonator (l = 2 m) smo potopili v vodo do polovice (h≅1 m). V resonančno cev smo na različnih višinah postavil oviro iz steklarskega kita, ki smo jo oblikoval kot kaže slika 21. Pri konstantnem nivoju smo nato spreminjali položaj ovire. V prvem nizu poizkusov je prečni presek ovire znašal več kakor 60% celotnega preseka resonatorja. Nato smo oviro zmanjšali na 25% celotnega preseka resonatorja in jo postavili na mesto, kjer je bil prej premik resonance najbolj izrazit.

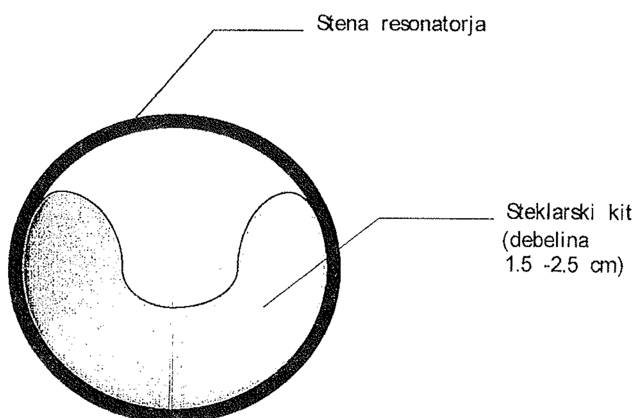

Slika 21 Oblika in namestitev testne ovire (obloge)

V naslednjih tabelah je prikazan vpliv postavitve ovire na pogrešek merilnika (S - prečni presek ovire, S_0 - presek resonatorja):

Oddaljenost od glave merilnika (ovira: S=60% S_0)	absolutni pogrešek	relativni pogrešek
10 cm	2.1 mm	0.16%
25 cm	17.3 mm	1%
50 cm	41 mm	2.2%

Oddaljenost od glave merilnika (ovira: S=25% S_0)	absolutni pogrešek	relativni pogrešek
50 cm	10.5 mm	0.58%

Na sliki 22 je tipična karakteristika za primer, ko v resonatorju ni ovire. Na slikah 23 in 24 sta tipični karakteristiki za primer, ko se ovira nahaja na sredini resonatorja (pogrešek je največji).

Na osnovi opravljenih poizkusov lahko sklepamo, da obloge na stenah resonatorja bistveno ne popačijo karakteristike. V primeru, da prečni presek oblog na stenah resonatorja ne preseže 30% nazivnega preseka resonatorja, se relativni pogrešek ne poveča za več kot 0.6%. Odstopanje je največje, kadar je ovira na sredi resonančnega prostora.

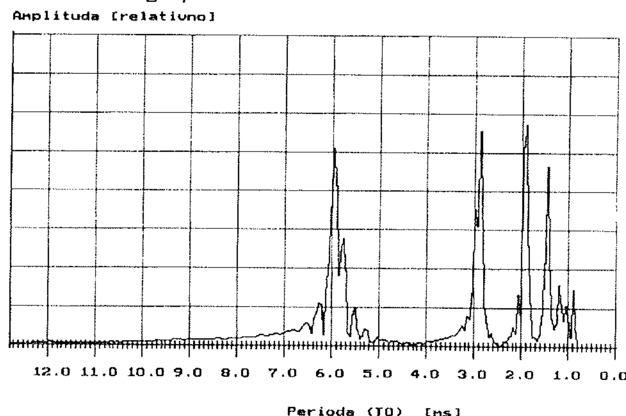

Slika 22 "Običajna karakteristika" brez ovire

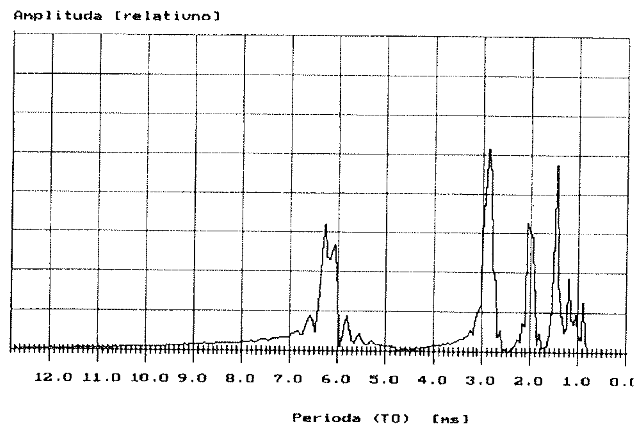

Slika 23 Karakteristika merilnika z oviro. Ovira je postavljena na sredino resonančnega prostora (površina ovire 60% nazivnega preseka resonatorja)

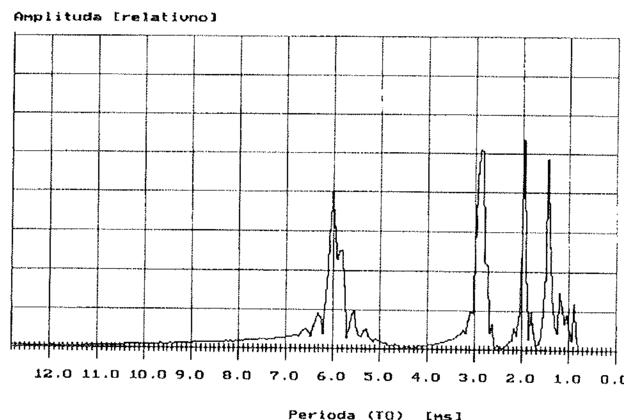

Slika 24 Karakteristika merilnika z oviro. Ovira je postavljena na sredino resonančnega prostora (površina ovire = 25% nazivnega preseka resonatorja)

Opravljeni poizkusi kažejo tudi, da na karakteristiko ne vpliva površinska obdelava sten resonatorja (hrapavost).

Vzrok za takšno obnašanje je v uporabi relativno velikih valovnih dolžin, saj je valovna dolžina zvočnega valovanja ob nastopu resonance dvakrat večja kot sam resonator. Valovna dolžina zvočnega valovanja je bistveno večja od ovire (obloge) in zato ovira bistveno ne vpliva na karakteristiko. Drugi vzrok je razporeditev hitrostne in tlačne amplitude znotraj resonatorja ter robni pogoji zaprtega resonatorja.

5. Zaključek

Akustična resonanca valovoda omogoča realizacijo učinkovitega detektorja ter merilnika nivoja fluidov. Detektor omogoča tudi zaznavanje različnih vrst sipkih snovi. Eksperimentalno sta bila realizirana in ovrednotena tako detektor, kakor tudi zvezni merilnik nivoja fluidov. Za obe izvedbi je značilna velika robustnost, ki se odraža v neobčutljivosti na spremenljive delovne pogoje, obloge, usedline, parazitne odboje, pene, zožitve, površinsko stanje fluida, itd.

Izjemna robustnost izhaja iz relativno veliki valovnih dolžin akustičnih valov, saj je valovna dolžina ob nastopu resonance dvakrat daljša, kakor resonančni prostor. Tako so morebitne ovire vselej bistveno manjše od valovne dolžine akustičnih valov, kar preprečuje parazitne odboje.

Akustični resonančni detektor nivoja je bil dodatno izboljšan z uporabo nevronske mreže, kar omogoča izjemno učinkovito klasifikacijo frekvenčnih karakteristik ter možnost prilagajanja na specifične delovne pogoje. Detektor je možno uporabiti tudi za zaznavanje akustično redkejših medijev, kot je npr. stiroporni granulat. Ob pravilnem učnem postopku je detektor uspešno zaznaval nivo tudi v primerih, ko je prišlo do več kakor 95% zamašitve resonatorja.

Akustični resonančni merilnik nivoja se odlikuje z relativno visoko ločljivostjo tudi pod ekstremnimi pogoji obratovanja, ko so v resonatorju prisotne izdatne obloge, ovire in druge neidealnosti. Merilnik lahko prenese zamašitve, ki presegajo 60% nazivnega preseka resonatorja.

Osrednja pomanjkljivost akustičnega merilnika in detektorja nivoja je v dinamiki obeh sistemov, saj se trajanje skaniranja celotnega območja povečuje z dolžino resonatorja in lahko znaša nekaj 10 s za 2 m dolg resonator.

Zgradba merilnika in detektorja nivoja je izjemno preprosta, kar omogoča relativno preprosto realizacijo ob uporabi srednje zmogljivih mikrokrmilnikov.

Reference:

/1/ H. Georgi, The physics of waves, Prentice Hall, New Jersey, 1993, ch. 7, pp. 155-171

/2/ L.E. Kinsler, A.R.Frey, A.B. Coppens and J.V. Sanders, Fundamentals of acoustics, third ed., John Wiley & Sons, 1982, ch. 9 and 10, pp. 200 - 242 , 154-156

/3/ R.E. Berg and D.G. Stork, The physics of sound, Prentice Hall, New Jersy, 1982, ch.3, pp. 63-88

/4/ B.Blitzer and U.Lamotte, Ultrasonic sensors for an energy-saving system, Sensors and Actuators A, 32(1992), pp. 545-549

/5/ S. Ros, J.M. Martin Abreu, T. Freire and L. Calderon, Digital techniques improve range measurement with ultrasound sensor, Sensors and Actuators A, 32(1992), pp. 550-555

/6/ W. Burda and W.-J.Becker, Ultraschall-Resonanz-Messgerat fuer die Fluid-Prozessmesstechnik, Technisches Messen, 60(1993), pp.375-382

/7/ C. E. Stapleton and J.T. Numata, Ultrasonic liquid measuring device for use in storage tanks containing liquids having a non-uniform vapor density, US patent 5,085,077 (1992)

/8/ E.M. Gregory and T.B. Williams, Sonic tank monitoring system, US patent 5,095,748 (1992)

/9/ J.S. Haynes, Tank sonic gauging system and methods, US patent 4,805,453 (1989)

/10/ K.S. Bates and D.B. Chang, Low frequency acoustic fuel sensor, US patent 5,251,482 (1993)

/11/ D.Đonlagic, M.Zavrsnik, D.Đonlagic, Low frequency acoustics resonance level detector with neural network classification, Sensors and Actuators A, 55 (1996), PP 99-106

mag. Denis Đonlagić, dipl.ing.el.
Fakulteta za elektrotehniko, računalništvo in informatiko,
Smetanova 17, 2000 Maribor
Tel.: 062 221 112
Fax: 062 225 013
El. pošta: ddonlagic@uni-mb.si

mag. Miha Završnik, dipl.ing.el.
Fakulteta za elektrotehniko, računalništvo in informatiko,
Smetanova 17, 2000 Maribor
Tel.: 062 221 112
Fax: 062 225 013
El. pošta: miha.zavrsnik@uni-mb.si

prof. dr. Dali Đonlagić, dip.ing.el.
Fakulteta za elektrotehniko, računalništvo in informatiko,
Smetanova 17, 2000 Maribor
Tel.: 062 221 112
Fax: 062 225 013
El. pošta: donlagic@uni-mb.si

Prispelo (Arrived): 12.3.2997 *Sprejeto (Accepted): 6.5.1997*

KONDENZACIJSKI VLAGOMER Z OPTIČNIMI VLAKNI

A. Babnik, A. Kobe, I. Bajsić, J. Možina
Fakulteta za strojništvo, Univerza v Ljubljani, Slovenija

Ključne besede: vlagomeri kondenzacijski z vlakni optičnimi, vlaga zraka, merjenje vlage, kondenzacija vlage, pogoji kondenzacije, vlakna optična, senzorji reflektivni, vlaga relativna, temperatura rosišča

Povzetek: Kondenzacijski ali rosiščni vlagomer je med najbolj točnimi merilniki vlažnosti zraka. Merjenje temelji na zaznavanju kondenzata na hlajeni kovinski površini in preračunu temperature rosišča vlažnega zraka v relativno oziroma absolutno vlažnost zraka. V obravnavanem prototipnem vlagomeru so elementi klasične optike nadomeščeni z novo postavitvijo odbojnostnega zaznavala z optičnimi vlakni. Eksperimentalno so preverjeni nekateri dejavniki, ki vplivajo na proces kondenzacije in s tem tudi na točnost vlagomera.

Fiber-optic Condensation Hygrometer

Key words: fiber-optic condensation hygrometers, air humidity, humidity measurement, humidity condensation, condensation conditions, optical fibers, reflective sensors, relative humidity, absolute humidity, dewpoint temperature

Abstract: The condensation dewpoint hygrometer is a very accurate instrument for measuring air humidity. Its working principle is based on the optical detection of dew forming on a chilled mirror and computing absolute or relative humidity from the temperature of the mirror at the optical treshold and the temperature of the surrounding air.

The optical detection system most commonly used consists of a laser source and a photodetector, built into a measuring chamber. This design enables the detection of light reflected from the chilled mirror. The most accurate instruments also detect scattered light. The use of optical fibres enables light source and photodetector to be placed outside the measuring chamber. In such optical configuration, the fibres are oriented to the mirror surface normal to detect reflected light.

The dewpoint hygrometer uses a temperature control system to actively chill the mirror. The protocol of setting the mirror temperature depends on the character of the measurement. Continuos mode hygrometer is sensitive to changes in thickness of the water layer on the mirror due to changes in humidity of the environment by adjusting the mirror temperature to maintain a constant water layer. Due to continous presence of water on the mirror surface, frequent cleaning is required. On the other hand, discrete mode hygrometers cool the mirror until dew is formed on it. This dew point temperature is measured and the mirror is heated back to the temperature of environment. Repeating the cycle enables changes in the humidity to be followed. Since dew is present on the mirror for only a short period of time in each cycle, frequent cleaning is no longer necessary.

A condensation dewpoint hygrometer using fibre optics and working in a discrete mode has already been proposed in literature. In this article several improvements of the basic design are proposed and implemented. Original inovations have improved properties of the hygrometer considerably, resulting in a very accurate yet simple instrument.

In preliminary experiments, detection of scattered light was found to be much more accurate in detecting dew formation then reflected light detection. This observation was implemented by placing a reflection-type fibre optic sensor at an angle to the mirror surface. The sensor was built using one transmiting and one receiving glass fiber with core diameters 100 μm and 500 μm, respectively.

Determination of the dewpoint temperature is more accurate using discrete mode, but only when heating and cooling optical detection (dew formation and evaporation) is performed. The dewpoint temperature must be calculated as an average of both temperatures that were measured at treshold condition. Only with such a procedure the inherent hysteresis of condensation and the thermal capacity of the mirror and temperature sensor are removed. Using only the temperature measured at first detection of dew forming, as described in the literature, can lead to unpredictable systematic errors.

Series of measurements were performed to obtain the dependence of the measured quantity on mirror position and orientation, velocity of the incoming air and cycle time. The hygrometer gave best results when the mirror faced downwards. Results with a vertical mirror are comparable, but a mirror facing upwards gave the largest fluctuations. Results were independent of the velocity of forced air over the mirror. Cycle time affects the width of hysteresis, but not the final result, if heating and cooling detection is employed. An emphasis was put on determining the systematic error caused by changing surface parameters of the metal mirror. This error depends on the surface roughness and varies for different surface compositions. The best repeatability with smallest systematic error was achieved using a polished surface with a thin anti-corrosion layer.

1. UVOD

Merjenje vlažnosti zraka je relativno neraziskano področje merilne tehnike, kar se kaže na uporabi starih in preverjenih načel delovanja merilnikov, ki so se ohranila iz preteklosti /1,2,3,4/. Novo smer je odprla šele uporaba elektronskih sestavnih elementov, ki omogočajo miniaturizacijo zaznavala in celotnega merilnika. Točnost določanja relativne vlažnosti večine takih merilnikov ne presega vrednosti od 1 do 2 % RH /5/. Izstopa kondenzacijski vlagomer, katerega točnost je za skoraj razred točnosti boljša /6/. Njegovo delovanje temelji na optičnem zaznavanju nastanka kondenzata na hlajeni kovinski površini. V ta namen sta v merilno sondo vgrajena polprevodniški laserski izvor in optični sprejemnik. Uporaba optičnih vlaken omogoča name-stitev obeh optičnih elementov izven merilne sonde /7,8,9/. V prispevku opisujemo nekatere izsledke razvoja kondenzacijskega vlagomera nove generacije, pri katerem smo kot detekcijski element uporabili izvirno postavitev odbojnostnega zaznavala z optičnimi vlakni, in katerega delovanje je nadzorovano z novim načelom krmiljenja /10/.

2. FIZIKALNE OSNOVE

Vlažen zrak je mešanica suhega zraka in vode. Slednja se v področju nenasičenosti nahaja v obliki vodne pare. Vsebnost pare se z zniževanjem temperature ne bo spreminjala do trenutka, ko so doseženi pogoji nasičenosti (delni tlak vodne pare doseže temperaturno odvisen tlak nasičenosti), nakar se bo pričela izločati iz zmesi v tekoči ali trdni obliki, odvisno od temperature zraka. Pojav je možno zaznati optično, kar je osnovno načelo delovanja vsakega kondenzacijskega in rosiščnega vlagomera.

Vsebnost vlage definiramo z razmerjem delnih tlakov sestavnih plinskih komponent v zraku. Absolutna vlažnost x je sicer razmerje mase vode in suhega zraka, v primeru opisa stanj v nenasičenem področju pa jo lahko izrazimo z razmerjem delnih tlakov vodne pare p_p in suhega zraka p_{sz} ter celotnega tlaka vlažnega zraka p:

$$x_p = 0{,}622\frac{p_p}{p_{sz}} = 0{,}622\frac{p_p}{p - p_p} \qquad (1)$$

Z relativno vlažnostjo φ opisujemo le stanja v nenasičenem področju in je razmerje dejanskega delnega tlaka pare p_p in nasičenega parnega tlaka p_s pri isti temperaturi:

$$\varphi = \frac{p_p(T)}{p_s(T)} = \frac{p_s(T_R)}{p_s(T)} \qquad (2)$$

Ker se vsebnost pare z zniževanjem temperature v področju nenasičenosti ne spreminja, lahko v gornji enačbi delni tlak pare nadomestimo z nasičenim parnim tlakom pri mejni temperaturi, ki jo imenujemo temperatura rosišča T_R. Ta temperatura je temeljni izmerek kondenzacijskega vlagomera, iz katerega lahko ob poznavanju temperature merjenega zraka T določimo relativno (enačba 2), oziroma absolutno vlažnost:

$$x_p = 0{,}622\frac{\varphi p_s}{p - \varphi p_s} \qquad (3)$$

Nasičeni parni tlak se eksponentno povečuje s temperaturo. Razmere na meji faz (gladini) čiste vode in vodne pare analitično opisuje Clausius-Clapey-ronova enačba /12/, ki pa je zaradi temperaturne odvisnosti uparjalne toplote vode le približna. Praktično se uporabljajo eksperimentalno izmerjene in tabelirane vrednosti, ki so točnejše od analitičnih /2,6/. V ostalih primerih se kondenzacijski pogoji spremenijo. Poleg uparjalne toplote je tedaj prisotna še "vezalna" toplota q_e, potrebna za premagovanje vezalne energije med molekulami vodne pare in mejo med fazama /2/. Mejni tlak, pri katerem se v tem primeru prične proces kondenzacije, imenujemo ravnotežni tlak (p_{pg}). Pri enakih ostalih pogojih je manjši od nasičenega parnega tlaka, razmerje med obema pa je odvisno od:

$$\frac{p_{pg}}{p_s}(T) = \exp\left(\frac{-q_e}{R_p T}\right) \qquad (4)$$

Pričetek kondenzacijskega procesa na obravnavani površini se torej prične pri višji temperaturi, kot bi se na vodni gladini. Pojav je izrazit na gladinah solnih raztopin (slika 1), medtem ko je na suhih trdnih površinah opazen le pri izvajanju natančnih meritev. Posledica pojava je sistemski pogrešek izmerka kondenzacijskega vlagomera, v katerem se proces kondenzacije vrši na kovinskem zrcalu.

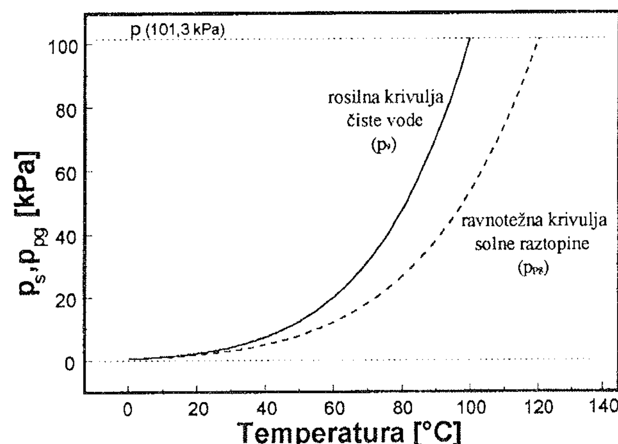

Slika 1: Temperaturna odvisnost nasičenega parnega tlaka nad čisto vodo (p_s) in solno raztopino (p_{pg})

Za veliko večino snovi in tudi za vodo je značilen nezvezen fazni prehod, ki povzroča pregretje tekočine (prenasičenost plinske mešanice) oziroma podhladitev pare /12/. V kolikšni meri bo ta pojav prisoten je odvisno od hitrosti spreminjanja temperature in gostote delcev, ki vzbudijo pričetek faznega prehoda - kali. V primeru kondenzacije na suhi trdni površini prevzemajo vlogo kali delci nečistoč na površini in sama površina snovi, ki ni idealno gladka.

3. RAZVOJ IN IZDELAVA KONDENZACIJSKEGA VLAGOMERA

Kondenzacijski vlagomer je v grobem sestavljen iz štirih podsistemov. Osrednji sestavni del kondenzacijskega vlagomera je hlajena kovinska zrcalna površina v toku merjenega zraka, na kateri se pri temperaturi rosišča vlažnega zraka prične pojavljati kondenzat v tekoči ali trdni fazi. Njena temperatura je nadzorovana z vgrajenim temperaturnim zaznavalom. Za hlajenje zrcala se v novejših merilnikih, zaradi enostavnega krmiljenja moči hlajenja z napajalnim tokom, izključno uporablja termoelektrični hladilni element (Peltier). Pričetek oziroma potek kondenzacije zaznava optični detekcijski sistem na podlagi spremembe intenzitete na kovinskem zrcalu odbite oziroma sipane svetlobe. Sistem je v komercialnih merilnikih izveden z v ohišje merilne komore vgrajenima polprevodniškim laserskim izvorom in optičnim sprejemnikom /5/. Uporaba vlaknaste optike omogoča namestitev obeh elektrooptičnih elementov izven merilne komore /8,9/. Naloga elektronskega krmilnika je nadzor nad merilnim procesom glede na režim delovanja merilnika in preračun izmerjene temperature rosišča v željene veličine, ki definirajo parametre vlažnega zraka. Celotni sistem vlagomera je shematsko prikazan na sliki 2.

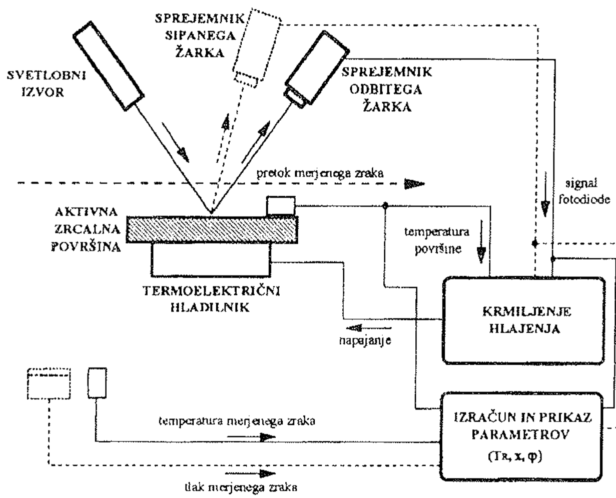

Slika 2: Shematski prikaz običajnega kondenzacijskega vlagomera

Merilnik lahko deluje v dveh režimih:

- zvezni režim delovanja izkorišča približno linearno odvisnost optičnega signala pri oblikovanju kondenzata na zrcalni površini. Krmilnik v tem primeru skrbi za vzdrževanje temperature zrcalne površine na vrednosti, ki bo pri dani vlažnosti merjenega zraka zagotavljala enakomerno debelino plasti kondenzata in s tem enakomerno razliko med merjenim in referenčnim signalom. Sistem torej odgovarja spremembi vlažnosti zraka s spremembo temperature površine (slika 3). V preteklosti se je izključno uporabljalo to načelo delovanja /5,13/. Pomanjkljivosti, kot so stalna prisotnost kondenzata na zrcalni površini, obvezna uporaba optične kompenzacijske metode in odmik izmerjene temperature od dejanske temperature rosišča, so botrovale razvoju merilnika z diskretnim režimom delovanja.
- pri diskretnem režimu delovanja se zrcalna površina enakomerno hladi. Ko je zaznana sprememba optičnega signala, povzročena s pojavom kondenzata, se proces obrne in poteka do trenutka, ko je zaznana sprememba na prvotno vrednost. Pri obeh mejnih trenutkih se odčita temperatura površine, srednja vrednost pa upošteva kot dejanska temperatura rosišča (slika 4). S tem so odpravljene po-

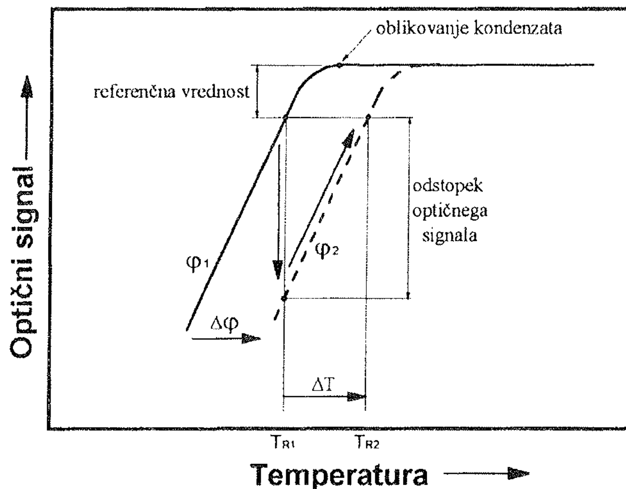

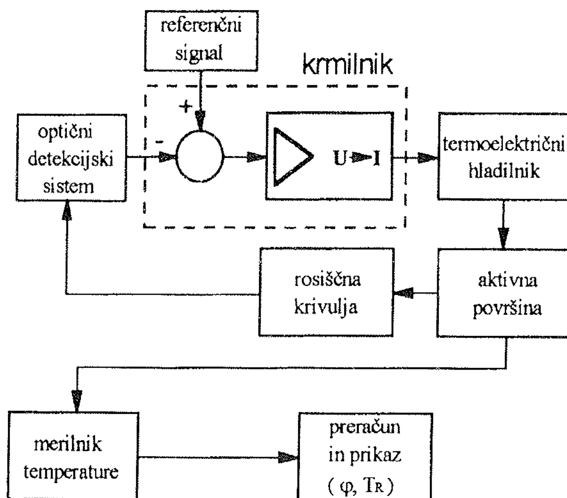

Slika 3: Zvezni režim - načelo delovanja in krmilnik

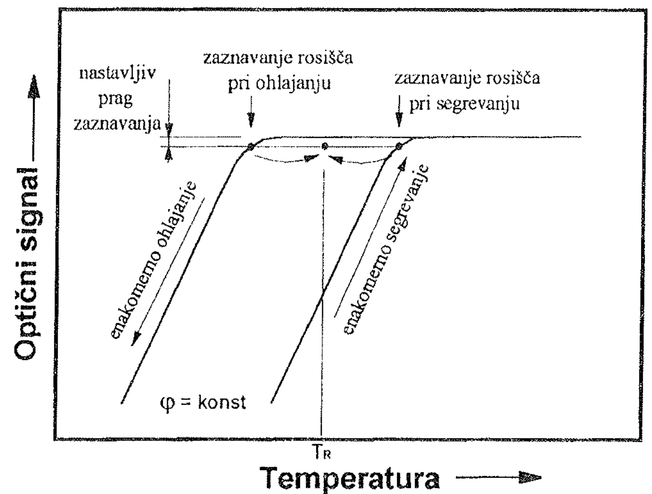

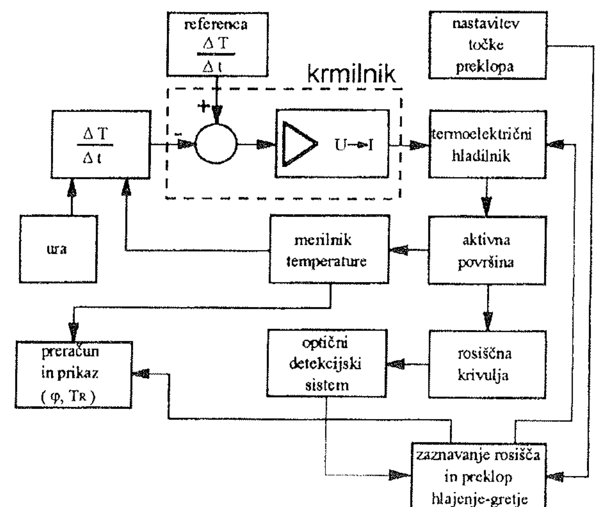

Slika 4: Diskretni režim - načelo delovanja in krmilnik

manjkljivosti zveznega režima na račun kompleksnejše krmilne zanke. Odčitek je namreč rezultat merilnega cikla, ki preide vsa stanja oblikovanja kondenzata od suhe površine do optično zaznavne debeline plasti kondenzata in to v smeri kondenzacije in izhlapevanja. Podoben režim delovanja je v literaturi že omenjen /9/, vendar izkorišča le območje kondenzacije, s čimer ni možno izločiti vpliva prenasičenja in dinamične značilnice temperaturnega zaznavala.

Značilnice kondenzacijskega vlagomera so določene z značilnicami temperaturnega zaznavala in optičnega detekcijskega sistema. Uporaba umerjenega uporovnega oziroma polprevodniškega temperaturnega zaznavala omogoča izmerke s točnostjo pod 0,1 K (0,7 %RH pri normalnih pogojih). Na izbiro vpliva predvsem zmožnost zagotovitve dobrega toplotnega spoja s kovinskim zrcalom in majhne toplotne vztrajnosti zaznavala. Obe zahtevi sta običajno s primernim oblikovanjem že zadovoljivo izpolnjeni. Razvoj optičnega detekcijskega sistema z vlaknasto optiko pa zasluži več pozornosti. Uporaba odbojnostnega zaznavala z optičnimi vlakni, nameščenega pravokotno na zrcalno površino, je v literaturi že omenjena /8,9/. S to postavitvijo se opazuje odbiti svetlobni žarek, kar onemogoča enostavno izvedbo optične kompenzacije za izločitev vplivov nihanja intenzitete izvora, spremembe absorpcije v obtekajočem zraku ter staranja zrcala (nanos nečistoč). Problem je v zadovoljivi meri rešljiv s poševno postavitvijo optičnega zaznavala, ki zaznava sipani žarek (slika 5). Sprememba optičnega signala pri pojavi kondenzata na zrcalu je tedaj bolj izrazita, kot v primeru pravokotne postavitve odbojnostnega zaznavala. S tem se poveča razmerje med koristnim signalom in motnjami, kar omogoča zaznavanje plasti kondenzata v začetni fazi oblikovanja in s tem točno določanje temperature rosišča.

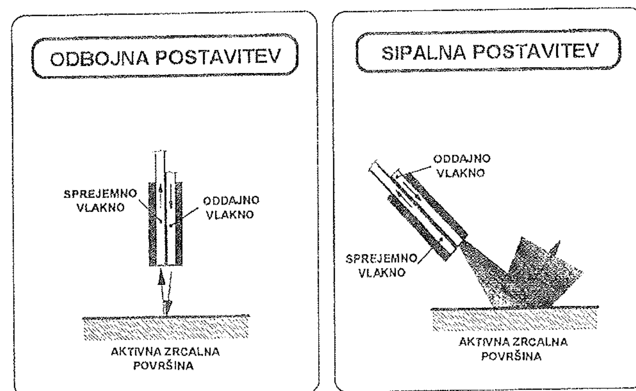

Slika 5: Primerjava pravokotne-odbojne in poševne-sipalne postavitve odbojnostnega zaznavala

Izdelani kondenzacijski vlagomer z optičnimi vlakni prikazuje slika 6. Običajno navzgor obrnjena zrcalna površina /7,8,10,13/ je v izdelku postavljena v nasprotni legi, s čimer se olajša izmenjava mejne zračne plasti ob zrcalu. Poleg tega zagotavlja konstrukcija komore optimalen obtok merjenega vlažnega zraka preko zrcalne površine. Obe konstrukcijski izboljšavi omogočata delovanje tudi pri zelo majhnih obtočnih hitrostih. Za merjenje temperature zrcalne površine je uporabljeno polprevodniško temperaturno zaznavalo z negativnim temperaturnim koeficientom (NTC), katero je v prvotni konstrukciji nameščeno na zrcalno površino, v končni obliki izdelka pa vgrajeno v samo osnovo zrcalne površine. Za oddajno vlakno odbojnostnega senzorja je bilo uporabljeno stekleno vlakno premera jedra 100 μm, sprejemno vlakno pa je bilo stekleno premera jedra 500 μm. Slika 7 prikazuje časovni potek temperature zrcalne površine in temperaturno odvisnost optičnega signala v enem merilnem ciklu zveznega režima delovanja. Slednji signal je identičen teoretičnemu s slike 4 z upoštevanjem sipalne postavitve optičnega sprejemnika.

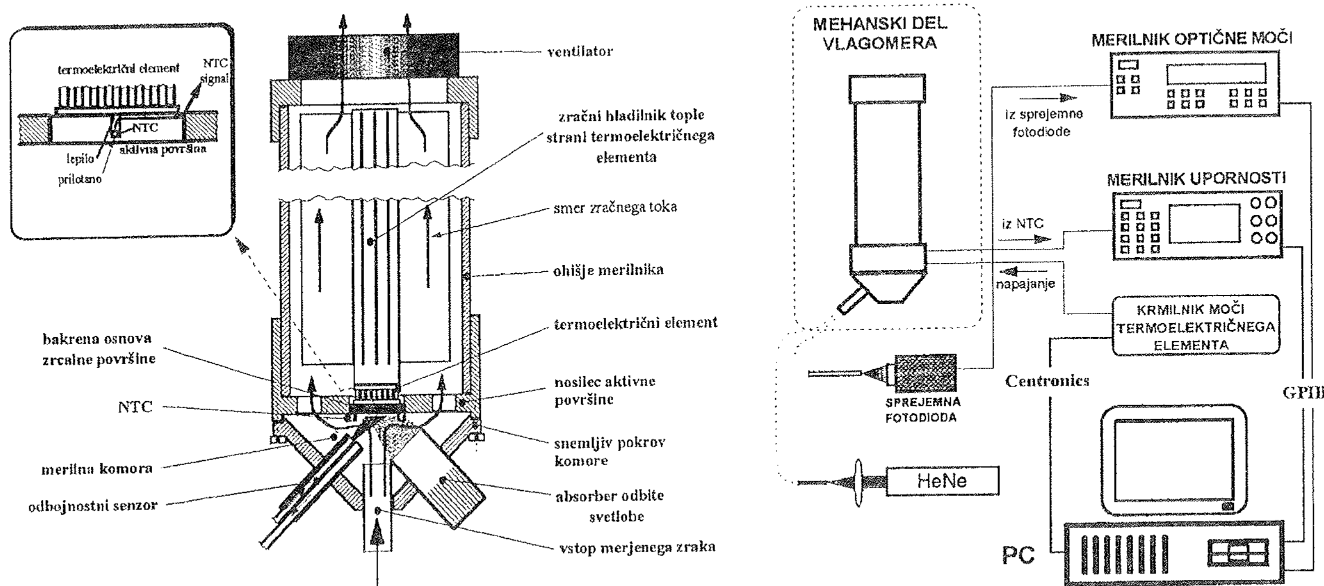

Slika 6: Prikaz izvedbe mehanskega dela in shema postavitve izdelanega kondenzacijskega vlagomera

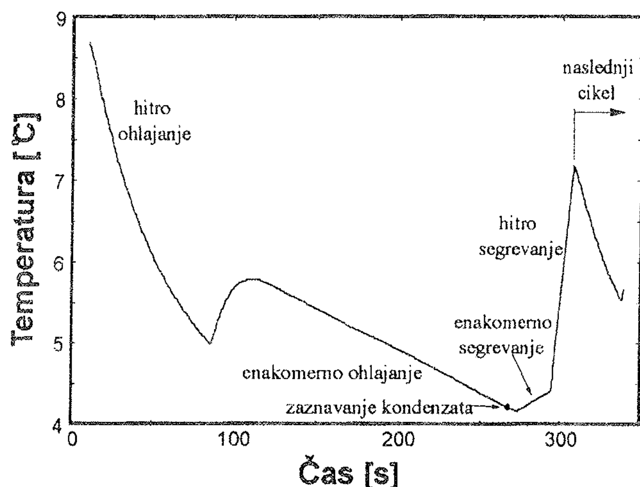

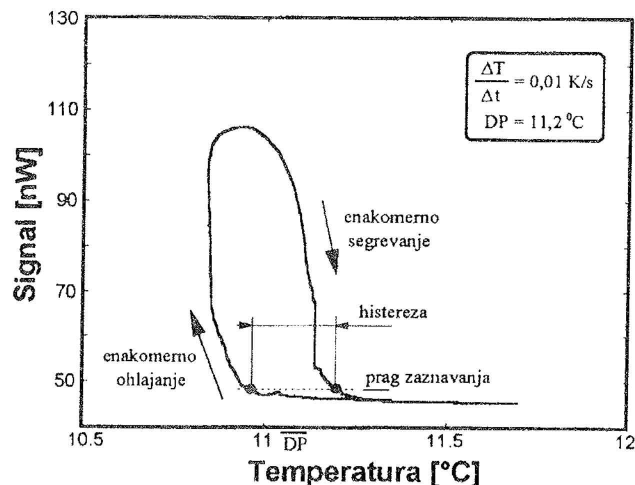

Slika 7: Časovni potek temperature zrcalne površine in temperaturna odvisnost optičnega signala v enem merilnem ciklu izdelanega vlagomera.

4. MERITVE ZNAČILNIC VLAGOMERA

Z izvedenimi preizkusi smo določili značilnice izdelanega vlagomera, kot tudi raziskali vpliv nekaterih dejavnikov na delovanje merilnika. Meritve so bile izvedene v zaprtem in glede poteka vlage kontroliranem prostoru s primerjavo odčitkov izdelanega in izbranega primerjalnega ali referenčnega merilnika.

Z uvodnimi preizkusi je bilo ugotovljeno, da odčitki kondenzacijskega vlagomera sledijo odčitkom referenčnega merilnika s sistemskim merilnim pogreškom (+3 ±0,5 % RH pri normalnih pogojih). Vzrok za nastalo sistemsko razliko smo prvotno iskali v postavitvi temperaturnega zaznavala, legi zrcalne površine, hitro-sti obtekanja merjenega zraka in hitrosti spreminjanja temperature zrcalne površine. Rezultati preizkusov, katerih namen je bil lociranje vzroka odstopka, so z navedbo odstopka relativne vlažnosti ΔRH in širine histereze optičnega signala podani v preglednicah 1 do 3. Navedene so povprečne vrednosti 10-ih ponovljenih meritev pri nespremenjenih zunanjih pogojih (referenčni merilnik: ROTRONIC MP 100A&C94 z deklarirano merilno točnostjo ± 1 % RH).

Preglednica 1: Vpliv lege zrcalne površine in dodatne toplot-ne izolacije temperaturnega zaznavala

lega	dodatna izolacija		brez dodatne izolacije	
	ΔRH [%RH]	histereza [K]	ΔRH [%RH]	histereza [K]
↑	4,5	±0,16	4,9	±0,16
→|	4,4	±0,24	4,8	±0,25
↓	5,7	±0,35	6,1	±0,35

Preglednica 2: Vpliv hitrosti obtekajočega zraka

hitrost obtekanja	konvekcija	0,2 m/s	0,8 m/s
ΔRH [%RH]	3,8	4,0	3,6
histereza [K]	0,24	0,16	0,15

Preglednica 3: Vpliv hitrosti spreminjanja temperature zrcalne površine

ΔT/Δt	0,01 K/s	0,03 K/s	0,06 K/s
ΔRH [%RH]	3,5	4,5	5
histereza [K]	0,11	0,27	0,41

Ker je vpliv dodatne toplotne izolacije temperaturnega zaznavala opazen, je treba tega vgraditi v samo osnovo zrcalne površine. S tem je preprečeno njegovo segrevanje zaradi obtekajočega zraka, ki je bistveno toplejši od zrcalne površine. Vpliv lege površine je očiten le pri navzgor obrnjeni površini, saj tanka plast ohlajenega zraka nad njo, ki je prisotna kljub prisilnem obtoku, deluje kot toplotni izolator. Pri ostalih dveh legah je izmenjevanje te plasti olajšano s konvekcijo. Hitrost obtekanja zraka na merilni pogrešek bistveno ne vpliva, medtem ko je vpliv hitrosti spremembe temperature opazen. Pojav je možno pojasniti s počasnim procesom kondenzacije in izrazitejšim vplivom dinamičnih značilnosti same zrcalne površine in temperaturnega zaznavala. Bistveni vzrok merilnega pogreška pa je očitno treba iskati v pomiku ravnotežne kondenzacijske krivulje (slika 1). Rezultat preverjanja vpliva hrapavosti in snovi zrcalne površine je prikazan na slikah 8 in 9

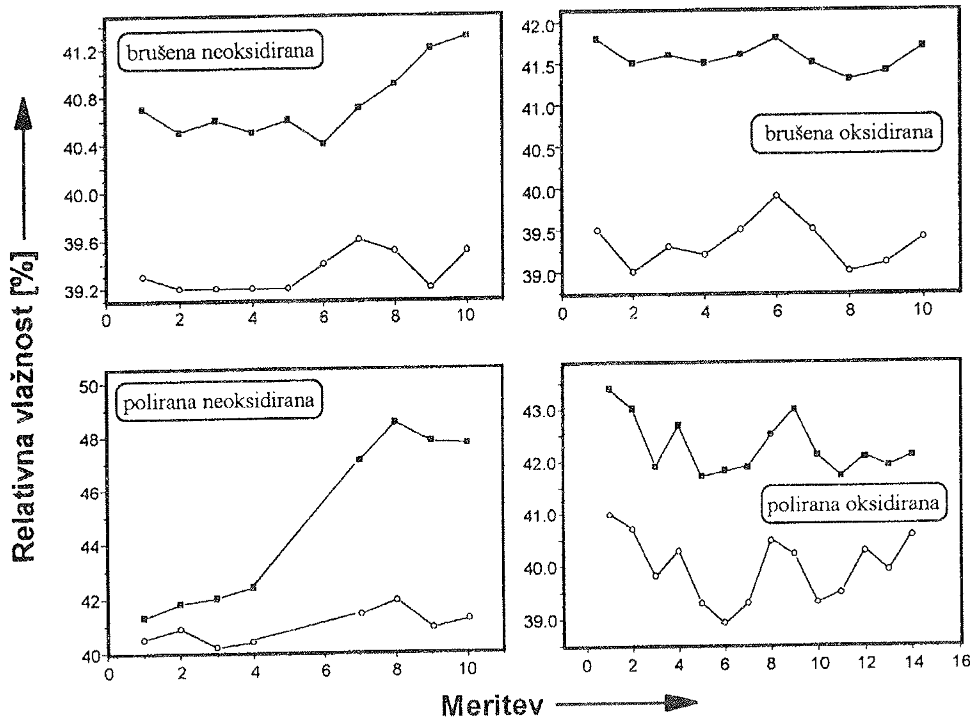

Slika 8: *Primerjava izmerkov električnega psihrometra (○) in kondenzacijskega vlagomera (■) z različnimi zrcalnimi površinami (baker; brušeno Ra =2 µm, polirano Ra < 0,6 µm)*

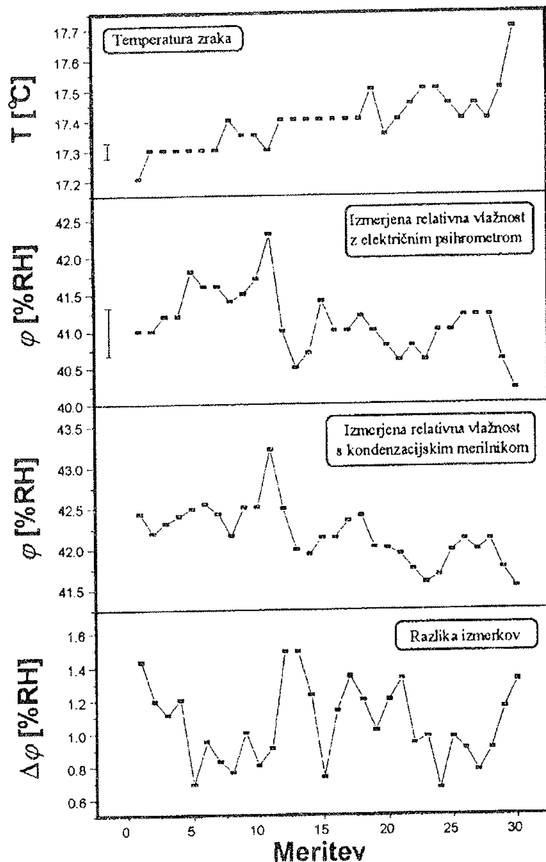

Slika 9: *Primerjava izmerkov električnega psihrometra in kondenzacijskega vlagomera s polirano zrcalno površino, prevlečeno s protikorozijskim slojem*

(referenčni merilnik: električni psihrometer Ahlborn Therm 2286-2). V vseh primerih je osnova zrcalne površine bakrena, medtem ko je sama površina brez oksidirane plasti (neposredno po obdelavi), s plastjo oksida, oziroma neposredno po obdelavi prevlečena s protikorozijskim neomočljivim slojem (ločilna pasta za poliestrske kalupe). Meritve so bile izvedene pri enakomernih ter nespremenjenih zunanjih pogojih.

Zaključimo lahko, da na pomik rosiščne krivulje (specifično vezalno energijo) bistveno vpliva oksidacija površine. Vpliv je bolj izrazit na polirani površini. Z nanosom protikorozijskega sloja preprečimo oksidacijo

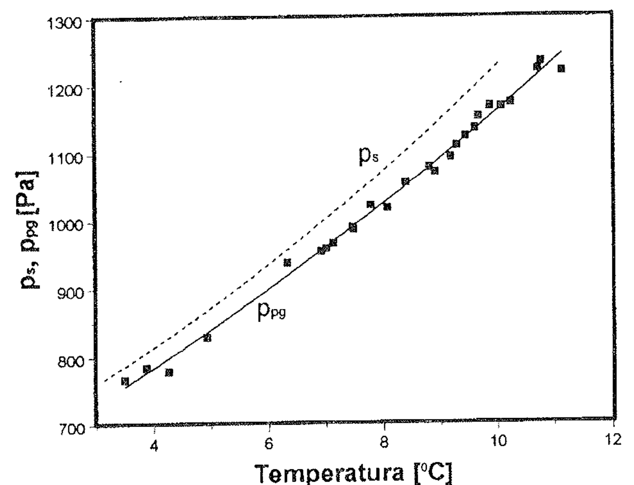

Slika 10: *Eksperimentalna ravnotežna krivulja (p_{Pg}) za polirano bakreno površino s protikorozijskim slojem v primerjavi z rosiščno krivuljo čiste vode (p_S)*

in zagotovimo časovno nespremenljive pogoje kondenzacije, kar se odrazi s časovno enakomernimi odstopki izmerkov pri enakomerni vlažnosti merjenega zraka.

Odstopek izmerka pri isti vezalni energiji je teoretično odvisen le od rosiščne temperature (enačba 4). Trditev smo preverili z izvedbo serije meritev pri spreminjajoči se vlažnosti merjenega zraka. Pomik ravnotežne krivulje za obravnavano zrcalno površino je prikazan na sliki 10.

5. SKLEPI

V prispevku je prikazan del razvoja prototipnega kondenzacijskega vlagomera z optičnim sistemom za detekcijo sipanega žarka, ki je izveden z odbojnostnim zaznavalom z optičnimi vlakni. Merilnik deluje v diskretnem režimu - upošteva temperaturi rosišča vlažnega zraka v obeh smereh faznega prehoda. Prikazani so eksperimentalno ovrednoteni vplivi lege zrcalne površine, hitrosti obtoka zraka, hitrosti spreminjanja temperature zrcala in snovi ter hrapavosti površine zrcala na merjeno vrednost rosiščne temperature. Metrološke značilnice obravnavanega kondenzacijskega vlagomera z upoštevanjem pomika ravnotežne krivulje presegajo značilnice uporabljenih referenčnih vlagomerov, zato navajamo naslednje ocene merilnotehničnih parametrov:

- ponovljivost vlagomera je manjša kot 0,35 %RH,
- relativni merilni pogrešek je manjši kot ±1 %RH,
- histereza določitve temperature rosišča je pri diskretnem režimu delovanja zanemarljiva,
- čas merilnega cikla znaša od 3 do 5 min odvisno od vlažnosti in temperature zraka ter izbrane hitrosti spreminjanja temperature zcalne površine.

6. LITERATURA

/1/ D. Stanković: Fizičko-tehnička merenja, Naučna knjiga, Beograd, (1987)

/2/ D. Voronjec, Đ. Kozić: Vlažan vazduh, Smeits, Beograd, (1980)

/3/ K. Carr - Brion: Moisture Sensors in Process Control, Elsevier Applied Science Publishers Ltd., London, (1986)

/4/ J. Perovnik, I. Bajsić: Pregled metod merjenja vlažnosti zraka, Strojniški Vestnik, Vol. 39, No. 3-4, 99, (1993)

/5/ Advanced Industrial Hygrometry and Process Instrumentation, katalog firme MICHELL Instruments

/6/ A Guide to the Measurements of Humidity, National Physical Laboratory, The institute of Measurement and Control, London, (1996)

/7/ V. J. Kardos, G. J. Sonek: A dewpoint temperature sensor based on Nd^{3+} doped fiber fluorescence, IEEE Photonics Tech. Lett., Vol. 7, No. 10, 1198, (1995)

/8/ S. Matsumoto, S. Toyooka: Laser dew-point hygrometer, Jpn. J. Appl. Phys., Vol. 34, 316, (1995)

/9/ F. Dadachanji: Humidity measurement at elevated temperatures, Measurement & Control, Vol. 25, 48, (1992)

/10/ A. Babnik: Nove vrste odbojnostnih senzorjev z optičnimi vlakni, disertacija, Fakulteta za strojništvo, Ljubljana, (1997)

/11/ D. A. Krohn: Intensity modulated fiber optic sensors: overview, Fiber Optic Sensors IV, SPIE 718, Massachusetts, 2, (1986)

/12/ M. Oprešnik:Termodinamika zmesi, Fakulteta za strojništvo, Ljubljana, (1988)

/13/ R. F. Pragnell: The modern condensation dewpoint hygrometer, Measurement and Control, Vol. 22, 74, (1989)

dr. Aleš Babnik, dipl. ing. str.
Andrej Kobe, dipl. ing. fiz.
doc. dr. Ivan Bajsić, dipl. ing. str.
prof. dr. Janez Možina, dipl. ing. fiz.

UNIVERZA V LJUBLJANI
Fakulteta za strojništvo,
Aškerčeva 6
1000 LJUBLJANA

Prispelo (Arrived): 16.6.1997 ***Sprejeto (Accepted): 23.6.1997***

CHARACTERISATION OF Al_2O_3 AND SrO MODIFIED $LaMnO_3$ FOR SOFC CATHODE MATERIAL

Danjela Kuščer, Janez Holc, Marko Hrovat, Slavko Bernik, Drago Kolar
Jožef Stefan Institute, Ljubljana, Slovenia

Keywords: SOFC, Solid Oxide Fuel Cells, high temperature SOFC, high temperature fuel cells with solid oxide electrolyte, lanthanum manganites, doping, microstructures, electrical resistivity, cathode materials, anode materials, solid electrolytes, YSZ, Yttrium Stabilized cubic Zirconium, environmental friendly, power generation, semiconducting perovskites, TEC, Thermal Expansion Coefficients, XRD analysis, X-Ray Diffraction analysis, EDS microanalysis, Energy Disperse x-ray System microanalysis

Abstract: The perovskites with nominal compositions $La(Mn_{1-x}Al_x)O_3$, strontium doped $(La_{0.8}Sr_{0.2})(Mn_{1-x}Al_x)O_3$ (for x between 0 and 0.94), and substoichiometric $(La_{0.8}Sr_{0.2})_{0.95}(Mn_{0.7}Al_{0.3})O_3$ were evaluated as possible solid oxide fuel cell (SOFC) cathodes. Cell parameters of solid solutions were calculated. The electrical and microstructural characteristics and high temperature interactions with yttria stabilised zirconia (YSZ) were studied. As compared with "pure" perovskites, doping with strontium and aluminum decreases and increases their specific resistivity, respectively. The incorporation of alumina substantially reduces the sinterability resulting in a rather porous, fine grained microstructure. The partial exchange of lanthanum with strontium and manganese with aluminum oxide significantly depress the reaction rate between perovskites and YSZ.

Karakterizacija $LaMnO_3$, modificiranega z Al_2O_3 in SrO, za katodni material za SOFC

Ključne besede: SOFC celice gorivne z elektroliti oksidnimi trdnimi, SOFC celice gorivne z elektroliti oksidnimi trdnimi visootemperaturne, manganiti lantanovi, dopiranje, mikrostrukture, upornost električna, materiali katodni, materiali anodni, elektroliti trdni, YSZ cirkonij kubični stabiliziran z itrijem, okolno prijazno, proizvodnja energije, perovskiti polprevodni, TEC koeficienti razteznosti termičnih, XRD analiza z uklonom Rentgen žarkov, EDS mikroanaliza z energijsko razpršenimi Rentgen žarki

Povzetek: Kot možne materiale za visokotemperaturne gorivne celice s trdnim elektrolitom (SOFC) smo sintetizirali in karakterizirali perovskite z nominalnimi sestavami $La(Mn_{1-x}Al_x)O_3$, s stroncijem dopirane $(La_{0.8}Sr_{0.2})(Mn_{1-x}Al_x)O_3$ (x med 0 in 0.94), in podstehiometričnega $(La_{0.8}Sr_{0.2})_{0.95}(Mn_{0.7}Al_{0.3})O_3$. Izračunali smo dimenzije osnovnih celic trdnih raztopin. Študirali smo električne in mikrostrukturne karakteristike ter visokotemperaturne interakcije s trdnim elektrolitom. Zamenjava dela mangana z aluminijem poveča specifične upornosti, medtem ko zamenjava dela lantana s stroncijem upornosti zmanjša. Obe vrsti dopiranja zelo zmanjšata reaktivnost med testiranimi perovskiti in trdnim elektrolitom.

INTRODUCTION

A fuel cell is a device for direct conversion of chemical energy into electrical energy. Basicaly it consists of cathode, anode and electrolyte. Oxidant is fed to the cathode and reducent (fuel) to the anode. The electrolyte, through which the ion current flows, prevents the mixing of oxidant and fuel. The concept is nearly 160 years old. The principle of fuel cell operation was reported in 1839 by Sir William Grove /1/. His fuel cell used dilute acid as an electrolyte and oxygen and hydrogen as oxidant and reducent, respectively.

High temperature fuel cells with a solid oxide electrolyte (SOFC) work at temperatures around 1000°C. Due to the high operating temperatures the choice of materials is limited mainly to ceramics. The solid electrolyte in SOFC cells is usually yttria stabilised cubic zirconia (YSZ). Cathodes are semiconducting perovskites and anodes are based on the mixture of metallic Ni and YSZ. An extensive and comprehensive review of materials for SOFC is presented in references /2,3/.

The oxygen accepts electrons at the cathode and moves as an ion through the dense ZrO_2 ceramic. At the anode ions combine with fuel and release electrons. The "force" driving oxygen ions through the electrolyte is the concentration gradient of oxygen between the cathode and the anode side. The fuel is hydrogen, a H_2/CO mixture, or hydrocarbons because the high operating temperature enables the internal (in situ) reforming of hydrocarbons with water vapour /4-6/. For the typical "working" conditions of an SOFC the open circuit voltage is around 1 V.

The advantage of high temperature solid oxide fuel cells for production of electrical energy is their high efficiency of 50-60%, while some estimates are even up to a yield of 70-80%. Also, nitrous oxides are not produced and the amount of CO_2 released per kWh, due to the high efficiency, is around 50 percent less than for power sources based on combustion, making SOFC "environmental friendly" power generation /7-11/.

The schematic diagram of the solid oxide fuel cell is shown in Fig. 1. Oxidant (air) is fed to the cathode and reductant (fuel) to the anode. The electrode reactions (for hydrogen as fuel) are:

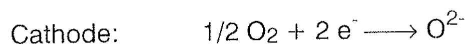

Cathode: $1/2\ O_2 + 2e^- \longrightarrow O^{2-}$

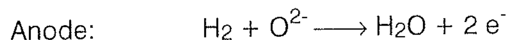

Anode: $H_2 + O^{2-} \longrightarrow H_2O + 2e^-$

The crossections of two basic constructions of SOFC, tubular and planar, are shown schematically in Figs. 2 and 3, respectively. Fuel cell elements - anode/solid

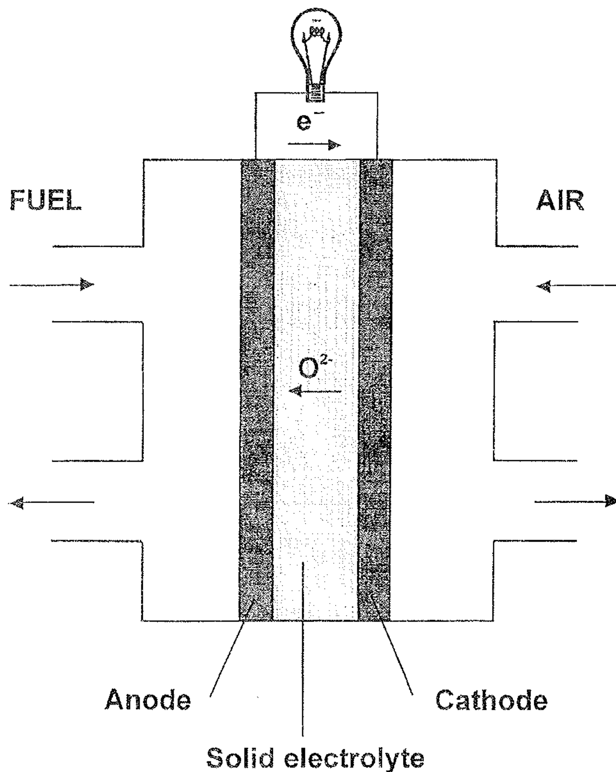

Fig. 1. Schematic diagram of the solid oxide fuel cell (SOFC). Air is fed to the cathode and fuel to the anode. The electrolyte, through which the ion current is flowing, also prevents the mixing of oxidant and fuel.

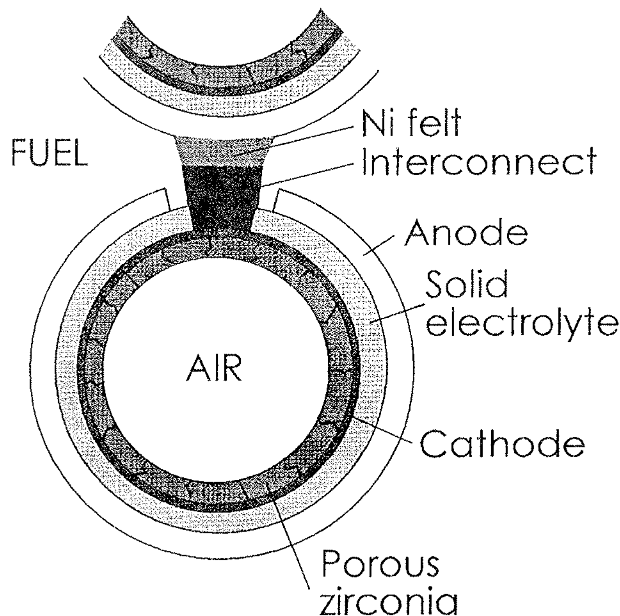

Fig. 2: Crossection of the tubular design of a SOFC (schematically). The porous cathode and its coating of dense solid electrolyte are deposited on the porous ZrO_2 based carrier tube. Electrical contact with the anode of the next cell is obtained with nickel felt. Air flows through carrier tube and the fuel flows between the tubes.

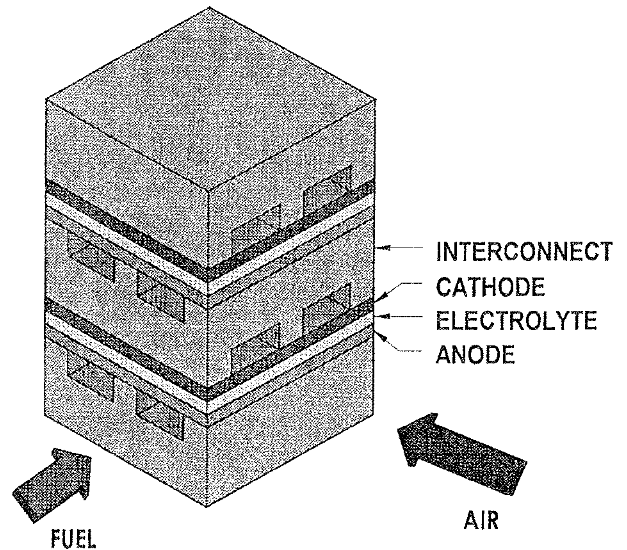

Fig. 3: Crossection of the planar design of a SOFC (schematically). The air and the fuel flow through channels in the interconnect.

electrolyte/cathode "sandwiches" are serially connected with an interconnect. Electrical charge flows as electrons through the interconnect and as oxygen ions through the solid electrolyte. In the case of tubular design air flows inside tubes over the cathode and fuel on the outside over anode while in the case of planar design air and fuel are flowing through the channels in the interconnect.

Cathode (air electrode) materials, which must withstand high operating temperatures and an oxidizing atmosphere, are at present based mostly on $LaMnO_3$ perovskites, doped with alkaline earth oxides, mainly SrO, to decrease specific resistivity. The thermal expansion coefficients (TEC) of $LaMnO_3$ is close enough to that of YSZ (11.2×10^{-6}/K and 10.5×10^{-6}/K, respectively), to prevent cracking or delamination of SOFC components either during high temperature operation or heating / cooling cycles /2,12,13/. Also, SOFC cathode materials must be porous to allow the diffusion of oxygen from the air to the solid electrolyte.

It is known that lanthanum perovskites, with the possible exception of $LaCrO_3$ /14/, react during high temperature ageing with zirconia from YSZ solid electrolyte, forming $La_2Zr_2O_7$ pyrochlore /15-19/. The specific electrical resistivity of $La_2Zr_2O_7$ is three to four orders of magnitude higher than that of $LaMnO_3$ (reported to be 1.5×10^3 ohm.cm /17/, or even 25×10^3 ohm.cm /20/ at 1000°C), which increases the cell losses and therefore decrease its yield due to increased internal resistivity.

In this paper an evaluation of the electrical and microstructural characteristics of $La(Mn_{1-x}Al_x)O_3$ and strontium doped $(La_{0.8}Sr_{0.2})(Mn_{1-x}Al_x)O_3$ (for x between 0 and 0.94) based materials as possible SOFC cathode materials is described. A range of solid solutions exists between $LaMnO_3$ and $LaAlO_3$ which enables some "tailoring" of material characteristics /21/. Although the

alumina-rich perovskites, i.e. x=0.94, are not interesting for SOFC cathodes due to their high specific resistivities, they are included to cover the entire Al_2O_3 concentration range. The literature data show that substoichiometry on "A" sites suppresses the reactivity with YSZ (see, for example, /18/) therefore some results on substoichiometric $(La_{0.8}Sr_{0.2})_{0.95}(Mn_{0.7}Al_{0.3})O_3$ will be also presented.

EXPERIMENTAL

For experimental work, $La(OH)_3$ (Ventron, 99.9%), $SrCO_3$ (Ventron, 99.9%), MnO_2 (Ventron, 99.9%), and Al_2O_3 (Alcoa, A-16, +99%) were used. The compositions of the samples were $La(Mn_{1-x}Al_x)O_3$ and $(La_{0.8}Sr_{0.2})_{0.95}(Mn_{1-x}Al_x)O_3$ (for "x" between 0 and 0.94) and $(La_{0.8}Sr_{0.2})_{0.95}(Mn_{0.7}Al_{0.3})O_3$. The samples were mixed in isopropyl alcohol, pressed into pellets, calcined at 1000°C and fired for 50 hours with intermediate grinding at 1200°C for $La(Mn_{1-x}Al_x)O_3$ and at 1300°C for strontium doped perovskites. During firing pellets were placed on platinum foils. To study the possible interactions at elevated temperatures, perovskites and YSZ powders were mixed in 1:1 molar ratio, pressed into pellets and fired at 1400°C for 300 hours. Samples were placed on platinum foils in alumina crucibles. The results were evaluated by XRD (X-ray powder diffraction analysis), SEM (scanning electron microscopy) and EDS (Energy Dispersive X-ray Microanalysis).

A JEOL JXA-840 scanning electron microscope equipped with a Tracor-Northern energy dispersive system (EDS) was used for overall microstructural and compositional analysis. Samples prepared for SEM were mounted in epoxy in cross-sectional orientation and then polished using standard metallographic techniques. Prior to analysis in the SEM, the samples were coated with carbon to provide electrical conductivity and avoid charging effects. In the case of standardless analysis the Tracor SQ standardless quantitative analysis program using multiple least-squares analysis and ZAF matrix correction procedure was used. Samples were analyzed under the following conditions: acceleration voltage 25 kV; probe current 250 pA; spectra acquisition time 100 s.

The phases in the sintered samples were determined using a Philips X-ray powder diffractometer using CuK_α radiation at a step size of 0.02° in the range $2\theta = 20°$ to 70°.

Electrical d.c. resistance was measured with four point method on sintered pellets with diameter of 6 mm and thickness of 2 mm with a Keithley 196 multimeter and a Keithley 580 Micro-ohmmeter instrument in the temperature range 20 - 925°C in air. Unfritted Pt electrodes were deposited as contacts on both sides of the samples and fired for 30 minutes at 1100 °C.

RESULTS AND DISCUSSION

The microstructures of $La(Mn_{1-x}Al_x)O_3$, $(La_{0.8}Sr_{0.2})(Mn_{1-x}Al_x)O_3$, and $(La_{0.8}Sr_{0.2})_{0.95}(Mn_{0.7}Al_{0.3})O_3$ are in Figs. 4, 5, and 6, respectively. The microstructures are porous and average grain diameters decrease with increasing Al_2O_3 content.

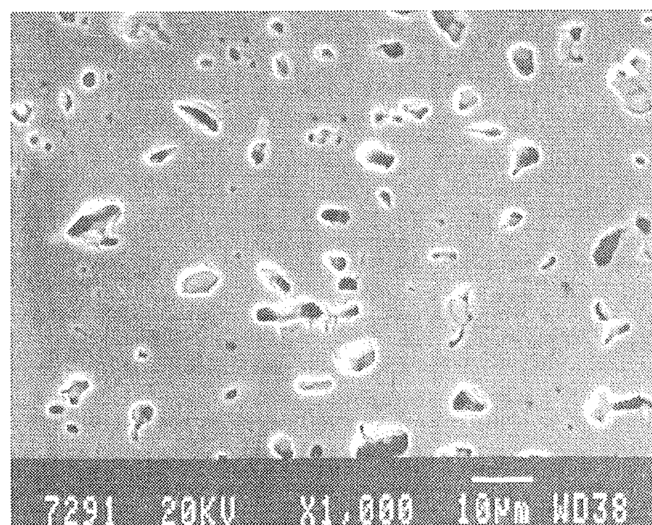

Fig. 4.a: The microstructure of $LaMnO_3$

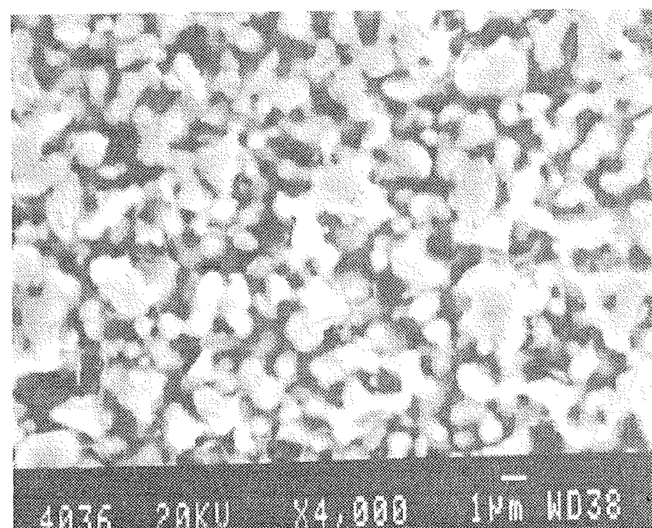

Fig. 4.b: The microstructure of $La(Mn_{0.8}Al_{0.2})O_3$

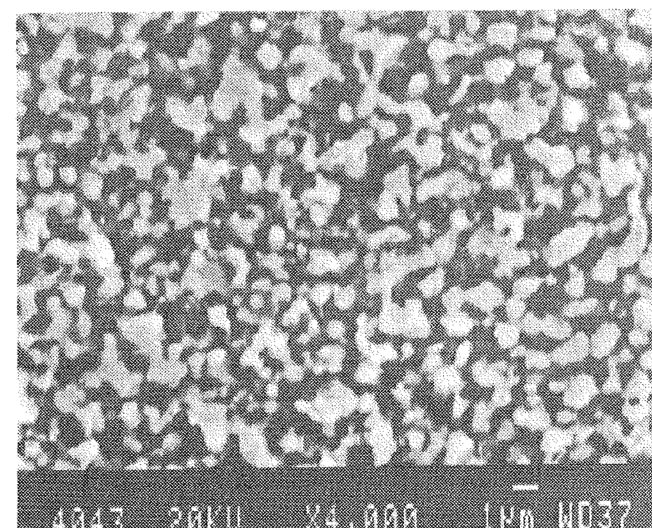

Fig. 4.c: The microstructure of $La(Mn_{0.5}Al_{0.5})O_3$

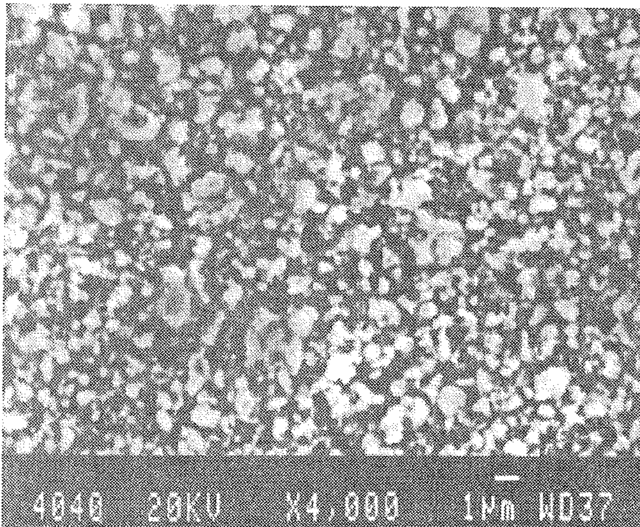

Fig. 4.d: The microstructure of $La(Mn_{0.06}Al_{0.94})O_3$

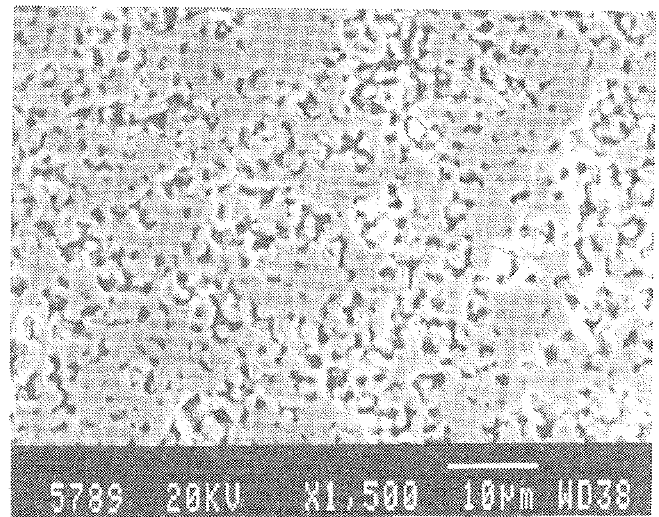

Fig. 5.b: The microstructure of $(La_{0.8}Sr_{0.2})(Mn_{0.7}Al_{0.3})O_3$

The microstructure of $La_{0.8}Sr_{0.2}MnO_3$ is well sintered (Fig. 5.a), but more porous than that of $LaMnO_3$ (Fig. 4.a). Data in the literature indicate that the partial replacement of the lanthanum with the strontium increased the density of sintered materials up to 10% substitution. For higher concentrations the densities of sintered samples decrease /22/. Substoichiometry on "A" sites increases the sintered density (Fig. 5.b - stoichiometric $(La_{0.8}Sr_{0.2})(Mn_{0.7}Al_{0.3})O_3$. and Fig. 6 - substoichiometric $(La_{0.8}Sr_{0.2})_{0.95}(Mn_{0.7}Al_{0.3})O_3$. Dark gray inclusions in Fig. 5.d (alumina rich $(La_{0.8}Sr_{0.2})(Mn_{0.06}Al_{0.94})O_3$ composition) are, according to the results of X-ray analysis and EDS microanalysis, $LaSrAlO_4$ compound.

In Table I and Table II the calculated cell parameters of $La(Mn_{1-x}Al_x)O_3$ and $(La_{0.8}Sr_{0.2})(Mn_{1-x}Al_x)O_3$ solid solutions, respectively, are given. Cell parameters were calculated from uncalibrated X-ray powder diffractometer data using the PARAM program. $LaMnO_3$, $LaAlO_3$ and solid solutions are indexed by a hexagonal cell, only $La_{0.8}Sr_{0.2}MnO_3$ is indexed by monoclinic cell. The

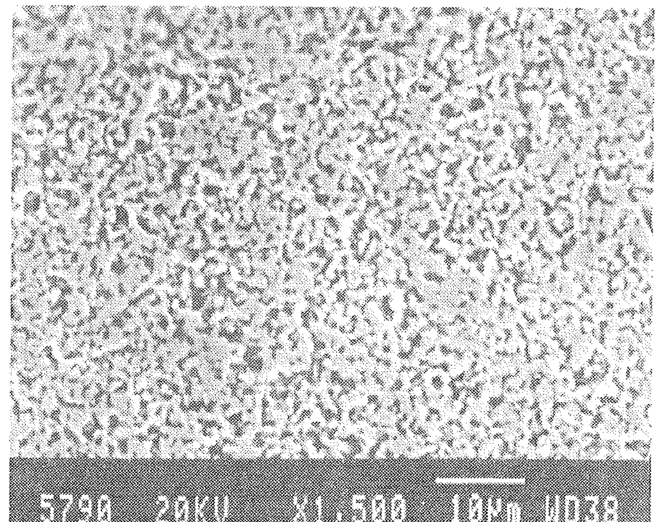

Fig. 5.c: The microstructure of $(La_{0.8}Sr_{0.2})(Mn_{0.5}Al_{0.5})O_3$

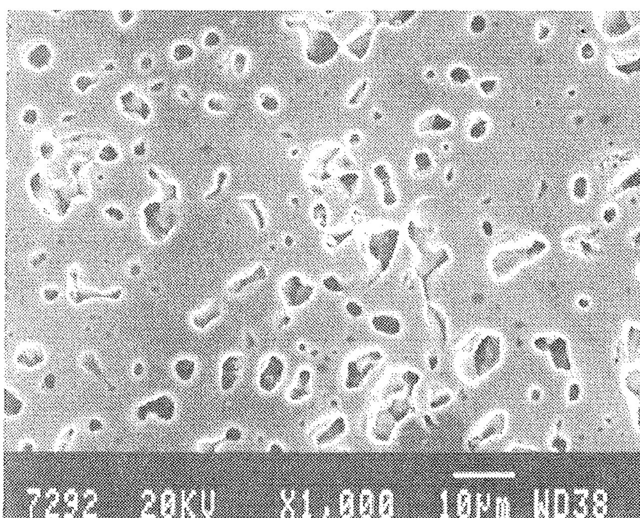

Fig. 5.a: The microstructure of $(La_{0.8}Sr_{0.2})MnO_3$

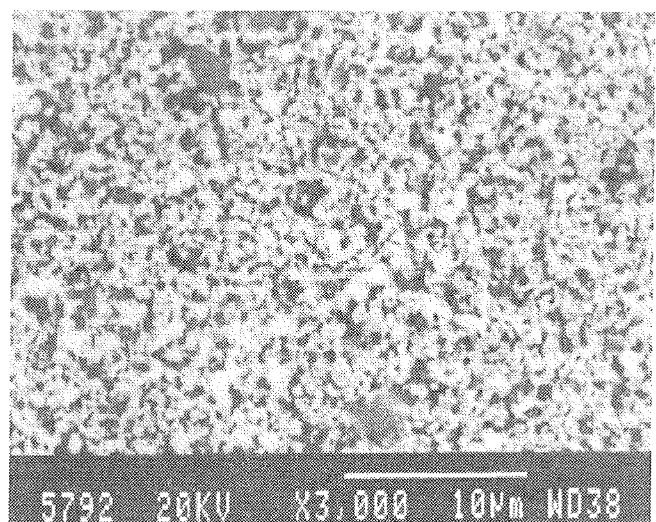

Fig. 5.d: The microstructure of $(La_{0.8}Sr_{0.2})(Mn_{0.06}Al_{0.94})O_3$

number in the bracket indicates the accuracy of the last significant digit. Subunit cell volumes are also shown in Fig. 7. Vertical bars indicate the accuracy of the calculated volume of perovskite subunit cells (the volume of unit cells in Table I and in Table II, divided by the number of subunit cells or pseudo-cells in the unit cell, i.e. 4 in the case of a monoclinic cell and 6 in the case of a hexagonal cell).

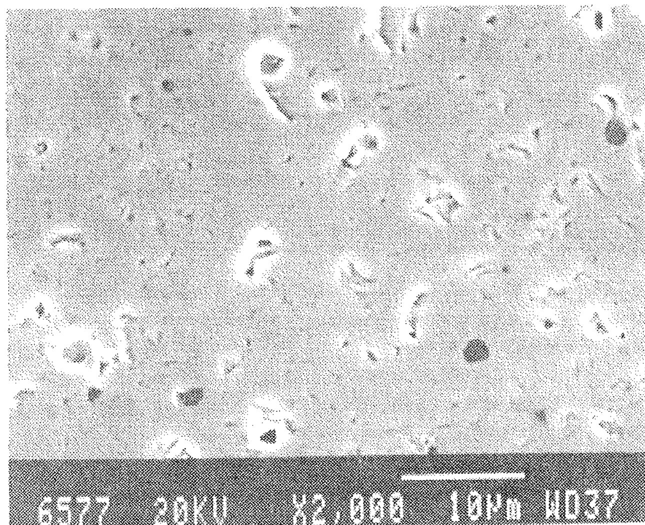

Fig. 6: The microstructure of substoichiometric $(La_{0.8}Sr_{0.2})_{0.95}(Mn_{0.7}Al_{0.3})O_3$

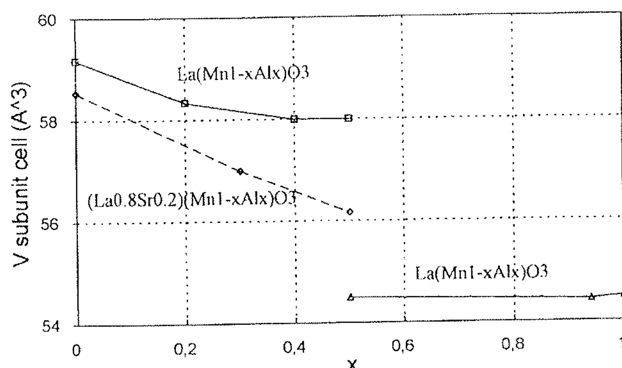

Fig. 7: Volume of perovskite subunit (or pseudo-) cells vs. composition for $La(Mn_{1-x}Al_x)O_3$ and strontium substituted $(La_{0.8}Sr_{0.2})(Mn_{1-x}Al_x)O_3$.

The values obtained for $LaMnO_3$, $LaAlO_3$, and $La_{0.8}Sr_{0.2}MnO_3$ are in fair agreement with data in JCPDS-ICDD 32-484, JCPDS-ICDD 31-22, and JCPDS-ICDD 40-1100 cards, respectively. The cell volume of $La(Mn_{1-x}Al_x)O_3$ linearly decreases with increasing alumina content from x=0 to x=0.4 which is the limit of solid solubility of $LaAlO_3$ in $LaMnO_3$ at 1200°C. It is due to the smaller ionic radius of Al^{3+} (Al^{3+} 0.535 Å and Mn^{3+} 0.645 Å). Strontium substituted perovskites $(La_{0.8}Sr_{0.2})(Mn_{1-x}Al_x)O_3$ have smaller cell volumes as their counterparts with the same aluminum / manganese ratio. The ionic radius of Sr^{2+} and La^{3+} are similar (La^{3+} 1.36 Å and Sr^{2+} 1.44 Å), therefore the contraction of volume occurs either due to formation of oxygen vacancies or smaller Mn^{4+} ions (Mn^{4+}=0.53 Å). Oxygen vacancies and/or Mn^{4+} ions are needed for charge compensation when the La^{3+} ion on "A" site is exchanged by the lower valence Sr^{2+} ion.

Table 1: Calculated cell parameters for materials with nominal compositions $La(Mn_{1-x}Al_x)O_3$

Nominal composition	a(Å)	c(Å)	V(Å^3)
$LaMnO_3$	5.531(5)	13.38(2)	355(1)
$La(Mn_{0.8}Al_{0.2})O_3$	5.512(4)	13.29(2)	350(1)
$La(Mn_{0.6}Al_{0.2})O_3$	5.502(5)	13.27(2)	348(1)
$La(Mn_{0.5}Al_{0.5})O_3$ *	5.497(7)	13.29(3)	348(2)
$La(Mn_{0.5}Al_{0.5})O_3$**	5.368(2)	13.12(3)	327(1)
$La(Mn_{0.06}Al_{0.94})O_3$	5.3630(9)	13.11(1)	326.6(4)
$LaAlO_3$	5.363(1)	13.5(2)	327(7)

* solid solution of Al_2O_3 in $LaMnO_3$

** solid solutions of Mn_2O_3 in $LaAlO_3$

Specific electrical resistivities are given for "as fired" samples and are not corrected for porosity of materials. The logarithm of resistivities of $La(Mn_{1-x}Al_x)O_3$ vs. reciprocal temperature is shown in Fig. 8. The logarithm of resistivities of $La(Mn_{1-x}Al_x)O_3$ vs. "x", i.e., alumina content is shown in Fig. 9 for 700°C and 900°C. Specific resistivities increase with increasing concentration of

Table 2: Calculated cell parameters for materials with nominal compositions $(La_{0.8}Sr_{0.2})(Mn_{1-x}Al_x)O_3$

nominal composition	a(Å)	b(Å)	c(Å)	β(°)	V(Å^3)
$La_{0.8}Sr_{0.2}MnO_3$	5.479(3)	5.523(3)	7.74(2)	90.5(1)	234.1(9)
$La_{0.8}Sr_{0.2}Mn_{0.7}Al_{0.3}O_3$ *	5.457(4)		13.25(2)		342(1)
$La_{0.8}Sr_{0.2}Mn_{0.5}Al_{0.5}O_3$	5.413(3)		13.27(3)		337(1)
$La_{0.8}Sr_{0.2}Mn_{0.06}Al_{0.94}O_3$	5.28(4)		13.2(2)		319(9)

* monoclinic cell

Al_2O_3. The change of slope in the resistivity vs. alumina content curves (Fig. 9) at x=0.4 is presumably due to the limit of solid solution in the $LaMnO_3$ rich region /21/.

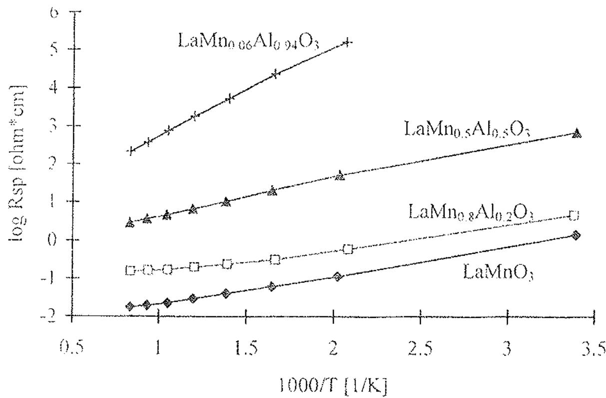

Fig. 8: The logarithm of resistivities of $La(Mn_{1-x}Al_x)O_3$ vs. reciprocal temperature

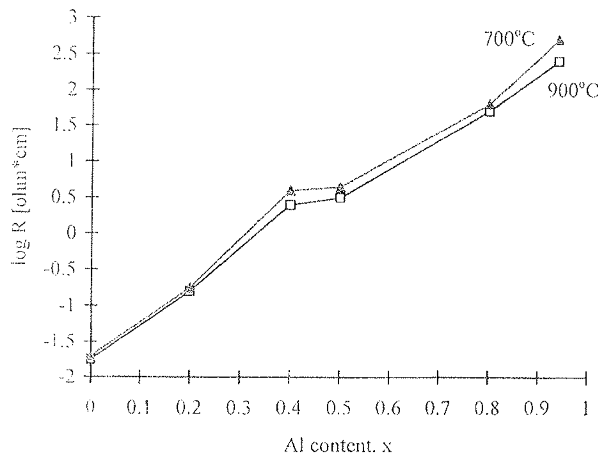

Fig. 9: Logarithm of specific resistivities of $La(Mn_{1-x}Al_x)O_3$ at 700°C and 900°C as a function of Al_2O_3 content.

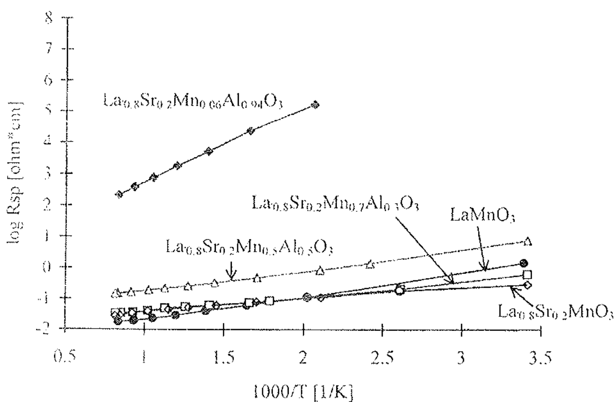

Fig. 10: Logarithm of resistivity of $(La_{0.8}Sr_{0.2})(Mn_{1-x}Al_x)O_3$ and $LaMnO_3$ vs. reciprocal temperature

The logarithm of resistivities of $(La_{0.8}Sr_{0.2})(Mn_{1-x}Al_x)O_3$ vs. reciprocal temperature is shown in Fig. 10. The resistivity of $LaMnO_3$ is presented for comparison. The resistivities of $LaMnO_3$ and $(La_{0.8}Sr_{0.2})(Mn_{1-x}Al_x)O_3$ for x=0 and 0.3 are nearly the same for the whole temperature range at temperatures over 200°C, whereas for x=0.5 the resistivity is higher by an order of magnitude. The specific resistivities of $(La_{0.8}Sr_{0.2})(Mn_{0.7}Al_{0.3})O_3$ are comparable or even slightly lower than the resistivities of $(La_{0.8}Sr_{0.2})MnO_3$ (without alumina).

For comparison, the resistivities of undoped $La(Mn_{1-x}Al_x)O_3$ samples and SrO doped $(La_{0.8}Sr_{0.2})(Mn_{1-x}Al_x)O_3$ samples are plotted together in Fig. 11. The resistivities of strontium doped samples are about one order of magnitude lower than those of undoped samples. While the resistivity of undoped $La(Mn_{0.7}Al_{0.3})O_3$ is an order of magnitude higher than the resistivity of $LaMnO_3$, for SrO doped samples the resistivities of similar compositions, i.e., $(La_{0.8}Sr_{0.2})MnO_3$ and $(La_{0.8}Sr_{0.2})(Mn_{0.7}Al_{0.3})O_3$ are nearly the same.

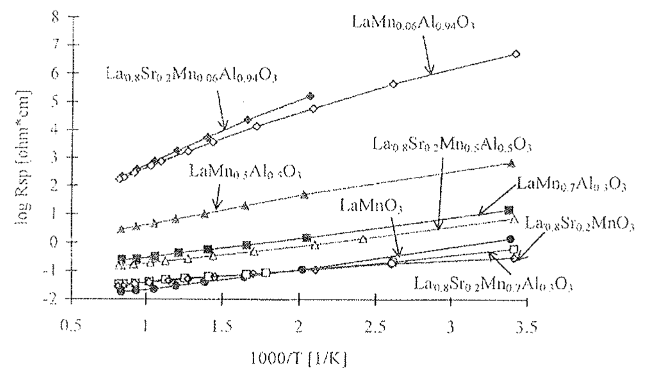

Fig. 11: Logarithm of resistivity of $La(Mn_{1-x}Al_x)O_3$ and $(La_{0.8}Sr_{0.2})(Mn_{1-x}Al_x)O_3$ vs. reciprocal temperature. Samples with partial exchange of lanthanum with strontium have an extension "S".

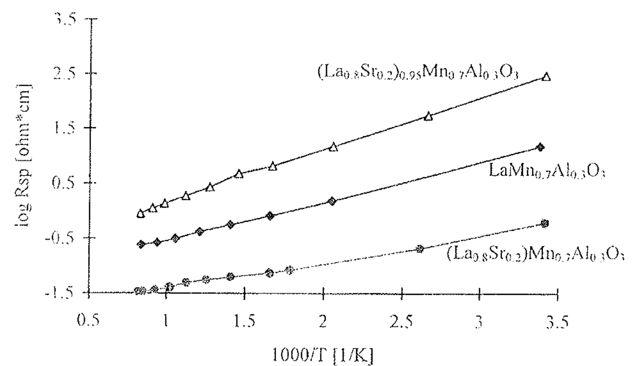

Fig. 12: The logarithm of specific resistivities vs. reciprocal temperature for $La(Mn_{0.7}Al_{0.3})O_3$, $(La_{0.8}Sr_{0.2})(Mn_{0.7}Al_{0.3})O_3$, and $(La_{0.8}Sr_{0.2})_{0.95}(Mn_{0.7}Al_{0.3})O_3$

Table 3. Specific resistivities of stoichiometric and substoichiometric samples at 25 °C, 400 °C, and at 900 °C (Ωcm)

Nominal composition	25°C	400°C	900°C
$LaMnO_3$	1.4 Ωcm	0.04 Ωcm	0.018 Ωcm
$La(Mn_{0.7}Al_{0.3})O_3$	8.2 Ωcm	0.57 Ωcm	0.12 Ωcm
$(La_{0.8}Sr_{0.2})(Mn_{0.7}Al_{0.3})O_3$	0.62 Ωcm	0.063 Ωcm	0.034 Ωcm
$(La_{0.8}Sr_{0.2})_{0.95}(Mn_{0.7}Al_{0.3})O_3$	280 Ωcm	4.8 Ωcm	0.35 Ωcm

It is interesting to note, however, that the composition with x=0.94 is an exception; namely, the resistivity of the undoped material is lower than the resistivity of the strontium oxide doped one. The reason for this unexpected characteristic is not known yet. The specific resistivities of $La_{0.8}Sr_{0.2}MnO_3$ and $(La_{0.8}Sr_{0.2})(Mn_{0.7}Al_{0.3})O_3$ are nearly temperature independent over the whole measured temperature range.

The logarithm of specific resistivities vs. reciprocal temperature for $(La_{0.8}Sr_{0.2})_{0.95}(Mn_{0.7}Al_{0.3})O_3$. is presented in Fig. 12. Values for $La(Mn_{0.7}Al_{0.3})O_3$, and stoichiometric strontium substituted $(La_{0.8}Sr_{0.2})(Mn_{0.7}Al_{0.3})O_3$ are shown for comparison. The partial exchange of lanthanum with strontium ions significantly decreases the resistivity. However, the resistivities of sub-stoichiometric compositions are higher than those of stoichiometric compositions.

Resistivities for materials with x=0.3, i.e., $La(Mn_{0.7}Al_{0.3})O_3$, $(La_{0.8}Sr_{0.2})(Mn_{0.7}Al_{0.3})O_3$, and substoichiometric $(La_{0.8}Sr_{0.2})_{0.95}(Mn_{0.7}Al_{0.3})O_3$ at room temperature, at 400°C, and at 900°C are summarized in Table III. Data for $LaMnO_3$ are also included for comparision. The partial exchange of lanthanum with strontium ions significantly decreases the resistivity. However, the resistivities of sub-stoichiometric compositions are higher than those of stoichiometric compositions.

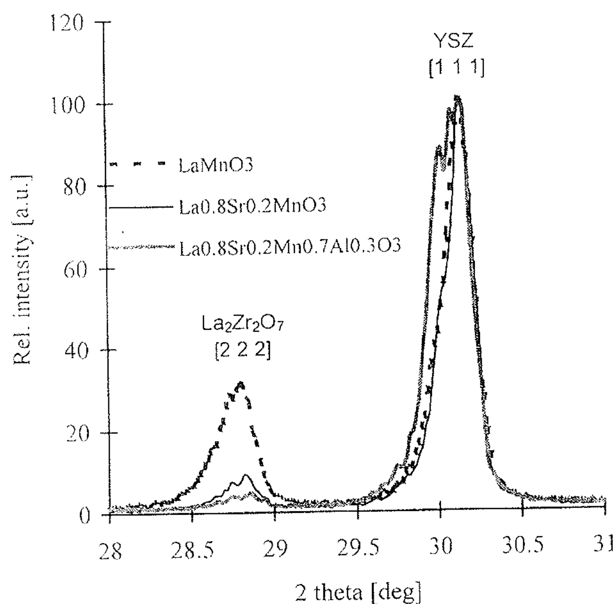

Fig. 13: Superimposed normalized X-ray spectra of $LaMnO_3$, $(La_{0.8}Sr_{0.2})MnO_3$, and $(La_{0.8}Sr_{0.2})(Mn_{0.7}Al_{0.3})O_3$ mixtures with YSZ after ageing for 300 hours at 1400°C. The [2 2 2] peak of $La_2Zr_2O_7$ at 2 θ=28.8° is shown.

Superimposed normalized X-ray spectra of $LaMnO_3$, $(La_{0.8}Sr_{0.2})MnO_3$, and $(La_{0.8}Sr_{0.2})(Mn_{0.7}Al_{0.3})O_3$ mixtures with YSZ after ageing for 300 hours at 1400°C, are presented in Fig. 13. The [2 2 2] peak of $La_2Zr_2O_7$ at 2 θ =28.8° is shown. The height of the peak is proportional to the quantity of $La_2Zr_2O_7$ pyrochlore phase which is formed during ageing. The results - the heights of the peaks - indicate that more pyrochlore phase is formed under the same ageing conditions between $LaMnO_3$ and YSZ than between $(La_{0.8}Sr_{0.2})MnO_3$ and YSZ. In the case of $(La_{0.8}Sr_{0.2})(Mn_{0.7}Al_{0.3})O_3$ the quantity of $La_2Zr_2O_7$ was minimized. It is known that the limited exchange of lanthanum oxide with alkaline earth oxides inhibits the formation of $La_2Zr_2O_7$ (see, for example, Ref. /18/. The results showed that the combination of strontium and aluminum oxide further depresses the formation of the undesirable high resistivity pyrochlore phase. No difference between $(La_{0.8}Sr_{0.2})(Mn_{0.7}Al_{0.3})O_3$ and substoichiometric $(La_{0.8}Sr_{0.2})_{0.95}(Mn_{0.7}Al_{0.3})O_3$ was observed.

CONCLUSIONS

Perovskites with nominal compositions $La(Mn_{1-x}Al_x)O_3$ and strontium doped $(La_{0.8}Sr_{0.2})(Mn_{1-x}Al_x)O_3$ (for x between 0 and 0.94) were synthesized as possible solid oxide fuel cells (SOFC) cathode materials. Some results on substoichiometric $(La_{0.8}Sr_{0.2})_{0.95}(Mn_{0.7}Al_{0.3})O_3$ were also obtained.

The microstructures of alumina substituted materials are porous and average grain diameters decrease with increasing Al_2O_3 content. $(La_{0.8}Sr_{0.2})(Mn_{1-x}Al_x)O_3$ perovskites are more densely sintered that those without strontium. Substoichiometry on "A" sites increases the sintered density.

From X-ray diffraction analysis data cell parameters were calculated. The cell volume of $La(Mn_{1-x}Al_x)O_3$ linearly decreases with increasing alumina content from x=0 to x=0.4 which is the limit of solid solubility of $LaAlO_3$ in $LaMnO_3$. Strontium substituted perovskites have smaller cell volumes as their counterparts with the same aluminum / manganese ratio.

Specific resistivities of $La(Mn_{1-x}Al_x)O_3$ increase with increasing concentration of Al_2O_3. The resistivities of $LaMnO_3$ and $(La_{0.8}Sr_{0.2})(Mn_{1-x}Al_x)O_3$ for x=0 and 0.3 are nearly the same for the whole temperature range at temperatures above 200°C, whereas for x=0.5 the resistivity is higher by an order of magnitude. The resistivities of strontium doped $(La_{0.8}Sr_{0.2})(Mn_{1-x}Al_x)O_3$ are about one order of magnitude lower than those of undoped samples. The resistivities of sub-stoichiometric compositions are higher than those of stoichiometric compositions.

To study the formation rate of the undesirable high resistive pyrochlore phase $La_2Zr_2O_7$, perovskites and YSZ mixtures were fired at elevated temperatures. The results showed that the combination of strontium and aluminum oxide significantly depress the formation of $La_2Zr_2O_7$. No difference between stoichiometric and substoichiometric materials was detected.

From described results it could be concluded that the optimized composition for SOFC cathodes is $(La_{0.8}Sr_{0.2})(Mn_{0.7}Al_{0.3})O_3$. It's resistivity is similar to $LaMnO_3$ while the reaction rate with YSZ is minimized.

ACKNOWLEDGEMENTS

This work was performed within the project "New SOFC Materials and Technology; JOU2-CT92-0063". The authors would like to express their thanks to Dr. Toma' Kosmač for helpful discussions. The financial support of the Ministry of Science and Technology of Slovenia is gratefully acknowledged.

REFERENCES

/1/ W. R. Grove, On voltaic series and the combination of gases by platinum, Phil. Mag., S.3., 14, (86), (1839), 127-130

/2/ N. Q. Minh, Ceramic fuel cells, J. Am. Ceram. Soc., 76, (3), (1993), 563-588

/3/ B. C. H. Steele, State-of-the-art SOFC ceramic materials, Proc. 1 st European Solid Oxide Fuel Cell Forum, European Fuel Cell Group, Ltd. and IEA Advanced Fuel Cell Programme, (Ed. U. Bossel), Lucerne, 1994, 375-397

/4/ K. Ledjeff, T. Rohrbach, G. Schaumberg, Internal reforming for solid oxide fuel cells, Proc. 2nd Int. Symp. on Solid Oxide Fuel Cells, Commission of the European Communities (Ed. F. Grosz, P. Zegers, S. C. Singhal, O. Yamatoto), Athens, 1991, 323-333

/5/ P. Stonehart, The unique features of the solid oxide fuel cell in a hydrocarbon energy world, Proc. 1 st European Solid Oxide Fuel Cell Forum, European Fuel Cell Group, Ltd. and IEA Advanced Fuel Cell Programme, (Ed. U. Bossel), Lucerne, 1994, 15-41

/6/ T. Aida, A. Abudula, M. Ihara, H. Komiyama, K. Yamada, Direct oxidation of methane on anode of solid oxide fuel cell, Proc. 4th Int. Symp. on Solid Oxide Fuel Cells, The Electrochemical Society, Inc. (Ed. M.Dokiya, O.Yamamoto, H. Tagawa, S.C. Singhal), Yokohama, 1995, 801-809

/7/ K. Kendall, Ceramics in fuel cells, Cer. Bull., 70, (7), (1991), 1159-1160

/8/ F. Gross, Solid oxide fuel cells R&D in Europe, Proc. 2nd Int. Symp. on Solid Oxide Fuel Cells, Commission of the European Communities (Ed. F. Grosz, P. Zegers, S. C. Singhal, O. Yamatoto), Athens, 1991, 7-2

/9/ M. Mogensen, N. Christiansen, Fuel cells - familiar principles for electricity generation, Europhys. News, 24, (1993), 7-9

/10/ H. Tagawa, Status of SOFC development in Japan, Proc. 3rd Int. Symp. on Solid Oxide Fuel Cells, The Electrochemical Society, Inc. (Ed. S. C. Singhal, H. Iwahara), Honolulu, 1993, 6-15

/11/ S. Kartha, P. Grimes, Fuel cells: energy conversion for the next century, Physics Today, 47, (11), (1994), 54-61

/12/ A. Mackor, T. P. M. Koster, J. G. Kraaijkamp, J. Gerretsen, Influence of La-substitution and -substoichiometry on conductivity, thermal expansion and chemical stability of Ca- or Sr-doped lanthanum manganites as SOFC cathodes, Proc. 2nd Int. Symp. on Solid Oxide Fuel Cells, Commission of the European Communities (Ed. F. Grosz, P. Zegers, S. C. Singhal, O. Yamatoto), Athens, 1991, 463-471

/13/ J. Gerretsen, A. Mackor, J. P. G. M. van Eijk, T. P. M. Koster, Standardization of thermal expansion coefficient (TEC) measurements for testing the compatibility of SOFC components, Proc. 2nd Int. Symp. on Solid Oxide Fuel Cells, Commission of the European Communities (Ed. F. Grosz, P. Zegers, S. C. Singhal, O. Yamatoto), Athens, 1991, 159-166

/14/ M. Hrovat, S. Bernik, J. Holc, D. Kolar, B. Dacar, Preliminary data on subsolidus phase equilibria in the La_2O_3 - Cr_2O_3 - Y_2O_3 and La_2O_3 - Cr_2O_3 - ZrO_2 systems, J. Mater. Sci. Lett., 14, (23), (1995), 1684-1687

/15/ H. Taimatsu, K. Wada and H. Kaneko, Mechanism of reaction between lanthanum manganite and yttria stabilized zirconia, J. Am. Ceram. Soc., 75 (2), (1992), 401-405

/16/ J. A. M. van Roosmalen and E. H. P. Cordfunke, Chemical reactivity and interdiffusion of $(La,Sr)MnO_3$ and $(Zr,Y)O_2$ solid oxide fuel cell cathode and electrolyte materials, Solid State Ionics, 52 , (1992), 303 - 312

/17/ J. A. Labrincha, J. R. Frade and F. M. B. Marques, $La_2Zr_2O_7$ formed at ceramic electrode/YSZ contacts, J. Mater. Sci. 28, (14), (1993), 3809-3815

/18/ G. Stochniol, E. Syskakis, A. Naoumidis, Compatibility studies between $La_{1-x}Sr_xMnO_3$ and 8YSZ, Proc. 5th IEA Workshop on SOFC, Materials, Process Engineering and Electrochemistry (Eds. P. Biederman, B. Krahl-Urban), Jülich FRG, 1993, 25-31

/19/ D. Kuščer, J. Holc, M. Hrovat, S. Bernik, Z. Samardžija, D. Kolar, Interactions between thick film $LaMnO_3$ SOFC cathode and ZrO_2 (8% Y_2O_3) during high temperature ageing, Solid State Ionics, 78, (1995), 79-85

/20/ F. W. Poulsen, N. van der Puil, Phase relations and conductivity of Sr- and La-zirconates, Solid State Ionics, 53-56, (pt. 2), (1992), 777-783

/21/ M. Hrovat, J. Holc, D. Kuščer, Z. Samardžija, S. Bernik, Preliminary data on subsolidus phase equilibria in the La_2O_3 - Al_2O_3 - Mn_2O_3 and La_2O_3 - Al_2O_3 - Fe_2O_3 systems, J. Mater. Sci. Lett., 14, (4), (1995), 265-267

/22/ A. Hammouche, E. Siebert, A. Hammou, Crystallographic, thermal and electrochemical properties of the system $La_{1-x}Sr_xMnO_3$ for high temperature solid electrolyte fuel cells, Mat. Res. Bull., 24, (3), (1989), 367-380

mag. Danjela Kuščer, dipl.ing.
dr. Janez Holz, dipl.ing.
dr. Marko Hrovat, dipl.ing.
dr. Slavko Bernik, dipl.ing.
dr. Drago Kolar, dipl.ing.
Jožef Stefan Institute
Jamova 39, 1000 Ljubljana, Slovenia
tel.: +386 61 1773418
fax: +386 61 1261029

Prispelo (Arrived): 25.3.1997 *Sprejeto (Accepted): 6.5.1997*

UDK621.3:(53+54+621+66), ISSN0352-9045

LOGIC PERTURBATIONS: A BASIS FOR DIGITAL CIRCUITS OPTIMIZATION

A. Žemva, B. Zajc
Faculty of Electrical Engineering, Ljubljana, Slovenia

Keywords: digital circuits, digital circuits optimization, logical perturbations, logic synthesis, test pattern generation, fault simulation, multi-level digital circuits, wave synthesis method, single-output circuits, multi-output circuits, experimental results, optimization algorithms

Abstract: In this paper, we introduce the concept of permissible logic perturbations as a method for logic optimization of multi-level digital circuits. The presented approach, denoted as a wave synthesis, refers to a sequence of procedures performed in order of logic levels that transform a perturbation region of multi-input, multi-output wires into a multi-input, multi-output logic subcircuit. Primary goal of the wave synthesis, which in contrast to the other methods for logic optimization relies on fault simulation and test pattern generation algorithms, is the area optimization of the initial, technology-independent multi-level circuit. We have verified the wave synthesis concept for several multi-input, multi-output combinational circuits and the experimental results obtained with the prototype software WASP confirmed the presented approach.

Logične perturbacije: Osnova za optimizacijo digitalnih vezij

Ključne besede: vezja digitalna, optimizacija vezij digitalnih, perturbacije logične, generiranje vzorcev testnih, simulacija napak, vezja digitalna večnivojska, metoda valovne sinteze, vezja enoizhodna, vezja večizhodna, rezultati eksperimentalni, algoritmi optimizacijski

Povzetek: V članku je predstavljena metoda za optimizacijo večnivojskih logičnih vezij na osnovi dovoljenih perturbacij. Predlagana metoda, imenovana valovna sinteza, temelji na zaporedju procedur s katerimi večvhodno, večizhodno perturbacijsko področje pretvorimo v večvhodno, večizhodno mutacijsko podvezje. Osnovni cilj valovne sinteze, ki v nasprotju z ostalimi metodami za logično optimizacijo temelji na algoritmih za generacijo testnih vzorcev ter simulacijo napak, je optimizacija vezij s stališča površine. Metodo smo preverili na množici testnih vezij in eksperimentalni rezultati so potrdili kvaliteto predlaganega pristopa.

1 Introduction

The increasing complexity of the modern VLSI circuitry is only feasible through the advanced CAD systems which as one of the important components include logic optimization tools. Automatic logic synthesis and optimization tools transform a high-level logic description into a multi-level network of realizable logic gates /1/.

The concept of logic perturbations has already been proven for optimizing multi-level logic combinational Boolean networks. It was first demonstrated in a transduction method, acronym for transformation and reduction, presented in /2/. Circuit transformations and reductions based on the permissible functions were repeatedly applied until a network of the sufficient lower cost was obtained. In this sense, the transduction method was significantly different from the known design methods. Optimization by logic perturbations has been further investigated in /3/. In particular, the replacement of a gate in a synchronous Boolean network was modeled by a perturbation of the gate functionality.

Perturbations presented in /4,5,6/ are based on redundancy addition and removal which can be efficiently computed using ATPG techniques. The heuristics for adding one redundant wire at a time and removing redundant wires caused by such perturbation was proposed in /4,5/. In /6/, the improved heuristics for identifying gates which are good candidates for a local functionality change, was described.

In this paper, logic optimization based on the concept of undetectable perturbations is discussed. The following discussion begins with the basic notations and definitions, followed by the description of the optimization method. Experimental results on the benchmark circuits confirmed the proposed method.

2 Notations and Definitions

We consider a synchronous multi-level Boolean network as shown in Figure 1; all flip-flops (FFs) are implicitly synchronized with a single clock. All combinational logic nodes of the direct acyclic graph (DAG) between primary/pseudo-primary inputs (PI/PPI) and primary/pseudo-primary outputs (PO/PPO) are assigned into two basic partitions: *a synthesized permissible mutation subcircuit* $M_i (1 \leq i < j)$ *and a remainder subcircuit* R_j. Both subcircuits are separated by a *target perturbation region* P_j. Initially, and as shown in Figure 1, this region consists of p directed edges or wires. We will refer to any pair of input pins of this region as (a, b), and the output pins as (a*, b*), respectively. Depending on the context, we may also refer to a wire pair (a, b) in P_j.

Perturbations in P_j are based on 2-in-2 perturbations introduced in /7/. These perturbations are special cases of k-in-p perturbations for k=2 and p=2. Examples of such perturbations within P_j are shown in Figure 2b. A pair of perturbations of type {$\underline{0}$ $\underline{1}$} is injected onto the wires sunk by output pins (a*, b*) - after decoding the signals on input pins (a=0, b=1). Similarly, a single of

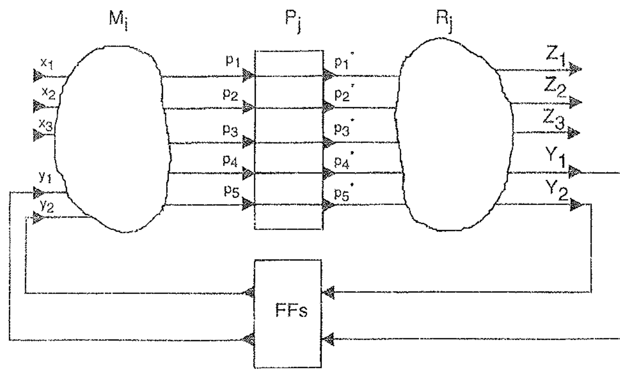

Fig. 1. Perturbation region in the Boolean network

perturbation of type $\{\underline{1}\ 0\}$ is injected onto the wire sunk by output pin (a*) - after decoding the signals on input pins (a=1, b=0). All $2^k \times (2^p-1) = 2^2 \times (2^2-1) = 12$ cases of detectability functions of 2-in-2 perturbations are thus summarized as follows:

$$\begin{aligned}
&\tau^{ab}_{\{\underline{0}\,\underline{0}\}} = \overline{f}_a \overline{f}_b O^{ab}_{\underline{0}\,\underline{0}}\ ; &&\tau^{ab}_{\{\underline{0}\,0\}} = \overline{f}_a \overline{f}_b O^{ab}_{\underline{0}\,0}\ ; &&\tau^{ab}_{\{0\,\underline{0}\}} = \overline{f}_a \overline{f}_b O^{ab}_{0\,\underline{0}}\\
&\tau^{ab}_{\{\underline{0}\,\underline{1}\}} = \overline{f}_a f_b O^{ab}_{\underline{0}\,\underline{1}}\ ; &&\tau^{ab}_{\{\underline{0}\,1\}} = \overline{f}_a f_b O^{ab}_{\underline{0}\,1}\ ; &&\tau^{ab}_{\{0\,\underline{1}\}} = \overline{f}_a f_b O^{ab}_{0\,\underline{1}}\\
&\tau^{ab}_{\{\underline{1}\,\underline{0}\}} = f_a \overline{f}_b O^{ab}_{\underline{1}\,\underline{0}}\ ; &&\tau^{ab}_{\{\underline{1}\,0\}} = f_a \overline{f}_b O^{ab}_{\underline{1}\,0}\ ; &&\tau^{ab}_{\{1\,\underline{0}\}} = f_a \overline{f}_b O^{ab}_{1\,\underline{0}}\\
&\tau^{ab}_{\{\underline{1}\,\underline{1}\}} = f_a f_b O^{ab}_{\underline{1}\,\underline{1}}\ ; &&\tau^{ab}_{\{\underline{1}\,1\}} = f_a f_b O^{ab}_{\underline{1}\,1}\ ; &&\tau^{ab}_{\{1\,\underline{1}\}} = f_a f_b O^{ab}_{1\,\underline{1}}
\end{aligned} \tag{1}$$

where for example, perturbation observability function $O_{\underline{1}\,\underline{1}}^{ab}$ is defined as

$$O^{ab}_{\underline{1}\underline{1}} = \sum_r Z_r(x, a^* = f_a, b^* = f_b) \oplus Z_r(x, a^* = \bar{f}_a, b^* = \bar{f}_b) \tag{2}$$

where Σ_r designates OR-ing the respective functions for all outputs. Given that P_j consists of m wires, a total of 12 x m x (m-1)/2 perturbations are considered. Permissible perturbation in P_j is defined for any pair of wires in P_j whose detectability, as per equations in (1), is identical to 0.

Basic properties of perturbation region P_j:

1. P_j is perturbable if there is at least one permissible perturbation in P_j;
2. P_j is non-perturbable if there is no permissible perturbation in P_j.

Permissible mutation function set $\{(f_{a^*}, f_{b^*})_i\}$ is synthesized from the pairwise permissible perturbations in P_j. We will also refer to this set as permissible pairwise mutations or simply permissible mutations. Suppose that we have the following number of permissible perturbations for a wire pair (a, b):

- n_{00} permissible perturbations for (a=0, b=0),
- n_{01} permissible perturbations for (a=0, b=1),
- n_{10} permissible perturbations for (a=1, b=0),
- n_{11} permissible perturbations for (a=1, b=1),

the size of the set of all permissible pairwise mutations is

$$|I_{ab}| = (n_{00}+1)(n_{01}+1)(n_{10}+1)(n_{11}+1) - 1 \tag{3}$$

and the set can be denoted as

$$\{(f_{a^*}, f_{b^*})_i \mid i \in I_{ab}\} \tag{4}$$

where the mutation index set I_{ab} is computed from the perturbation indices as follows:

$$I_{ab} = \{i \mid i = j4^3 + k4^2 + l4^1 + m4^0\} \forall (j,k,l,m) \in P_{ab} \tag{5}$$

and P_{ab} is a 4-tuple of permissible perturbation indices. For example, for (a=0, b=0) we have:

j=0: no perturbation is permissible for $\{0\ 0\}_{ab}$;

j=1: perturbation $\{0\ \underline{0}\}_{ab}$ is permissible;

j=2: perturbation $\{\underline{0}\ 0\}_{ab}$ is permissible;

j=3: perturbation $\{\underline{0}\ \underline{0}\}_{ab}$ is permissible;

and k, l and m are defined similarly for (a=0, b=1), (a=1, b=0) and (a=1, b=1).

Permissible Mutation Subcircuit M_j is formed with the permissible mutations from $\{(f_{a^*}, f_{b^*})_i\}$ as a maximum cover at the minimum cost. A greedy heuristics for this cover is given in the next section.

Illustrative Example. We have already discussed the target perturbation region such as P_j in Figure 2a. Given that any of the three perturbations illustrated in Figure 2b are permissible ($n_{00}=0$, $n_{01}=1$, $n_{10}=1$ and $n_{11}=1$), we can synthesize up to 2·2·2-1=7 permissible mutations as shown in Figure 2c. In Figure 2d, we have tabulated permissible mutations in terms of their respective perturbation and mutation indices, along with yet to be defined mutation cost of each function, $\$_i$. For example, the first permissible mutation $f_{a^*} = f_a f_b$, $f_{b^*} = f_b$ in Figure 2d is synthesized by considering perturbation $\{\underline{1}\ 0\}$ permissible (l=2). Associated perturbation index P_{ab}=0.0.2.0 and the corresponding mutation index $I_{ab} = 0+0+2\cdot 4^1+0 = 8$.

If all 12 perturbations were permissible, we would have a choice of 4·4·4·4 - 1 = 255 permissible mutations for the wire pair (a, b).

Free and Bound Wire. Wire a is referred as free if $f_{a^*} = f_a$, $f_{a^*} = \bar{f}_a$, $f_{a^*} = f_b$ or $f_{a^*} = \bar{f}_b$; otherwise it is referred as bound or covered. The same applies for wire b.

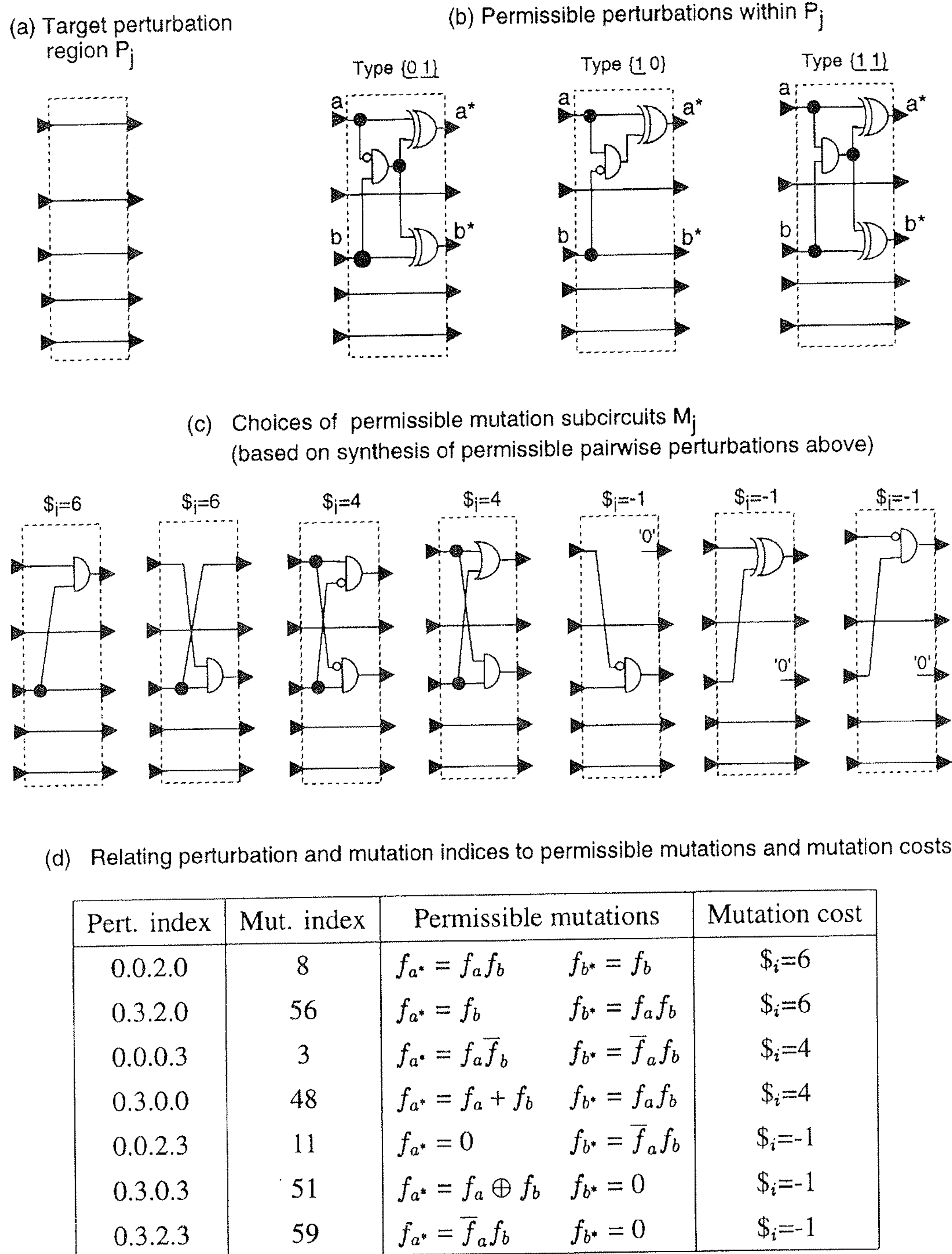

Pert. index	Mut. index	Permissible mutations		Mutation cost
0.0.2.0	8	$f_{a^*} = f_a f_b$	$f_{b^*} = f_b$	$\$_i$=6
0.3.2.0	56	$f_{a^*} = f_b$	$f_{b^*} = f_a f_b$	$\$_i$=6
0.0.0.3	3	$f_{a^*} = f_a \overline{f}_b$	$f_{b^*} = \overline{f}_a f_b$	$\$_i$=4
0.3.0.0	48	$f_{a^*} = f_a + f_b$	$f_{b^*} = f_a f_b$	$\$_i$=4
0.0.2.3	11	$f_{a^*} = 0$	$f_{b^*} = \overline{f}_a f_b$	$\$_i$=-1
0.3.0.3	51	$f_{a^*} = f_a \oplus f_b$	$f_{b^*} = 0$	$\$_i$=-1
0.3.2.3	59	$f_{a^*} = \overline{f}_a f_b$	$f_{b^*} = 0$	$\$_i$=-1

Fig. 2 Permissible perturbation and synthesized mutation functions

Cost Classes of Permissible Mutations. For each wire pair (a, b) and each permissible mutation i, we define a cost $\$_i$ as follows:

$$\$_i = \$(a) + \$(a^*) + \$(b) + \$(b^*) \qquad (6)$$

where

$\$(a)$ = -4 if the input pin is floating
= 0 otherwise

$\$(a^*)$ = 4 if the output pin is driven by a free wire
= 2 if the output pin is driven by a bound wire
= 1 if the output pin is driven by a bound wire and is logically equivalent to the other output pin
= 1 if the output pin is driven by a free wire and is logically equivalent to the other output pin
= -3 if the output pin is driven by a constant.

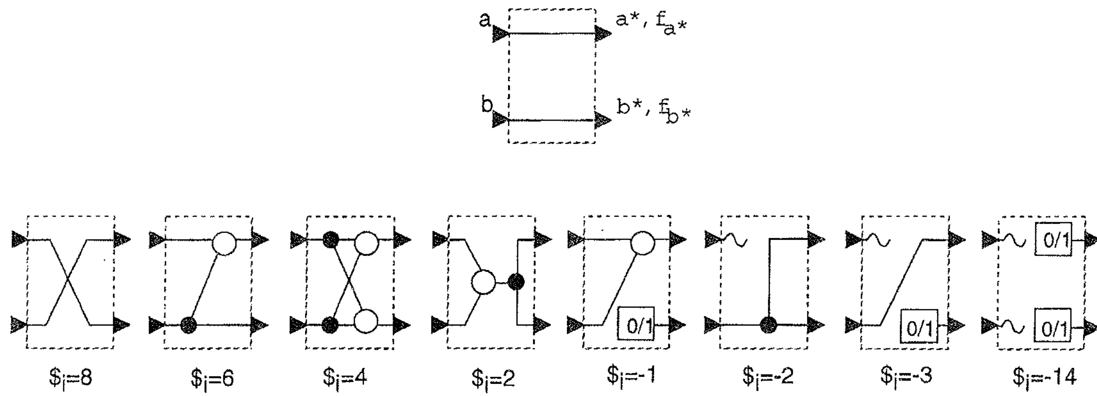

Class size	Mutation cost $\$_i$	Cost			
		$\$(a)$	$\$(b)$	$\$(a^*)$	$\$(b^*)$
7	$\$_i$=8	0	0	4	4
80	$\$_i$=6	0	0	2	4
80	$\$_i$=4	0	0	2	2
20	$\$_i$=2	0	0	1	1
40	$\$_i$=-1	0	0	2	-3
8	$\$_i$=-2	-4	0	1	1
16	$\$_i$=-3	-4	0	4	-3
4	$\$_i$=-14	-4	-4	-3	-3

Fig. 3 Partitioning of 255 mutation functions into 8 cost equivalence classes

and where \$(b) and \$(b*) are calculated similarly.

For the set of permissible perturbations in Figure 2b, the costs of permissible mutations range from 6 to -1 as shown in Figure 2c-d.

The cost assignment to I/O nodes of the permissible mutations as shown in (6) induces a partition of all 255 permissible mutations into 8 cost equivalence classes (CEC). Generic topology of 2-input, 2-output permissible mutations into the 8 CECs is shown in Figure 3, along with the table that depicts the size of each class, associated with the mutation cost $\$_i$. Shaded nodes represent fanout nodes, unshaded nodes represent logic nodes that can implement all irredundant functions of 2-inputs. The square node with 0/1 represents a constant 0/1 signal that can prune logic nodes in the forward path. The wire terminated with ~ represents a floating wire that can prune logic nodes driving this wire. Wires show no inverters, although inverters may be presented without affecting the cost function. The cost of the permissible mutation in each class ranges from 8 to -14. The lower the cost of the mutation, the more pruning potential we associate with the mutation.

Since we can precompute and store all possible 2^{12}-1 perturbation indices that map into the 255 mutation indices ranked by its cost, we can determine the minimum cost mutation by simple table look-up, given the 4-tuple of permissible perturbation indices.

3 Optimization Algorithm

Consider a sample circuit shown in Figure 4, consisting of 20 2-input gates on 6 levels with a maximum fanout of 4, generated with SIS /8/ for a given minimal two-level specification. Starting at the primary inputs, we introduce a perturbation region P_1 as a set of directed wires that connect primary inputs to the inputs of the original circuit, designated as a remainder R_1, as shown in Figure 4.

Given the perturbation region P_1, we assign to each wire pair a set of 2-in-2 perturbations introduced in /7/, and determine which, if any, of these perturbations are permissible. Permissible mutation subcircuit M_j is formed by inserting permissible pairwise mutations from $\{(f_{a^*}, f_{b^*})_i\}$ for each pair.

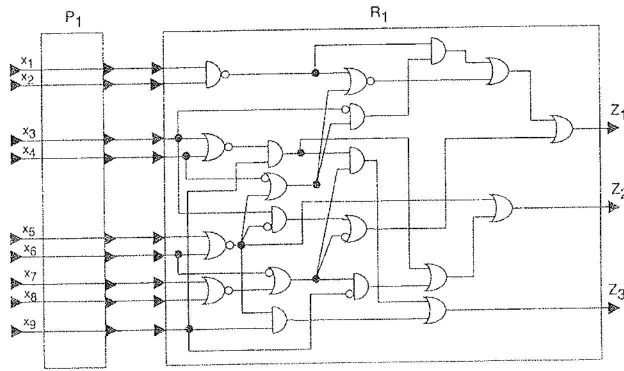

Fig. 4 Sample multi-output circuit

Cost of permissible mutation subcircuit M_j. Cost of permissible mutation subcircuit M_j, denoted as $\$_{Mj}$, is defined as:

$$\$_{M_j} = \sum_{i=1}^{m}(\$(a),\$(a*)) \qquad (7)$$

where \$(a) and \$(a*) are the cost of input and output pins as defined in the previous section.

Heuristics for M_j **synthesis.** We are formulating the problem of M_j synthesis as the problem of a maximal covering at the minimum cost. Assigning initially a tuple of (0,4) to all wires in M_j, the synthesis problem is related to the problem of finding a minimum cost $\$_{Mj}$ for a given set of permissible mutations $\{(f_{a*}, f_{b*})_i\}$.

Given a set of $|l_{ab}|$ permissible mutations per pair (a,b), the upper bound of the syntheses on m-output M_j is:

$$|M_j| = |l_{ab}|^{m(m-1)/2} \qquad (8)$$

Greedy heuristics is used for the synthesis of permissible mutation subcircuit M_j. Permissible mutations, starting with the lowest cost, are assigned one after another to the free wires until all wires are bound or there are no more permissible mutations. The approach is illustrated in Figure 5 for M_1 of the sample circuit in Figure 4. For M_1, $f_{x1*}=f_{x1}f_{x2}$, $f_{x2*}=0$ and $f_{x7*}=0$, $f_{x8*}=f_{x7}+f_{x8}$ are selected first from the set of 36 pairs. The number of free lines is reduced by 4 and $f_{x3*}=f_{x3}$, $f_{x4*}=f_{x3}+f_{x4}$ and $f_{x5*}=f_{x5}+f_{x6}$, $f_{x6*}=f_{x6}$ are selected from the set of the remaining 10 pairs. The number of free lines is reduced to 1 (x_9) and the procedure is terminated. Complexity of the greedy heuristics used is $O(m^2)$, where m is the number of wires in P_j.

Using the proposed greedy approach, one of the cost equivalent mutation subcircuit is constructed. In order to construct Mj with different $\{(f_{a*}, f_{b*})_i\}$, a backtracking capability is embedded into the algorithm for M_j synthesis.

As shown in Figure 5, new perturbation region P_2 consists of directed wires driven by the synthesized permissible mutation subcircuit M_1. Remainder R_2 is the remaining circuit driven by the output wires of P_2. Applying the same procedure on P_2, mutation subcircuit M_2 is synthesized as shown in Figure 6.

The steps illustrated in Figures 5 and 6, denoted as the wave synthesis, are repeated until either the size of the perturbation region has been reduced to the two wires and the remainder itself becomes the last permissible mutation subcircuit or the perturbation region is found unperturbable.

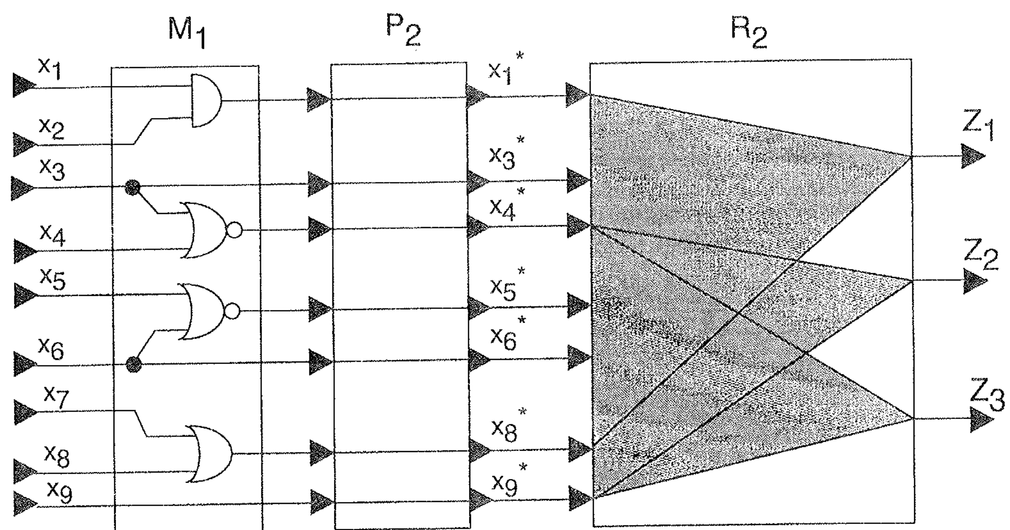

Fig. 5 Synthesis of M_1 for the sample circuit

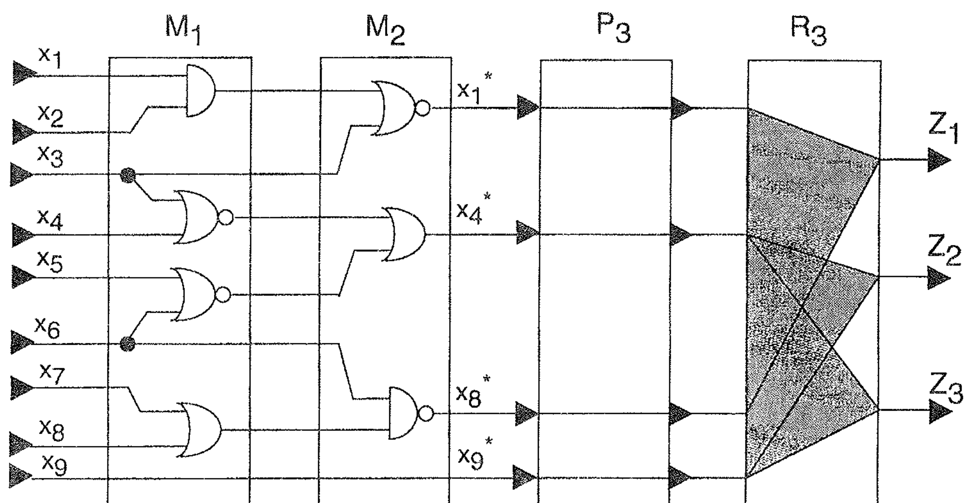

Fig. 6 Case of unpertutbable perturbation region in multi-output circuit

Case of Unperturbable Perturbation Region.

The problem arises when we reach the perturbation region such as P_3 in Figure 6, which is unperturbable. In this case, we have to consider a partitioning strategy for the remainder such as R_3 in Figure 6. Remainder R_j is partitioned into two parts: one with a single output and the other with the remaining outputs. Our decision to select the 'best single output candidate partition' is based on the notion of the extraction potential. Our definition of the extraction potential expands the notation of replication potential introduced in /9/.

Let $A_{Z1}=[1\ 1\ 1\ 0]^T$, $A_{Z2}=A_{Z3}=[0\ 1\ 1\ 1]^T$ denote the adjacency vectors of the remainder R_3. The purpose of the adjacency vector is to show the dependency of the primary outputs of the circuit to the wires in the perturbation region. A value of 1 for the k-th wire in the adjacency vector denotes that there is at least one path from the k-th wire to the PO Z_i, while a value of 0 denotes that there is no path from the k-th wire to the PO Z_i.

The extraction potential ψ_{Zi} for each PO Z_i of the remainder is then

$$\psi_{Z_i} \hat{=} \left\| \left(A_{Z_i} \oplus \prod_{j=1;j\neq i}^{m} A_{Z_j} \right) \right\| \qquad (9)$$

All operations performed in (9) are defined as follows:

- Logical XOR. For example, given $A_{Z1}=[1\ 1\ 1\ 0]^T$ and $A_{Z2}=[0\ 1\ 1\ 1]^T$, $A_{Z1} \oplus A_{Z2} = [1\ 0\ 0\ 1]^T$.
- Logical AND. For example, given $A_{Z1}=[1\ 1\ 1\ 0]^T$ and $A_{Z2}=[0\ 1\ 1\ 1]^T$, $\Pi^2_{j=1} A_{Zj}=A_{Z1} \cdot A_{Z2} = [0\ 1\ 1\ 0]^T$.
- Norm. For example, given $A_{Z1}=[1\ 1\ 1\ 0]^T$, $\|A_{Z1}\| = 3$.

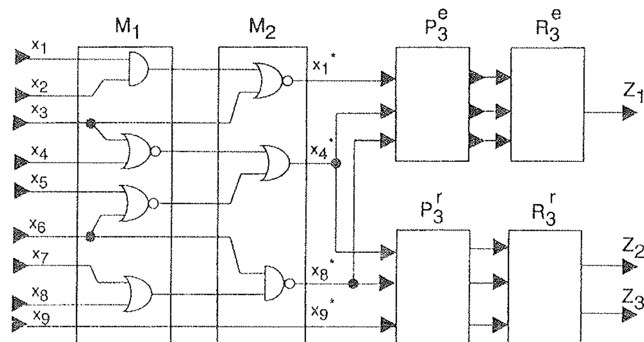

Fig. 7 Partitioning perturbation regions

Single-output partition with the highest extraction potential ψ_{Zi} is selected. The higher is the extraction potential for Z_i, the lower is the number of common wires of P_j driving Z_i and the remaining POs. Similarly, $\psi_{Zi}=0$ denotes that all wires of P_j drive Z_i and the remaining POs. For the adjacency vectors of the remainder R_3 in Figure 6, $A_{Z1}=[1\ 1\ 1\ 0]^T$, $A_{Z2}=A_{Z3}=[0\ 1\ 1\ 1]^T$, we find $\psi_{Z1}= \|\ ([1\ 1\ 1\ 0]^T \oplus [0\ 1\ 1\ 1]^T)\ \| = 2$ and $\psi_{Z2} = \psi_{Z3} = \|\ [0\ 1\ 1\ 1]^T \oplus [0\ 1\ 1\ 0]^T)\ \|=1$. Primary output Z_1 is extracted and the remainder R_3 is partitioned into $R_3^e=\{Z_1\}$ and $R_3^r=\{Z_2,Z_3\}$ as illustrated in Figure 7. Perturbation region P_3^e consists of wires $\{x_1^*,x_4^*,x_8^*\}$ and perturbation region P_3^r of wires $\{x_4^*,x_8^*,x_9^*\}$. Applying the same concept on remainder R_3^r, the final circuit is shown in Figure 8. It is composed of 13 2-input gates on 4 levels with a maximum fanout of 3.

By inserting M_j, redundancy may be introduced in the previously synthesized permissible mutation subcircuits M_i ($1 < i < j$) as well as in the remainder R_j. We postpone redundancy removal until the optimization procedure terminates.

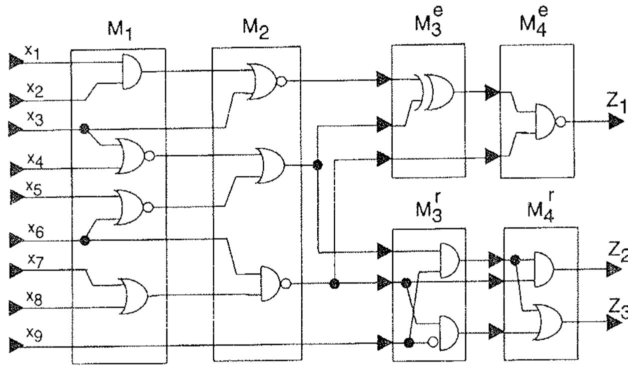

Fig. 8 Final synthesized multi-output circuit

4 Experimental Results

We have implemented the wave synthesis algorithm as a program WASP in Programming Language C and run it on Sun SPARC 10 workstation. In this section, we report our experimental results obtained with the circuits from the Benchmark set from /10/.

In Table 1, we compare WASP results to the results obtained with SIS, using the commands from script algebraic. The initial benchmark circuits exist in the multi-level form or in the minimum two-level representation (circuits market with p). Since the final, technology-independent circuits generated by WASP consist of 2-input nodes, we used command xl_split-n2 for the SIS generated circuits to split any logic nodes with more than 2 inputs into 2-input gates. For all circuits, we then report the number of 2-input nodes, logic levels and the maximum fanout. The results are summarized in Table 1. We have improved the number of 2-input nodes for 15.64%, number of logic levels for 5.08% and the maximum fanouts for 23.01%. This confirms that the presented algorithm for logic optimization optimizes the area and the maximum fanout by in general any additional increase of the delay.

5 Conclusions

In this paper, we have introduced the concept of wave synthesis for optimization of digital circuits. The premise of the proposed concept is exploiting permissible perturbations evaluated for wire pairs within the perturbation regions. Given a set of permissible functions associated to any pair with permissible perturbations, permissible mutation subcircuit of the lowest cost is synthesized and inserted into the nominal circuit. The

Table 1: Comparison of technology-independent circuit

Circuit Name	Inp. Nmb	Out. Nmb	SIS			WASP		
			Gates	Levels	Fanout	Gates	Levels	Fanout
cm82a	5	3	13	5	3	12	5	3
$rd53^p$	5	3	34	6	8	22	7	4
cm138a	6	8	20	4	8	20	4	8
$rd73^p$	7	3	59	10	8	44	9	4
z4ml	7	4	18	9	3	18	8	3
inc^p	7	9	100	9	19	94	10	13
$5xp1^p$	7	10	94	10	15	75	9	12
$rd84^p$	8	4	61	14	6	49	10	3
$misex1^p$	8	7	49	7	7	50	7	8
$clip^p$	9	5	99	10	14	88	11	13
$sao2^p$	10	4	128	12	17	108	13	14
x2	10	7	42	7	9	37	7	8
cm85a	11	3	36	6	5	26	8	3
t481	16	1	27	9	4	15	4	1
Total			780	118	126	658	112	97
Improvement [%]			Gates: 15.64		Levels: 5.08		Fanout: 23.01	

proposed approach is feasible for single and multi-output circuits. Experimental results on the benchmark circuits demonstrated the proposed method by optimizing circuits in terms of area and wiring.

References

/1/ G. De Micheli. Synthesis and Optimization of Digital Circuits. McGraw Hill, New York, 1994.

/2/ S. Muroga, Y. Kambayashi, H. C. Lai, and J. N. Culliney. The Transduction Method - Design of Logic Networks Based on Permissible Functions. IEEE Transaction on Computer Aided Design, 38(10):1404-1424, October 1989.

/3/ M. Damiani and G. De Micheli. Don't Care Set Specifications in Combinational and Synchronous Logic Circuits. IEEE Trans. on Computer-Aided Design, CAD-12(3):365-388, March 1993.

/4/ K.-T. Cheng and L. A. Entrena. Multi-Level Logic Optimization By Redundancy Addition and Removal. In European Conference on Design Automation, pages 373-377, 1993.

/5/ L. A. Entrena and K.-T. Cheng. Sequential Logic Optimization By Redundancy Addition and Removal. In International Conference on Computer Aided Design, pages 271-276, 1993.

/6/ S.-C. Chang and M. Marek-Sadowska. Perturb and Simplify: Multi-level Boolean Network Optimizer. In International Conference on Computer Aided Design, pages 2-5, 1994.

/7/ A. Žemva and F. Brglez. Detectable Perturbations: A Paradigm for Technology Specific Multi-Fault Test Generation. In VLSI Test Symposium, pages 350-357, April 1995.

/8/ SIS -Release 1.2. UC Berkeley Soft. Distr., July 1994.

/9/ R. Kužnar, F. Brglez, and B. Zajc. Multi-way Netlist Partitioning into Heterogeneous FPGAs and Minimization of Total Device Cost and Interconnect. In ACM/IEEE 31st DAC, pages 238-243, June 1994.

/10/ Logic Synthesis Benchmarks, 1994 Available under Benchmarks at http://www.cbl.ncsu.edu/www/. For autoreply about benchmarks, send e-mail to benchmarks@cbl.ncsu.edu.

Dr. Andrej Žemva, dipl.ing.
Prof. Dr. Baldomir Zajc, dipl.ing.
Faculty of Electrical Engineering
Tržaška 25, 1000 Ljubljana, Slovenia
Tel.: +386 61 176 83 46
Fax: +386 61 126 46 30
E-mail: andrej.zemva@fe.uni-lj.si

Prispelo (Arrived): 24.4.1997 *Sprejeto (Accepted): 6.5.1997*

INFRARED SPECTROSCOPY AS ANALYSING TOOL FOR MATERIALS USED IN MICROELECTRONICS 2. Thin films

Marta Klanjšek Gunde
National Institute of Chemistry, Ljubljana, Slovenia

Keywords: materials for modern technologies, infrared spectroscopy, microelectronics, thin films. IR beams, infrared beams, LO modes, Longitudinal Optical modes, Berreman effect, IRE, Internal Reflection Element, ATR, Attenuated Total Reflection, MNOS, Metal/Si-Nitride/Oxide/Semiconductor materials, Metal/Insulator/Semiconductor material, PECVD, Plasma-Enhanced Chemical Vapour Depositions, epitaxial layers, SiO_2, silicon oxides, silicon nitrides, a-Si, amorphous silicon, PSG, phospho-silicate glasses, BPSG, boro-phospho-silicate glasses, fluorinated-silica glasses, semi-insulating polycrystaline silicon, aluminium oxides, aluminium nitrides, strontium titanates, gallium nitride, superlattice, multilayer materials

Abstract: The application of infrared spectroscopy to analyse thin solid films used in modern technology devices has been reviewed. A variety of problems related to chemical bonding and morphology are possible to solve for amorphous, polycrystalline, and crystalline films as well as for low-dimensional structures. Determination of the sort and amount of dopants is now routinely applied to control the technological process. Together with relevant scientific hypothesis and with others appropriate characterisation methods, infrared spectroscopy may be efficiently used in research and development in material science.

Uporaba infrardeče spektroskopije pri analizi materialov za mikroelektronsko industrijo 2. Tanke plasti

Ključne besede: materiali v modernih tehnologijah, spektroskopija infrardeča, mikroelektronika, plasti tanke, IR žarki infrardeči, LO načini valovanja optični longitudinalni, TO načini valovanja optični transverzalni, Berreman efekt, IRE elementi notranji refleksijski, ATR refleksija totalna dušena, MNOS materiali kovina/Si-nitrid/oksid/polprevodnik, MIS materiali kovina/izolator/polprevodnik, PEVCD nanosi CVD plazemsko izboljšani, plasti epitaksialne, SiO_2 oksidi silicijevi, nitridi silicijevi, a-Si silicij amorfni, PSG stekla fosfor-silikat, BPSG stekla bor-fosfor-silikat, stekla fluor-silikat, silicij polikristalni pol-izolatorski, oksidi aluminijevi, nitridi aluminijevi, titanati stroncijevi, nitriti galijevi, superkristali, materiali večplastni

Povzetek: Članek predstavlja pregled uporabe metod infrardeče spektroskopije za analizo tankih plati, ki se uporabljajo v modernih tehnologijah. Mogoče je rešiti različne probleme, ki so povezani s kemijskimi in strukturnimi lastnostmi v amorfnih, polikristalnih in monokristalnih tankih plasteh, pa tudi v strukturah s kvantnimi dimenzijami. Določanje vrste in vsebnosti dopantov se že rutinsko uporablja za spremljanje in morebitne korekcije v tehnološkem procesu. Z ustreznimi znanstvenimi hipotezami in skupno z drugimi analiznimi metodami lahko infrardeča spektroskopija nudi odlično pomoč praktično na vseh nivojih raziskav in razvoja materialov.

I. INTRODUCTION

In this paper the application of infrared (IR) spectroscopy to analyse most frequently used microelectronic materials is considered with special attention to the recent literature. In the first part, the semiconductor substrates were discussed /1/. In the second part (present article), IR spectroscopy of thin solid films deposited or formed on such substrates is reviewed. The literature published in 1990 and later is considered mostly.

Thin films are one of the crucial components of the microelectronic and other modern technology devices. To ensure high yield of devices, the films must satisfy a large set of chemical, structural, and electrical requirements. Film composition and thickness have to be strictly controlled. Defects and imperfections present in these films are critical for small device geometries, therefore their densities have to be low. Excellent adhesion, low stress, conformable step coverage, and appropriate surface topography are demanded /2/. A large variety of films are used for this purpose. They can be metals, semiconductors, or insulators. They may be crystalline, polycrystalline, or amorphous. They may have high density or they may be porous.

The formation of such films is accomplished by a large variety of techniques that can be divided into two groups: (a) film growth by interaction of a vapour-deposited species with the substrate material; and (b) deposition of film without causing changes to the substrate. The first category includes thermal oxidation and nitridation of single crystal silicon, formation of silicides by direct reaction of a deposited metal and substrate /2/, as well as electrochemical etching that forms porous layers (e.g. porous silicon, /3/). The second group includes three subclasses: chemical vapour deposition (CVD), physical vapour deposition (PVD) and coating of the substrate with liquid, which is then dried to form the solid thin film. By the CVD process single crystal thin films (epitaxy), amorphous, or polycrystalline films may be formed. The PVD includes sputtering, evaporation, and molecular beam epitaxy (MBE). For the coating of substrate with liquid, most common the spin-coating technique is applied /2/.

The crystallographic structure of prepared thin films can vary from a highly disordered (amorphous) state to a well-ordered (e.g. epitaxial growth on a single crystal substrate). Dielectrics are frequently observed in amorphous state, while most metals result in polycrystalline structure. Silicon films can be amorphous, polycrystalline, or single crystal, depending on the deposition temperature and on the substrate material /2/.

The properties of thin films are closely related to their chemical composition, material structure, order, and method of preparation and may be substantially different from those of the corresponding material in bulk. For extensive characterisation of films, a non-destructive method is desired to apply. Such demands are fulfilled by optical techniques. Among them, IR spectroscopy is potentially the ideal one for characterising thin films. It is especially essential if the nature of chemical bonds at the surface or at some interface have to be understood, where any sample preparation may induce serious artificial effects.

IR spectroscopy has been used to solve a variety of structural problems for amorphous, polycrystalline, and crystalline films and to investigate the dependence of the film structure upon the deposition parameters. The greatest volume of work was performed for silicon and silicon-containing films /4-7/.

II. THEORETICAL BACKGROUND

The spectroscopic characterisation of thin solid films and surfaces includes analysis of their chemical composition, concentration of impurities, film thickness, or/and concentration profiles. For conducting layers the properties of free electrons or holes in some cases can be determined also. The analyses are based on spectroscopic measurements of the contribution of vibronic excitations and of free carriers to the dielectric properties of the sample: the frequency dependent dielectric function includes informations about molecular vibrations and about conduction electrons. IR spectroscopy is used mainly for films that contain metal-hydrogen or metal-oxygen bonds that absorb in the mid IR spectral region. Structures of films with metal-hydrogen or metal-metal bonds or heavier oxides have IR absorptions that fall in the far-IR and can be studied by far-IR spectroscopy and Raman spectroscopy.

The goal of the successful spectroscopic analysis is to apply the optimised optical conditions of the sampling technique to obtain unambiguous data also on very thin films or on multilayered structures. Therefore, many diversified techniques to observe spectra for many configurations of the sample have been developed. Polarised and unpolarised beams may be applied with optionally chosen incidence angle. The interpretation of obtained spectra has become more and more complex especially if extracted data are expected to be very precise and as complete as possible. Samples required in modern technology applications usually include silicon in monocrystalline, polycrystalline, or amorphous forms. Their high refractive indices cause a considerable reflection of the IR beam on each surface boundary. In thin films ($d \approx \lambda$) the observed spectral features are not only due to the nature of the dielectric function, but interferences of the partial waves reflected at the surface and/or interfaces of the layers also occur. The so-called Fabry-Perot fringes carry informations about optical constants and thickness of the layer. The interference fringe patterns obscure the baseline, impede detection of weak peaks, and alter the intensity. The broad region where anomalous dispersion in refractive index of dielectric materials takes place, shifts the position of IR absorption bands and additionally changes their shapes and intensities. All effects act simultaneously and cause strongly pronounced optical effects in IR spectra of such samples. It is well known that optical theory can predict or eliminate these effects from certain spectra /8-11/.

III. SAMPLING TECHNIQUES

Avariety of techniques are available for obtaining IR spectra of different thin solid supported films. The choice of sampling technique depends on the type of the sample and on the information desired from the analysis. In the following, some more pertinent techniques for thin film analysis are described briefly. Essentially the same techniques are used as described in the previous paper /1/. To apply them on thin films and multilayers, some modifications have to be done.

III.1. Transmission

The transmission experiment is the most familiar to anyone who uses IR spectroscopy on a routine basis. During measurements, the light passes through the sample, and its absorption from the entire thickness of the film (multilayer, superlattice) and of the substrate is measured.

The substrate must be transparent or low-absorbing so that a portion of light lost due to absorption and/or scattering on them is small. Typical substrates for transmission work in the mid IR spectral region are polished crystal discs made of alkali halides (e.g. KBr, NaCl, KCl). For the modern technology applications it is of much importance, that low-level doped silicon and GaAs slices are also suitable for this purpose.

Transmission studies are used for dielectric films with thickness on the order of μm that have been deposited on transparent or semitransparent substrates. The thickness restriction is due to overdamping of intense absorption lines.

Routine quantitative analysis of transmittance spectra of thin supported films are made from their negative logarithm (i.e. absorbance spectra). The intensity diminish due to absorption in the substrate is account for by subtraction of the corresponding absorbance spectrum (Figure 1). It is assumed that the absorption bands in the so obtained spectrum are proportional to the absorption coefficient of respective vibration, concentration of the corresponding species, and optical path length (Beer-Lambert law). The approxima-tion neglects the effects of refractive index as well as all optical effects. It is routinely used for organic materials where absorptions are small, although some errors are still introduced. In precise work especially with inorganic

materials, the more complex analytical methods of chemometrics have to be applied /6/. Another possibility is to apply optical theories to account for optical effects that are strongly pronounced in spectra of these samples /8,9,11,12/. In some situations this is the only way to minimise the error of quantitative analysis.

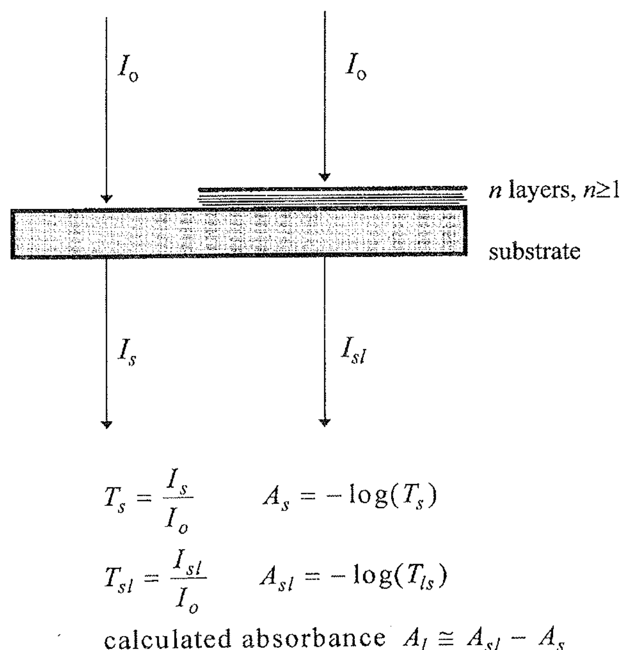

Figure 1. Normal incidence transmittance (T) measurement of the substrate (index s) and of n layers deposited on them. Absorbance (A) of the unknown layer (index l) is obtained by subtraction of the corresponding data for the known composition. Example for one layer (n=1).

In spite of all sorts of problems, the most simple transmission technique is very important. Before the extensive use of computers, the studies reported in the literature were done more or less only by the simple transmission measurement and even today studies using this approximate method are often reported. It is used especially to identify the basic chemical composition of the film. Many times it is the most convenient method to follow the changes in sample materials after some process (e.g. thermal annealing) qualitatively. By this procedure, very recently some small changes in spectra of superlattices were measured /13, 14/.

III.2. External reflection

When a one- or multilayered structure is deposited on a reflective substrate, the reflection of the IR beam from the sample may bear worthy information about its optical properties. If the incident and reflected beams lie outside the sample, the method is called the external reflection. Due to high refractive indices, silicon as well as III-V compound materials have considerable reflectance even in low-level doped form. Increasing doping, the reflectance of slices is increased further. Therefore, the semiconductor substrates are appropriate reflective substrates for external reflection spectroscopy to be performed. Additional possibility to apply external reflection for thin films analysis are the metal layers used in various types of MOS devices. For the impinging light, these layers act as reflecting mirrors. For that reasons, the external reflection is relevant analysing method for most films used in microelectronic industry.

There are many ways to measure the external reflection of thin solid supported films. All of them measure the specular reflectance obeying Snell's laws. Optionally polarised beam impinges on the sample at a certain angle. The radiation passes trough the sample until it reflects on the reflective surface somewhere inside the sample. Then, the beam returns trough the sample towards the detector (Figure 2.). By increasing number of reflections on the upper surface of the sample, the sensitivity of measurement can be further increased (see /1/, Fig. 5.).

For films thicker than the wavelength (2.5 - 25 μm for the whole mid IR), the intensity of the reflected light is similar to that of the transmitted light trough the sample with an twofold effective pathlength. In such cases the term reflection-absorption spectroscopy (RAS) is usually used to describe the experiment.

For thinner films, the absorption of the radiation inside the sample will be strongly influenced by the reflecting surface, by the polarisation of the incoming radiation, by the incident angle, and by the orientation of dynamic dipoles inside investigated material with respect to the reflective surface. The polarisation of the incoming radiation influences the intensity of absorption. Most intensity is collected in the component that is polarised parallel to the plane of incidence, whereas the contribution of the perpendicular component is very small. The absorption of light inside thin film reaches its maximum when the incident angle is about equal to the Brewster's

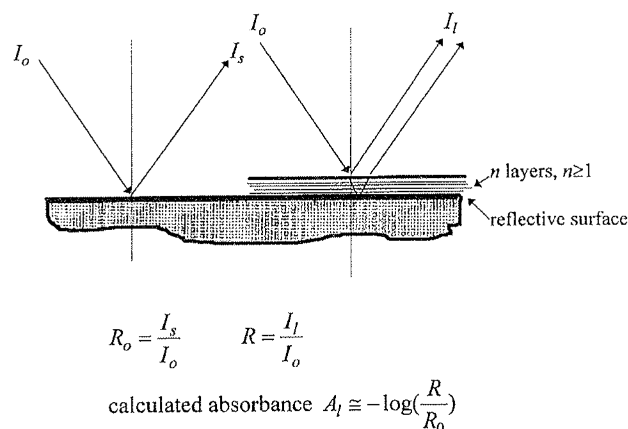

Figure 2. External reflection measurement of substrate (index s) and layers deposited on them (index l). Any incident angle and polarisation of the incident beam may be applied. Absorbance of the unknown layer is obtained as negative logarithm of layer reflectance that was normalised by the reference reflectance.

angle for the reflective material. For metals, this angle is very large (~90°), whereas for silicon smaller incidence angle is preferable (~60°). The largest angle that can be obtained experimentally, is about 85°. When the experiment is performed at this largest angle, the term near grazing incidence angle reflection spectroscopy (NGIA) is used.

External reflection spectroscopy of molecules that were adsorbed on metal surface was formulated 30 years ago /15/. It gained full advantage of increasing sensitivity by parallel polarisation and near grazing incidence angle. The experimental conditions together with the optical consideration of the three-phase system leads to the so-called metal surface selection rules that can be used to determine the orientation and molecular ordering at the surface /16/. A small blue shift of the adsorbate band maxima respect to the corresponding bands in transmission was thought to be due to optical effects inherent in the experiment.

For inorganic thin films, that are extensively used in modern technologies, the most important is the so-called "Berreman effect" /17/. He made an experiment with very thin (<2 μm) crystal films, deposited on metallic substrates. The component of the beam polarised normal the film (parallel to the plane of incidence), causes absorption bands at frequencies of the zeros of film dielectric function. These are the frequencies of the longitudinal optical (LO) polar modes. They depend strongly also upon intrinsic material properties, e.g. the effective charge and mass of all species participating the corresponding mode, dielectric properties of the surroundings etc. /18/. The Berreman effect is an macroscopic phenomenon of electrodynamics and offers the possibility of an precise analysing tool for very thin dielectric layers. However, the interpretation of the results is substantially different from measurement in transmission. In polar materials the band frequencies appearing in both experimental configurations are much apart so that the difference can not be described as a "small blue shift" as it is relevant for organic adsorbates. Furthermore, only some factors affecting absorption frequencies obtained in transmittance and in external reflection of parallel polarised light are the same. For all these reasons, the full understanding and interpretation of measured spectra also for thicker layers, other polarisation, incidence angles and substrates was not performed until recently when various spectral simulations with extensive computer support were accomplished /19-21/.

III.3. Internal reflection

In internal reflection spectroscopy, the incident radiation is reflected from the interface between a material with higher refractive index and a material with lower refractive index as shown in Figure 3. The higher refractive index material is called internal reflection element (IRE) and is cut to a specific geometry. In microelectronic applications, the semiconductor sub-strate (low-level doped silicon or III-V compound materials) usually represent an IRE. The material to be sampled (single layer or layered structure) is coated directly on IRE.

For total internal reflection, the incidence angle must exceed the critical angle. In this circumstances, the lower refractive index material is probed by that portion of radiation (called the evanescent wave) that passes trough the boundary of the IRE crystal surface. The evanescent field is characterised by refractive indices of the two materials, incident angle, state of polarisation, and upon the wavelength of the beam in the IRE crystal. However, the decay of this field inside the optically rarer medium (its penetration depth) is independent upon the polarisation. The obtained spectrum is similar to a transmission spectrum. The method is often called attenuated total reflection (ATR).

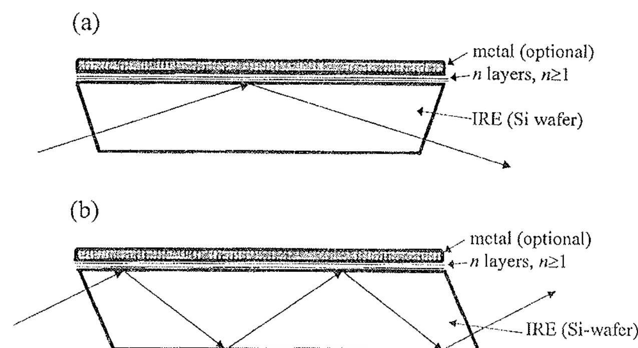

Figure 3. Internal reflection experiments with one reflection (a) and two reflections (b). For more experimental configurations, see /1/, Fig. 6.

Internal reflection spectroscopy is especially useful for films that are too thin for the spectrum to be measured in transmission. In microelectronic and photovoltaic systems as metal/oxide/semiconductor (MOS), metal/Si-nitride/oxide/semiconductor (MNOS), and metal/insulator/semiconductor (MIS) are of interest. In those systems a very thin oxide interlayer between M and S has to be characterised. In an IR experiment, the interlayer is illuminated via polished areas of the border of the Si-wafer that acts as an IRE (Fig. 3). In the oxide film, absorption of the IR light due to vibronic resonances is only possible for p-polarisation (parallel polarisation) where it is still amplified by the metal film (M). By this configuration, the 1.3 nm thick oxide on silicon within a MIS structure was measured /22/ (see also Fig. 3).

Various experimental configurations of internal reflection spectroscopy appearing in the recent literature /23-25/ are essentially ATR experiments. Among them, there is also excitation of surface polaritons, called also surface electromagnetic waves (SEW). The echo from the back of the thin layer can be avoided by residual vacuum gap of nm range between a sample and IRE (Otto geometry). The later method is not always possible to perform.

By the ATR measurements, the optical depth of the material may be profiled. The method makes use of angle-dependent penetration depth of evanescent wave /26/. The procedure represents one possibility to detect and analyse the depth-dependent composition of films.

IV. EXAMPLES

A large variety of films used in modern technologies represent relevant measurable samples for IR spectroscopy. Metal layers can not be analysed but they may play an important role in using some of the reflection techniques. All other type of films can in principle be analysed in terms of their intrinsic properties such as chemical composition, structure, order, free charge carriers, thickness, etc.

The examples of IR spectroscopy application for thin films are divided in representative groups as epitaxial layers, silicon oxide films, silicon nitride films, amorphous silicon, various glass-type films, other films, multilayers, heterostructures, and superlattices.

IV.1. Epitaxial layers

Epitaxial layers are grown on a surface of a single crystal substrate whereas its crystallographic orientation is retained. Therefore, epitaxial layer is an extension of a substrate. In homoepitaxial layers, the layer and the substrate are the same material such as silicon on silicon. Heteroepitaxial layers are made from different materials, such as silicon on sapphire or mercury-cadmium-telluride on cadmium telluride /27/. The most interesting property of epi-layers is that they can be doped to a different extent than the substrate.

Most epi-layers used in production environment are produced by CVD process involving silane halides, whereas MBE growth technique is used mostly for the research and development. Many factors of a finished devices depend upon the exact thickness of the epi-layer involved. The measurement of epi-layer thickness by the IR interference method is known from 1961 by Spitzer and Tanenbaum /28/ where the basic requirements for the interference fringes to be seen in the external reflection spectrum are defined. There has to be a suitable spectral range in which the epi-layer is transparent. Provided that on the interface between the epi-layer and the substrate the impurity concentration suddenly changes, the incident radiation will be reflected both at the surface of the epi-layer and at the interface. Since the waves transverse the layer, these so-called Fabry-Perot fringes carry information about layer thickness as well as about its optical constants. The onset of the fringes will occur at a wavelength governed by the carrier concentration of the heavily doped substrate. The spectra are measured by external reflection technique using unpolarised IR beam at normal incidence /27, 28/. To increase the sensitivity of the method, oblique incidence of polarised beam may be applied /5/.

For the method to be applied for homoepitaxial Si layers, the substrate resistivity has to be less than 0.02 Ωcm (at 23°C) and the resistivity of the epi-layer more than 0.2 Ωcm (at 23°C). In these circumstances, the technique is capable of measuring the thicknesses of both n- and p-type layers greater than 2 μm thick. With reduced precision the technique may also be applied to both n- and p-type layers from 0.5 to 2 μm thick. The external reflection spectra of some homoepitaxial Si layers are shown in Figure 4.

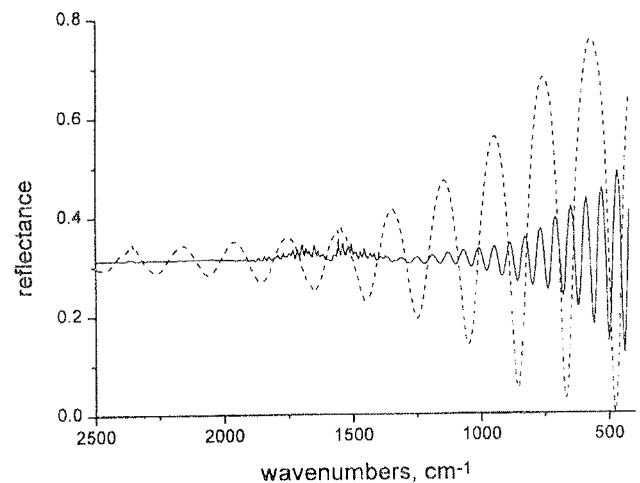

Figure 4. External reflection spectra of two silicon homoepitaxial layers.
full line: substrate: 0.015 Ωcm, Sb-doped, n-type,
epi-layer: P-doped, n-type, 1-6 Ωcm, measured thickness 23.4 μm
dashed: substrate: 0.002-0.004 Ωcm, As-doped, n-type,
epi-layer: P-doped, n-type, 2.0-2.4 Ωcm, measured thickness 7.2 μm

By the same technique, the thickness of the heterostructures of III-V semiconductors epitaxially grown on GaAs substrate were measured. Simultaneously, the diffusion profile in epitaxial Si-layers were studied /5/.

IV.2. Silicon oxide films

Silicon oxide films are one of the most crucial films for the microelectronic industry. Their ability to form highly passivating, stable, and insulating films represents the basis for planar processing of silicon integrated circuits.

Silicon oxide is the simplest form of glass and appears also in most mixed glasses. Therefore, the study of its properties may help in understanding the whole group of materials. Silicon oxides fabricated in the laboratory condense into amorphous solids noted by SiO_x. If x=0 we have amorphous silicon and if x=2 the silicon dioxide was formed. The structure of amorphous layers compose of statistical mixture of $Si\text{-}(Si_yO_{4\text{-}y})$, y=0,1,2,3,4 tetrahedra. The final structure represents a three-dimensional random network where some of the tetrahedra joins to each other by an oxygen ion. This ion is called bridging oxygen and is shared between two touching polyhedra. In the crystalline SiO_2, all oxygens are bridging oxygens. The greatest the ratio of bridging to non-bridging oxygens in amorphous form, the better the cohesiveness of the glass /2,29/.

IR spectra of silicon oxide films can be obtained as absorbance spectra recorded in normal incidence transmission (see Figure 1). As deposited silicon oxide films are different by the stoichiometry, as well as by the porosity and bonded impurities. In Figure 5, absorbance spectra of thermal oxide and of two differently

formed CVD silicon oxide layers are shown /30/. Beside strongly pronounced vibration of bridging oxygen in SiO_4^- random network tetrahedra, also vibrations due to other species in films (e.g. SiOH, Si_2O_3, H_2O) are obtained. By thermal annealing at temperatures above 800°C for 10-15 min, densification of layers is complete and absorbance spectra of all silicon oxide films are indistinguishable from each other and from the thermal oxide which is SiO_2 /30/.

This simple form of IR analysis was frequently used to study the properties of various silicon oxide films /31,32/ also if they were very thin /33,34/. For precise analysis and to extract more data from measured spectra, optical effects have to be taken into account /35,36/. Applying optical analysis it was shown that the position of absorption peak due to asymmetrical stretching vibration of Si-O-Si bond may acts as an detector of differences among films: increasing the annealing temperature yields to stronger bonds in the oxide structure /37,38/.

To increase the sensitivity for very thin films (d<100nm), oblique incidence angles or some of the reflection techniques using polarised IR beam may be applied. This way the structural nature of the Si/SiO_2 interface was studied /39-43/. These analyses are important to understand the properties of the so-called conduction channel formed at this interface.

IV. 3. Silicon nitride films

In recent years, special attention has been devoted to the use of silicon nitride in semiconductor device technology, since it can be used safely for interlayer isolation, device passivation, and mechanical protection /44/.

The most important method to produce silicon nitride thin films is plasma-enhanced CVD (PECVD) that enables the formation of thin film dielectrics at low temperatures (200-500°C). PECVD silicon nitride films tend to be nonstoichiometric what is chemically represented as $Si_xN_yH_aO_b$ with a and b being much less than x and y. The IR absorbance spectrum of such film obtained by transmission measurement (see Fig. 1) is represented in Figure 6. The main absorption region (750-950 cm^{-1}) is dominated by the antisymmetrical stretching mode of the Si-N-Si molecular group. The symmetrical stretching of the same molecular group leads to the much smaller band at 490 cm^{-1}. An appreciable amount of hydrogen in the form of Si-H and N-H bonds is recorded at 2170 and 3340 cm^{-1}, respectively. A small band due to Si-O vibration is found at 1160 cm^{-1}.

The changes in position, shape, and intensities of absorption bands were observed at various preparation ways as well as after heat treatments. These changes are possible to relate to the properties of local environment of the constituent atoms and hence to the molecular structure of the layer. Such data may lead to conclusions about important intrinsic properties as follows: stoichiometry, identification of densification or structural loosening of the film, passivating the dangling bonds of silicon and nitrogen (these are the principal source for the localised gap states), reduction of mechanical strain within the network etc. /44/. The studies may be performed applying the normal incidence transmission /45/ or some of reflection techniques /46, 47/.

The ultrathin silicon nitride film (0.4<d<4 nm) deposited on a top of 1.3 nm thick silicon oxide film thermally grown on crystalline silicon was analysed. For this purpose, the internal reflection at grazing incidence (due

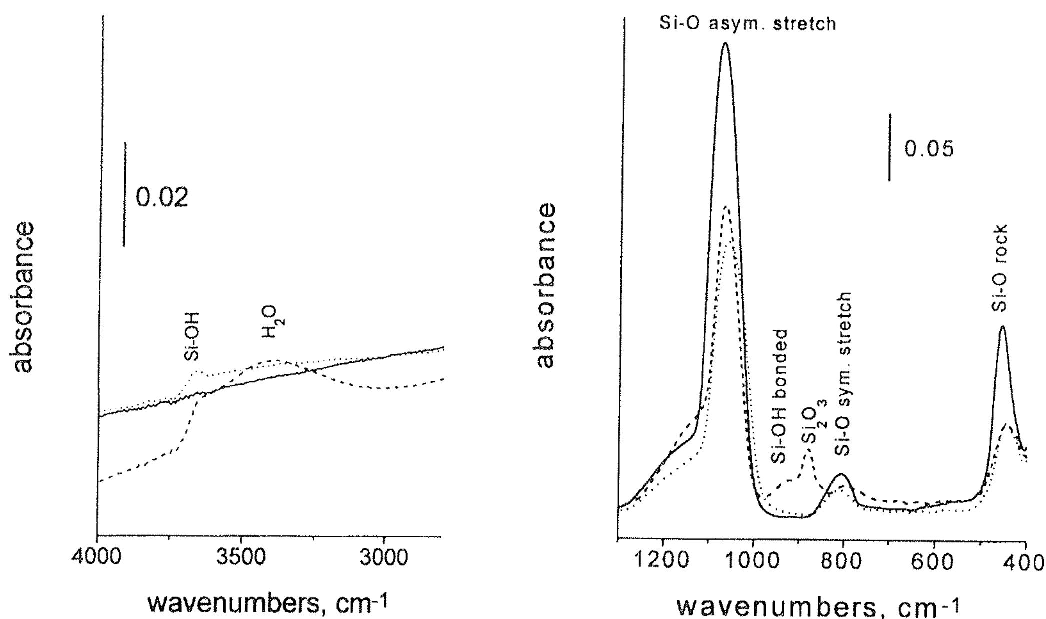

Figure 5. Absorbance spectra of as-deposited silicon oxide films formed by thermal oxidation (full line) and by CVD process (broken line, points). Thermal oxidation was performed in the diffusion owen at 750°C, the deposition rate was 0.19 nm/min and the layer thickness obtained is 114.4 nm. Data for CVD oxides: broken line: O_2:SiH_4=1.5, deposition at 160°C, 3.5 nm/min, final thickness 221.2 nm; points:O_2:SiH_4=3, deposition at 355°C, 20.1 nm/min, final thickness 168.1 nm

to metallized rear side) was applied to analyse the vibrational properties of the sample. During the direct-plasma-enhanced CVD of nitride film, the ultrathin silicon oxide layer changes due to ion bombardment. Applying the remote-plasma-enhanced CVD, this damage process did not occurre /46/.

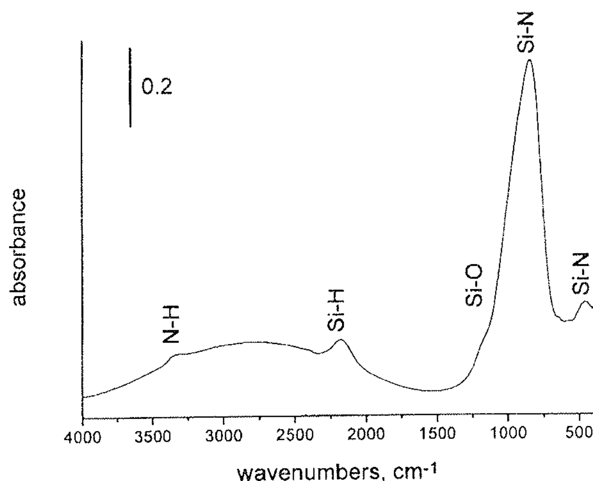

Figure 6. Absorbance spectrum of PECVD silicon nitride film. A radial flow reactor operating at 300°C was used. Reactant gasses were N_2, NH_3, and SiH_4 at gass flow rates of 735, 405, and 173 cm^3/min, respectively. The film thickness is 0.945 μm. The spectrum was obtained by the normal-incidence transmis-sion method. The origin of absorption lines is noted in the figure. The broad absorption is due to interference in the film.

The resist pattern deformation in chemical amplification resists on SiNx layers were observed. Applying the ATR technique, the Si-OH surface groups were found to cause the pattern deformation /47/.

One of the most interesting publication is the analysis of silicon nitride which forms occasionally and can not be etched in concentrated HF. The authors analysed the 10 μm diameter nitride spot. By the help of IR spectroscopy, they were able to conclude, that this unintentionally formed etch-resistant silicon nitride has the crystalline structure /48/.

The results obtained from IR spectra may be defined precisely if optical effects were taken into account. It is well known that these effects may change the position, intensity, and shape of absorbance lines in spectra of thin films. The most prominent are changes due to film thickness /9/. Optical analysis of silicon nitride /49/ and silicon oxynitride /50/ films can be found in the recent literature.

IV.4. Amorphous silicon films

IR spectroscopy can be used to study a variety of problems related to chemical bonding and morphology in amorphous silicon films. In crystalline films, absorption bands are sharper and more resolved. Some of them may split due to crystalline phase. In most work, the main region of interest is incorporation of hydrogen. There are several IR absorptions caused by hydrogen in amorphous silicon. An example is shown in Figure 7. These bands enables an insight into homogeneity, morphology, long-term stability, structural defects etc. Among all absorptions appearing in the absorbance spectrum of hydrogenated amorphous silicon, the most frequently studied spectral region is 2200-1800 cm^{-1} where the silicon-hydrogen stretching vibrations occur. This way the source of light-induced changes in the optical properties of hydrogenated amorphous silicon were measured. These changes are one of the key properties that determines the durability of solar cells made of amorphous silicon. On the basis of the silicon-hydrogen stretching vibrations measured by ATR method, a reversible shift in the Fermi level after light illumination for 38 hours was observed /51/.

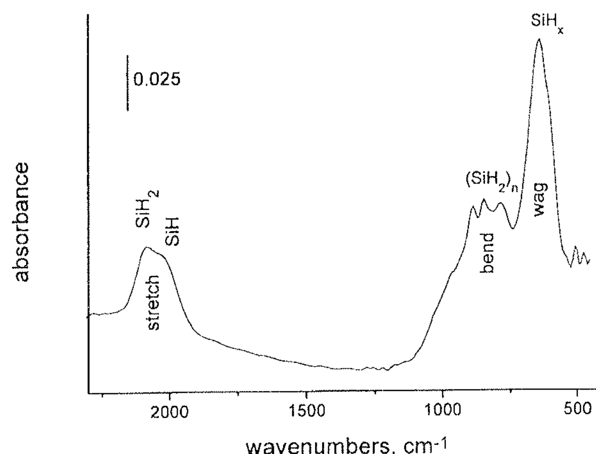

Figure 7. Absorbance spectrum of amorphous hydrogenated silicon film. ~300 nm thick film was prepared by magnetron sputtering.

Very recently, nucleation of amorphous hydrogenated silicon on the H-terminated surface of crystalline silicon was monitored by in situ near normal transmission spectra (11° incidence angle) /52/. The film thickness was measured simultaneously by the quartz crystal microbalance. For layer thickness from 4 Å up to 150 Å, the evolution of the bonding configuration in the SiH stretching mode region was followed. The absorption bands due to stretching modes of SiH, SiH_2, and SiH_3 bonds in each spectrum were deconvoluted. From obtained results the authors were able to conclude that the coalescence point of monohydride SiH bond clusters occurs at about 20 Å layer thickness.

IV.5. Doped silicon oxide films

Dielectric thin films of doped silicon oxide glasses have some important advantages over undoped glasses as in preventing diffusion of dopants into underlying layers, passivating device junctions, reducing film stress relative to pure SiO_2 etc. The films used for such purpose range in thickness from 0.5 and 1.0 μm. Another use of these films is to taper and planarise irregular device topographies.

Two most important doped silica glasses are **phospho-silicate-glass (PSG)** and **boro-phospho-silicate-glass (BPSG)**. In these films, phosphorus and/or boron oxides have been added into a silicon matrix in order to achieve desired film properties. The chemical, physical and electrical properties of PSG and BPSG films are determined by the dopant levels and film thickness.

PSG consists of two compounds, P_2O_5 and SiO_2 - therefore it is a binary glass (or binary silicate). Phosphorus acts to provide trapping sites for alkali ions and thus minimises impurity penetration. PSG can be flowed at high temperatures (1000-1100°C) to create a smoother surface topography /2/.

BPSG is a ternary oxide system (three component): B_2O_3-P_2O_5-SiO_2. In such films, boron plays an important role in lowering glass viscosity: by adding boron dopant into PSG glass, flow temperatures as low as 700°C can be obtained. Increase in boron concentration of 1 wt. % decreases flow temperature by 40°C, whereas an upper limit of boron concentration is deter-mined by stability: BPSG films containing over 5 wt. % boron tends to be very hygroscopic and unstable /2/.

Flow and reflow temperatures are critical for minimising vertical and lateral diffusion of dopants. For adequate maintenance of films, the (B,P) dopant contents and other critical parameters must be precisely controlled. Small changes in film composition and thickness may lead to significant changes in the thin film properties, especially film reflow temperature.

IR spectroscopy is the most common method to measure PSG and BPSG composition. Doped silicon oxide glasses are multicomponent oxide solids where the band absorptions may be overlapped by a considerable extent. Optical effects due to reflections on the reflective silicon wafer and due to inteferences within thin film are also present. All these complexities together complicate the quantitative analysis of spectra. For this purpose, univariate as well as multivariate calibration techniques for normal incidence transmission /6,53/ or external reflection /54,55/ measurements were developed. It was found, that in chemo-mechanical polishing, boron is more effective than phosphorus /56/. A simple method for quantitative and simultaneous determination of composition and thickness of BPSG films based on IR ellipsometry was described with precision of the order of 0.1 wt. % on thė boron and phosphorus /57/. All of these IR methods are based on measuring heights and/or areas of two absorption peaks for each component determination: net B-O (at ~1370 cm^{-1}) to total Si-O (at ~1090 cm^{-1}) for boron content, and net P=O (at ~1316 cm^{-1}) to total Si-O (at ~1090 cm^{-1}) for phosphorus content. Absorption bands due to B-O and P=O in BPSG films are highly overlapped and the various determination methods used throughout the literature differ to each other in a way how they account for this fact.

Another form of doped silica glasses used in microelectronic industry is **fluorinated-silica-glass (FSG)**. These films show the ability to reduce the dielectric constant while providing enhanced gap fill over undoped oxide films. All these properties are in close relation to the dopant concentration within the film: increasing fluorine content, the dielectric constant decreases and the gap fill improves. Fluorine dopant levels in FSG films is commonly determined by IR spectroscopy: the ratio of the Si-F peak (at ~937 cm^{-1}) area to the Si-O bond stretch peak (at ~1090 cm^{-1}) area is used to quantify the fluorine doping levels /58/.

IV.6. Other films

Several solid inorganic films are used in modern technologies. The most basic are made of silicon and silicon containing materials mentioned in previous chapters. In this chapter, the application of IR spectroscopy for some of the other materials having interesting properties for many potential applications is examined. In most cases, their investigation is still in progress.

Semi-insulating polycrystalline silicon (SIPOS) has many potential applications, e.g. as a resistive plate, as an active passivating layer, for SIPOS/Si heterojunctions, etc. Understanding the phenomena that determines SIPOS characteristics and how to design their material properties is still in progress.

SIPOS is a mixture of silicon and silicon oxide phases. The Si-phase can be amorphous or microcrystalline, depending on the oxygen content, anneal, and deposition temperature. The evolution of the micro-structure is strongly related to chemical composition.

Recently, the strong relationship between microstructure and electrical conduction mechanisms in SIPOS was studied /59/. Several techniques were used for this purpose as X-ray photoelectron spectroscopy (XPS), secondary ion mass spectroscopy (SIMS), IR spectroscopy, Raman spectroscopy, photoluminiscence, and electroluminiscence. By IR transmission at normal incidence, the presence of SiO_2 phase was followed. Thin SIPOS films were deposited by low-pressure CVD of SiH_4 and N_2O or SiH_4 and CO_2. As deposited materials were amorphous and may contain all five possible tetrahedra, from Si-Si_4 to Si-O_4, corresponding to the five possible oxidation states of Si. In low temperature annealed films (700-800°C), only tetrahedra of the extremes, i.e. Si-Si_4 and Si-O_4 were formed. At higher temperatures (790-1000°C) Si-nanoclusters and SiO_2 phase were formed /59/.

Aluminium oxide is an attractive material for microelectronics as well as for other applications. It has high chemical stability, high radiation resistance, high thermal conductivity, and very low permeability of alkali ions and other impurities. These properties depend upon deposition temperature and upon post-deposition heat treatment as it was reported for PECVD aluminium oxide films /60/. In this investigation, IR spectroscopy plays an important role: the chemical composition was possible to follow via functional groups such as Al-CH_3, Al-O, and O-H /51/. The most important is the possibility to detect the hydrogen bonds which are not detectable by Auger electron spectroscopy (AES) or by XPS. The concentration of hydrogen was followed by the area of O-H stretching mode in absorbance spectrum of corresponding sample /60/.

Aluminium nitride in a wurtzite crystal structure is a wide energy band gap semiconductor (6.2 eV) and has many valuable properties as high thermal conductivity, high electrical resistivity, high ultrasonic velocity etc.

There are many troubles in producing large areas of high quality AlN thin films. Dependence of material properties upon the deposition conditions were reported for ion-beam assisted deposition /61/. The most important factor that impacts the crystal quality is the stress in the film. A process-induced biaxial compressive stress in the plane of film as well as stress produced by differences in the thermal expansion coefficient among the substrate (Si(111)) and the film was examined. In IR absorbance spectra, only one peak was detected. As the ion-beam voltage employed during deposition was reduced from 200 V to 50 V, the spectral position of this transverse optical (TO) mode was shifted monotonically towards lower wavenumbers (higher wavelengths), approaching the TO mode value for bulk crystalline material. Simultaneously, the width of the peak was decreased and its intensity increased. All these results shows that decreasing the ion-beam voltage, the structural disorder decreases. Therefore, the authors concluded: to produce films approaching single crystal quality, the ion-beam voltages have to be the lowest possible.

Strontium titanate, $SrTiO_3$, is a very promising ferroelectric material for use in e.g. micro-size thin film capacitors, as a gate insulator for MIS field-effect transistors with extremely high carrier concentrations. For these applications, films with good crystallinity and high dielectricity have to be ensured. For these reasons, the correlation between IR spectra and temperature coefficient of the dielectric constant of $SrTiO_3$ thin films was studied /62/. 130-230 nm thick films were deposited on the Pt/MgO substrate by the rf-magnetron sputtering at various deposition temperatures (T_D) ranging from 350 to 710°C. IR absorption spectra were measured in external reflection mode. In obtained spectra, LO phonon modes associated with crystallinity of films were followed against T_D. A close correlation was found between dependence of the LO phonon modes upon T_D and the temperature coefficient of the dielectric constant. This is a well known phenomenon: the frequencies of the LO modes depend strongly upon dielectric properties of the medium /18/ (see also chapter III.2.).

Gallium nitride is one of the III-V compound materials with very interesting properties. As grown GaN is semi-insulating when grown in a hydrogen-rich ambient whereas in absence of hydrogen, it is a p-type conductor. The final properties of the layer are defined by the post-growth treatments whereas hydrogen play an important role.

Measuring normal incidence transmittance at cryogenic temperature, very recently the direct spectroscopic evidence of local vibrational modes of hydrogen with the shallow acceptors in Mg-doped GaN thin film (4 μm thick films, CVD deposited on double side polished sapphire substrate) was reported /63/. In spectra of undoped and Si-doped GaN, these local vibrational modes were absent. The authors concluded, that hydrogen is able to passivate Mg acceptors in these type films. This way they were able to answer the question as to whether the high resistivity of as-grown GaN:Mg arises from compensation of hydrogen passivation.

IV.7. Multilayers, heterostructures, and superlattices

The parallel-faced piles of layers used in modern technologies are named as multilayers, heterostruc-tures, or superlattices. Heterostructure consists of different materials (e.g. Ge and Si) whereas in multilayer the same material having different properties (e.g. different doping, different porosity etc.) may appear (homolayers). The name superlattice is used to point out the quantum-sized dimensions. For an electron, such layers form quantum wells and barriers between them. Due to tunnelling, minibands of allowed energies are formed in the superlattice. Such samples may be formed by carefully controlled deposition of atomic layers onto a crystal (MBE). Applying this procedure, quantum wells, quantum wires, or quantum dots may be formed, offering admirable possibility to tune the properties of the final material. The superlattice may have properties quite different from those of any naturally occurring materials. Throughout the literature, multilayer and heterostructure are used also for samples with low-dimensional (quantum) structures /22,64,65/.

In principle, an n-layers pile may be measured by each of three basic IR sampling techniques (see Figs. 1-3). In these experiments, many complications may appear. The coherent reflections and transmissions of the IR beam trough the multilayered stack may produce all sorts of optical effects. By suitable calculation procedure (matrix formalism), they may be taken into account /66,67/. When some of the layers are thick enough to support evanescent waves, it leads to the numerical instability. The solution of this problem was proposed /68/. Such calculations were applied in problems of optical gratings and the graded-index problem, but rarely in the field of IR spectroscopy. The reason for this may be the complexity of the problem.

If IR measurements are performed enough skilful, the interpretation of measured spectra will not be too complicated. The changes in selected part of the sample may be observed only, whereas the remainder may be taken as an reference. Some experimental techniques enable to select the vibrational modes that is to be monitored. Nevertheless, the interpretation of IR spectra of these complicated structures requires much more knowledge both from the field of optics and solid state theory. For more simple samples, such knowledge is not obviously required.

In MNOS structure, the concentration of hydrogen bonds in 12 nm thick silicon nitride layer was determined. For this purpose, the internal reflection spectroscopy at grazing incidence was applied. Despite of an ohmic Al contact, silicon wafer was used as an IRE /22/.

Conducting GaAs multilayers were analysed by external reflection spectroscopy at oblique and at normal

incidence angles. From spectral position of Fabry-Perot and Berreman structures, layer thickness and free carrier concentrations in them were obtained. In the procedure, the coupled LO phonon plasmon polaritons appearing in polar semiconductors were taken into account /65/.

A GaAs superlattice incorporating 50 carbon δ-doped layers (1 nm thick) with 50 nm superlattice periode was analysed by IR spectroscopy. High resolution (0.1-0.5 cm^{-1}) spectra were measured at ~10K in normal transmission mode. By IR localised vibrational modes due to hydrogen and carbon, the sites of the superlattice occupied by the carbon atoms were detected and their bonding properties were studied /13/.

The temperature and electric field dependence of the interminiband absorption in a doped GaAs/AlGaAs superlattice was monitored /14/. To measure IR trans-mittance of the superlattice during electric field pulses used to heat the electron system, a step-scan/time-resolved extension for spectrometer was applied.

IR ATR spectroscopy in the long-wavelenght region (far IR) was used to study the phonon parameters of a short period GaAs/AlAs superlattice /69/. By ATR spectroscopy in Otto configuration (sample is separated from IRE by a small gap), it is possible to excite the modes localised at a surface of superlattice (localised surface polaritons). In special cases, ATR can excite also surface modes on the superlattice-substrate interface. This can occur only just above LO frequencies of the superlattice or of the substrate. Guided wave polaritons are confined within the superlattice and may be excited in both polarisations. These modes together with polariton dispersion curves near the centre of first Brillouin zone helped the authors to analyse the parameters of the superlattice. IR measurements were performed at 77K with a resolution of 0.5 cm^{-1} /69/.

V. CONCLUSIONS

IR spectroscopy is an efficient non-destructive analysing tool for materials used in modern technologies.

It may be applied to determine the sort and amount of dopants in the investigated materials. Some of these analysis are used routinely in the technological process. These are determination of dopants in silicon wafers (interstitial oxygen, substitutional carbon, /1/) and dopants in doped silica glasses (P in PSG and P,B in BPSG). Amount of these dopants are crucial parameters for efficient fabrication of well-operated devices.

Other applications of IR spectroscopy are strongly connected with research and development. Here, IR spectroscopy may be used as purely analytical technique, offering an insight into the chemical properties of the sample. Connected to scientific hypothesis, and accompanied by other characterisation methods, the obtained data may be of great importance to the material scientists who are able to master the fabrication techniques to high sophisticated levels.

In the preparing the future of microelectronics and all other up-to date technologies, IR spectroscopy may play a considerable role. Provided that more and more knowledge about surface chemistry and chemistry of local environments, about optics, electromagnetics, and solid state theory will be incorporated, the role of IR spectroscopy may be more and more prominent. For the researchers, it is important due to all advantages of IR spectroscopy. Simultaneously, the important parts of Fourier-transform spectrometers (the source and detecting systems, interferometer, scanning mecha-nism, computing power, beamsplitters, polarisers etc.) are improving to so high level that they may fully support high demands of specialists applications.

VI. REFERENCES

/1/ M. Klanjšek Gunde, Informacije MIDEM, 27 (1997), 23-30

/2/ S. Wolf and R. N. Taubner: Silicon Processing for the VLSI Era, volume 1: Process Technology, Lattice press Sunset Beach, California (1986)

/3/ M. H. Ludwig, Crit. Rev. Sol. St. Mater. Sci. 21 (1996), 265-351

/4/ U. Techner and K. Hübner, Phys. Stat. Sol. (b), 159 (1990), 917-926

/5/ P. Grosse, Microchim. Acta, 11 (1991), 309-323

/6/ J. E. Franke and T. M. Niemczyk, and D. M. Haaland, Spectrochim. Acta 50A (1994), 1687-1723

/7/ A. Sassella, Adv. Mater. 8 (1996), 349-352

/8/ M. Klanjšek Gunde, B. Aleksandrov, Appl. Opt. 30 (1991), 3186-3196

/9/ M. Klanjšek Gunde, Appl. Spectrosc. 46 (1992), 365-372

/10/ M. Milosevic and S. L. Berets, Appl. Spectrosc. 47 (1993), 566-574

/11/ K. Yamamoto, H. Ishida, Vib. Spectrosc. 8 (1994), 1-36

/12/ K. Yamamoto, H. Ishida, Appl. Opt. 34 (1995), 4177-4185

/13/ B. R. Davidson, L. Hart, R. C. Newman, T. B. Joyce, T. J. Bullough, C. C. Button, J. Mater. Sci: Mater. Electron. 7 (1996), 355-360

/14/ W. Hilber, M. Helm, K. Alavi, R. N. Pathak, Appl. Phys. Lett. 69 (1996), 2528-2530

/15/ R. G. Greenler, J. Chem. Phys. 44 (1966), 310-315

/16/ H. Brunner, U. Mayer, H. Hoffmann, Appl. Spectrosc. 51 (1997), 209-217

/17/ D. W. Berreman, Phys. Rev. 130 (1963), 2193-2198

/18/ M. Klanjšek Gunde, disertacija, Univerza v Ljubljani, Fakulteta za matematiko in fiziko, Oddelek za fiziko (1996)

/19/ A. N. Parikh, D. L. Allara, J. Chem. Phys. 96 (1992), 927-945

/20/ J. A. Mielczarski, J. Phys. Chem. 97 (1993), 2649-2663

/21/ K. Yamamoto, H. Ishida, Appl. Spectrosc. 48 (1994), 775-787

/22/ R. Brendel, Appl. Phys. A 50 (1990), 587-593

/23/ P. Grosse, V. Offermann, Vib. Spectrosc. 8 (1995), 121-133

/24/ W. Offermann, P. Grosse, M. Feuerbacher, G. Dittmar, Vib. Spectrosc. 8 (1995), 135-140

/25/ K. Yamamoto, A. Masui, H. Ishida, Vib. Spectrosc. 13 (1997), 119-132

/26/ S. Ekgasit, H. Ishida, Appl. Spectrosc. 50 (1996), 1187-1195

/27/ K. Krishnan, P. J. Stout, M. Watanabe, in Practical Fourier Transform Infrared Spectroscopy p. 285-349, Academic Press (1990)

/28/ W. G. Spitzer, M. Tanenbaum, J. Appl. Phys. 32 (1961), 744-745

/29/ M. Klanjšek Gunde, Informacije MIDEM 20 (1990), 83-86

/30/ M. Klanjšek Gunde, B. Aleksandrov, Informacije MIDEM 20 (1990), 138-141

/31/ Y. Uchida, S. Takei, M. Matsumura, Jpn. J. Appl. Phys. 35 (1996), 1460-1463

/32/ W. Bensch, W. Bergholz, Semicond. Sci. Technol. 5 (1990), 421-426

/33/ K. B. Clark, J. A. Bardwell, J. M. Baribeau, J. Appl. Phys. 76 (1994), 3114-3122

/34/ O. Sneh, M. L. Wise, A. W. Ott, L. A. Okada, S. M. George, Surf. Sci. 334 (1995), 135-152

/35/ A. Kučírková, K. Navrátil, Appl. Spectrosc. 48 (1994), 113-120

/36/ R. Ossikovski, B. Drévillon, M. Firon, J. Opt. Soc. Am. A 12 (1995), 1797-1804

/37/ M. Klanjšek Gunde, B. Aleksandrov, Appl. Spectrosc. 44 (1990), 970-974

/38/ M. Klanjšek Gunde, B. Aleksandrov, Informacije MIDEM 20 (1990), 201-204

/39/ J. E. Olsen, F. Shimura, J. Appl. Phys. 66 (1989), 1353-1358

/40/ H. Shirai, Jpn. J. Appl. Phys. 33 (1994), L94-L97

/41/ R. A. B. Devine, Appl. Phys. Lett 68 (1996), 3108-3110

/42/ J. Okuno, K. Park, Appl. Phys. Lett. 69 (1996), 541-543

/43/ T. Kanashima, Y. Kurioka, T. Imai, H. Yamamoto, M. Okuyama, Jpn. J. Appl. Phys. 36 (1997), 2460-2463

/44/ M. Gupta, V. K. Rathi, R. Thangaraj, O. P. Agnihotri, Thin Sol. Films 204 (1991), 77-106

/45/ T. S. Chao, W. H. Chen, T. F. Lei, Jpn. J. Appl. Phys. 34 (1995), 2370-2373

/46/ T. Balz, R. Brendel, R. Hezel, J. Appl. Phys. 76 (1994), 4811-4816

/47/ R. Yamanaka, T. Hattori, T. Mine, T. Tanaka, Jpn. J. Appl. Phys. 34 (1995), 6794-6799

/48/ H. G. Tompkins, M. Dydyk, P. W. Deal, J. Electrochem. Soc. 137 (1990), 2003-2004

/49/ K. Yamamoto, A. Masui, Appl. Spectrosc. 6 (1996), 759-763

/50/ M. Firon, C. Bonnelle, A. Mayeux, J. Vac. Sci. Technol. 14 (1996), 2488-2492

/51/ D. M. Back, in Advances in Physics (1990), p. 265-312

/52/ J. Knobloch, P. Hess, Appl. Phys. Lett. 69 (1996), 4041-4043

/53/ D. M. Haaland, Anal. Chem. 60 (1988), 1208-1217

/54/ J. E. Franke, L. Zhang, T. Niemczyk, D. M. Haaland, J. H. Linn, J. Electrochem. Soc. 140 (1993), 1425-1429

/55/ L. Zhang, J. E. Franke, T. M. Niemczyk, D. M. Haaland, Appl. Spectrosc. 51 (1997), 259-264

/56/ C. W. Liu, B. T. Dai, C. F. Yah, Thin Sol. Films 270 (1995), 607-611

/57/ R. Ossikovski, N. Blayo, B. Drévillon, M. Firon, B. Delahaye, A. Mayeux, Appl. Phys. Lett. 65 (1994), 1236-1238

/58/ R. Swope, W. S. Yoo, J. Vac. Sci. Technol. B 14 (1996), 1702-1705

/59/ S. Lomardo, S. U. Campisano, Mater. Sci. Engn. R17 (1996), 281-336

/60/ Y. C. Kim, H. H. Park, J. S. Chun, W. J. Lee, Thin Sol. Films 237 (1994), 57-65

/61/ J. H. Edgar, C. A. Carosella, C. R. Eddy, Jr., D. T. Smith, J. Mat. Sci.: Mater. Electron. 7 (1996), 274-253

/62/ K. Matsui, M. Taga, T. Kobayashi, Jpn. J. Appl. Phys. 32 (1993), L796-L798

/63/ W. Götz, N. M. Johnson, P. D. Bour, M. D. McCloskey, E. E. Haller, Appl. Phys. lett. 69 (1996), 3725-3727

/64/ Z. I. Alferov, Phys. Scripta T68 (1996), 32-45

/65/ P. Grosse, B. Harbecke, B. Heinz, W. Jantz, M. Maier, Appl. Phys. A 50 (1990), 7-12

/66/ B. Harbecke, Appl. Phys. B 39 (1986), 165-170

/67/ K. Ohta, H. Ishida, Appl. Opt. 29 (1990), 2466-2473

/68/ C. Schwartz, L. F. DeSandre, Appl. Opt. 26 (1987), 3140-3144

/69/ A. A. Hamilton, T. Dumelow, T. J. Parker, S. R. P. Smith, J. Phys. Condens. Mater. 8 (1996), 8027-8039

dr Marta Klanjšek Gunde, dipl. ing.
Kemijski Inštitut,
Hajdrihova 19
1115 Ljubljana, Slovenija
tel. +386 61 1760 291
fax: +386 61 1259 244
e-mail: marta.k.gunde@ki.si

Prispelo (Arrived):13.6.1997 ***Sprejeto (Accepted):23.6.1997***

APLIKACIJSKI ČLANKI - APPLICATION ARTICLES

Total Organic Carbon - TOC in Water

Part II: Pharmaceutical and Semiconductor Applications

I. Šorli, R. Ročak, Z. Bele
MIKROIKS d.o.o., Ljubljana, Slovenia

1.0 A Brief History of TOC Analysis

TOC is the acronym for total oxidizable carbon, sometimes referred to as total organic carbon. Original TOC methods were developed to help correlate information obtained from chemical oxygen demand (COD) and biochemical oxygen demand (BOD) tests in drinking water and wastewater. The TOC methods were designed to be more efficient than the COD (requires hazardous agents) and BOD (requires 5 days to complete) tests. During the past decade, the impor-tance of measuring TOC in drinking water and wastewater as well as the water used in the pharmaceutical, semiconductor, and power generation industries has increased dramatically. Today, new government regu-lations for TOC levels are demanding a more sensitive, flexible, and convenient method for TOC analysis.

Drinking water

The emphasis on drinking water and wastewater is increasing and government agencies, most notably the EPA (Environmental Polution Agency), are instituting rules to monitor municipal systems more closely. It is important to monitor the level of TOC, especially in drinking water, because of the potential for chlorine, the primary drinking water disinfectant, to react with the organics in the water and form halogenated hydrocarbons. These byproducts have been implicated to be carcinogenic.

Pharmaceutical applications

The pharmaceutical industry has maintained an oxidizable substances test for Purified Water (PW) and Water for Injection (WFI) in the United States Pharmacopeia (USP) for more than a century and has been sensitive to the advantages of TOC analysis for many years. As of November 15, 1996, the USP requires a TOC test or oxidizable substances test for PW and WFI. It is now being proposed that the oxidizable substances test be eliminated and replaced by the recently implemented TOC test. Measurement of TOC is a direct reflection on the quality of water being produced and can have a significant impact on the manufacturing process of drug products.

One of the new evolving pharmaceutical applications for TOC monitoring is cleaning validation. The FDA expects companies to provide written procedures detailing the validation of cleaning process for various pieces of equipment (e.g. fermentation tanks). This validation includes testing for residual cleaning agents which can involve TOC analysis.

Semiconductor Applications

TOC in ultrapure water has been recognized as a contaminant and a major contributor to increased product defects in the semiconductor industry for more than 10 years. Today, device geometry reductions accompanied by increases in circuit densities are imposing challenging demands on the purity of water used in production. Semiconductor manufacturers must monitor TOC levels in all stages of the water purification, including at the point-of-use. Since even the slightest increase in TOC levels can effect production yield, the industry has incorporated on-line TOC monitoring to provide more information throughout the entire water purification process.

Power Generation Applications

The power generation industry recognizes TOC as a significant corrosion contributor. TOC found in water is a source of corrosive organic acids that can reduce the life of boilers, reactors, and turbine blades. High-purity water is necessary for continuous operation of power facilities, hence the importance of TOC monitoring.

2.0 Pharmaceutical applications

2.1 Introduction and Background

Since the late 1980's the Pharmaceutical Research and Manufacturers of America P*h*RMA (formally known as the Pharmaceutical Manufacturer's Association) Water Quality Committee (WQC) has investigated and studied new methods for testing the quality of USP PW and WFI. They determined that existing test methods were not ideal and that they should be updated to better reflect current analytical techniques. Table 1 shows the WQC's proposed changes for testing the quality of pharmaceutical water.

The committee proposed that (a) the calcium, sulfate, chloride, ammonia and carbon dioxide tests be re-

placed by single conductivity analysis, (b) heavy metals, total solids, and coliforms tests be deleted because they are irrelevant in any modern high-purity water system and (c) the oxidizable substance test be replaced by the non-selective and highly sensitive TOC method.

Table 1: List of old methodology and proposed new methodology

OLD METHODOLOGY	NEW METHODOLOGY
pH	Maintain
BET	Maintain
Calcium	
Sulfate	
Chloride	Conductivity
Ammonia	
Carbon dioxide	
Oxidizible Substances	Total Organic Carbon (TOC)
Heavy Metals	Delete
Total Solids	Delete
Coliforms	Delete
Microbial Count	Add (Information Chapter only)

The official methods for TOC and Conductivity were published in the USP 23 Fifth Supplement, November 15, 1996. Table 2 lists the acceptable limits of these methods and others for determining the quality of pharmaceutical water. Recommended microbial levels for PW and WFI water have been included in an information chapter.

Table 2: Acceptable limits for tests to meet the USP requirements for pharmaceutical waters

TOC	500 ppb maximum	
Conductivity	limits of 4.7 µS/cm (depending on pH)	
Bacterial Counts	Purified water:	100 cfu/ml
	Water for Injection:	10 cfu/100 ml
Endotoxin (WFI water) only	0.25 EU per LAL test	
pH	5-7	

2.2 Calibration and System Suitability for USP TOC Analysis Using On-line Instrumentation

To ensure correct operation and accurate results the USP TOC method requires the instrument used for analysis be standardized or calibrated with 500 ppb sucrose solution and the suitability of the instrument be tested by analyzing a solution containing 500 ppb 1,4-benzoquinone.

In order to perform the USP calibration and system suitability, methods needed to be developed that allowed solutions to be transported to the installed on-line instrument eliminating the need to remove the instrument and take it to the laboratory for testing. One method that has become quite popular for performing the USP calibration and system suitability was originally suggested by a large pharmaceutical company and is available commercially. Figure 1 shows how a stainless steel vessel can be cleaned with high purity water, filled with test solution, either sucrose or 1,4 benzoquinone, and the entire contents (typically 4 L) pressurized to approximately 25 psig (1.7 bar) through a series of three way valves. The vessel can then be transported to the installed on-line instrument, figure 2, and be connected to the inlet by another three way valve. The valve is then opened and the instrument can take as many as seven or eight measurements.

An alternate mechanism for delivering test solutions to on-line instruments that are installed is shown in figure 3. This method involves preparing the test solutions directly into 2 L volumetric flask and pumping the solution through the TOC analyzer. Because there is a potential for contamination due to exposure of the test solution to the outside air, this method should only be used for instruments that are installed in relatively clean environments.

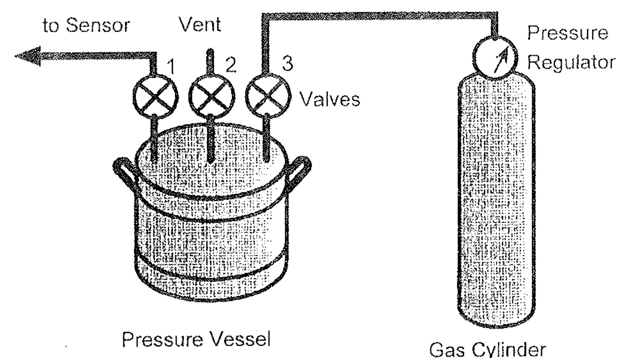

Figure 1: A stainless steel pressurized vessel system for transporting test solutions to an installed, on-line instrument

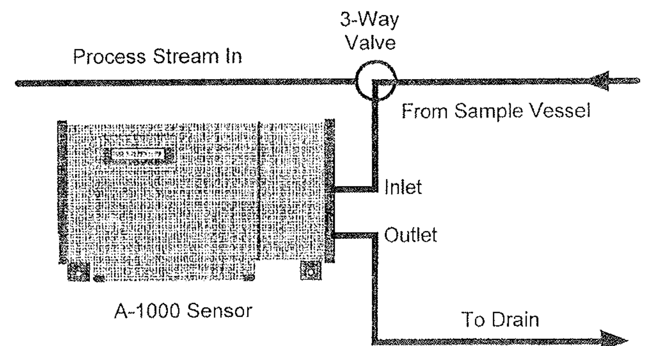

Figure 2: Connection of the stainless steel vessel to the installed on-line TOC sensor

Table 3: Data obtained with stainless steel pressurized vessels; values are an average of three measurements

Sucrose, Expected TOC Value (pppb)	Sucrose Measured TOC Value (ppb)	1,4-Benzoquinone, Expected TOC Value (ppb)	1,4-Benzoquinone, Measured TOC Value (ppb)	% Response Efficiency
500	540	500	470	87
500	547	500	507	93
500	524	500	496	95

Table 4: Data obtained with a volumetric flask and pump; values are an average of three measurements

Sucrose, Expected TOC Value (pppb)	Sucrose Measured TOC Value (ppb)	1,4-Benzoquinone, Expected TOC Value (ppb)	1,4-Benzoquinone, Measured TOC Value (ppb)	% Response Efficiency
500	525	500	531	101
500	553	500	549	99
500	534	500	545	102

Table 3 and 4 show the performance of test solutions delivered to installed on-line TOC instrumentation. The response efficiencies are all within the USP specified values of 85% to 115%.

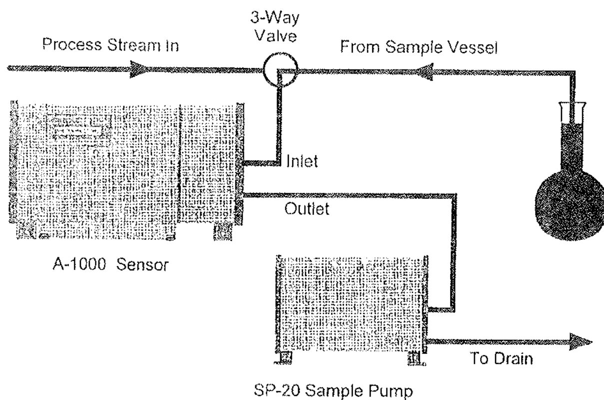

Figure 3: A one step preparation and delivery of test solutions to an installed, on-line instrument

2.3 USP Requirements for Measuring Conductivity

The USP conductivity test is comprised of three stages and meeting the requirements of any one of them is acceptable for pharmaceutical water manufacturers. Stage 1 consists of measuring the temperature and the conductivity of the water using a non-temperature-compensated conductivity probe. The measurement can be performed as a laboratory test, but optimally should be performed on-line. Since the conductivity of high-purity water increases as a function of temperature, the USP has established a list of allowed conductivity values at temperatures ranging from 0°C to 100°C (table 5). These conductivity values are based upon the contributing conductivity of the maximum allowable limits for the chloride and ammonia ions previously specified in the USP (before the USP 23 Fifth Supplement, November 15, 1996).

If the conductivity of the water is higher than the stated table value for the corresponding temperature, then the water must be tested according to Stage 2. Stage 2 requires that the water be equilibrated with air at 25°C and that the conductivity of the water be less than 2.1 μS/cm. If the conductivity of the atmospheric, 25°C equilibrated water is greater than 2.1 μS/cm, then the pH of the water must be measured and the conductivity fall in the acceptable range as shown in figure 4.

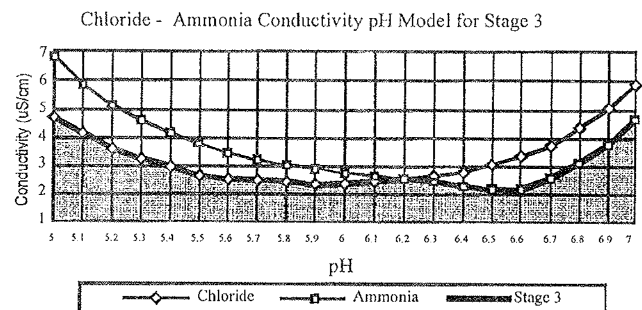

Figure 4: Stage 3 pH and conductivity requirements for the USP Conductivity Method <645>; the chloride and ammonia ions are the models used to determine the acceptable conductivity

Table 5: Temperature and conductivity requirements for USP Conductivity Method <645>, Stage 1: for non-temperature compensated conductivity measurements only.

Temperatue, °C	Conductivity, µS/cm
0	0.60
5	0.8
10	0.9
15	1.0
20	1.1
25	1.3
30	1.4
35	1.5
40	1.7
45	1.8
50	1.9
55	2.1
60	2.2
65	2.4
70	2.5
75	2.7
80	2.7
85	2.7
90	2.7
95	2.9
100	3.1

2.4 USP Calibration Requirements for Conductivity Measurements

The USP conductivity method requires the cell constant of the instrument to be determined within ±2% of a known reference. Procedures can include measuring a solution of known concentration such as the conductivity standard used in American Society of Testing and Materials (ASTM) method D1125, or by comparing the instruments readings to values from a known certified probe. Of the two methods the latter is preferable because electrolyte solutions can be very difficult to prepare and measure consistently, and commercially available solutions are higher in conductivity than the USP limits. Figure 5 shows a comparison between an on-line TOC sensor and a NIST traceable Thorton® conductivity probe that has a known cell constant. A homogenous atmosphere equilibrated water sample was allowed to flow simultaneously, in parallel, to both instruments using a "tee" in the sample line. The results demonstrate excellent agreement between the two instruments, well within the USP requirement of ±2%.

The USP conductivity method also requires that the instrument or meter accuracy be 0.1 µS/cm excluding cell constant. A well designed on-line conductivity instrument or meter will contain metal film precision resistors that are accurate to within ±0.01% of the stated value. These resistors verify the measuring electronic circuitry prior to each conductivity measurement to ensure that the instrument's accuracy is within ±0.1 µS/cm.

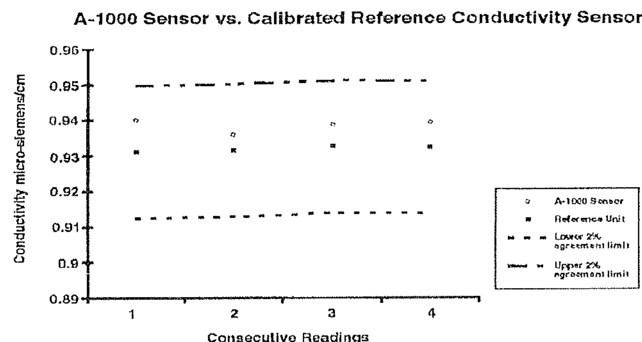

Figure 5: Conductivity measurements comparing the performance of an on-line conductivity sensor to a calibrated, NIST traceable conductivity probe

2.5 Pretreatment Strategies for TOC Reduction in WFI and USP PW

TOC by its nature is nonionic; therefore, deionization (DI) resins have little effect on TOC reduction. For deionization to work properly, TOC must be deionized. The ionization of TOC can be accomplished by oxidation, whether complete or partial, with HO•. These free-radical hydroxyls help in the formation of by-products, including organic acids. Organic acids are compounds with anion valences. In these organic acid forms, the anion resin beads can produce excellent results. Figure 6 represents various pretreatment schemes for identical water systems. All readings were generated from an A-100 TOC analyzer (Anatel, Boulder, Colorado). The top set of readings shows TOC measurements between 1000 and 1300 ppb using deionizing resin beads in a mixed-bed configuration. There was no pretreatment of the water other than rough particle filters at 10 µm and 1 µm. The raw water was municipally treated water, which complies with the Federal Safe Drinking Water Act (42 USC 300 g-1).

The middle set of TOC readings in figure 6 was taken after the addition of granulated activated carbon (GAC) module. GACs are regularly used for pretreatment in water purification systems to reduce or eliminate chlorine and help reduce TOC loading, especially of volatile compounds. The addition of GAC module with the existing DI system reduced the TOC loading in the water system by almost half. The system maintained 600 ppb of TOC, rather than the 1200 range. Although the reduc-

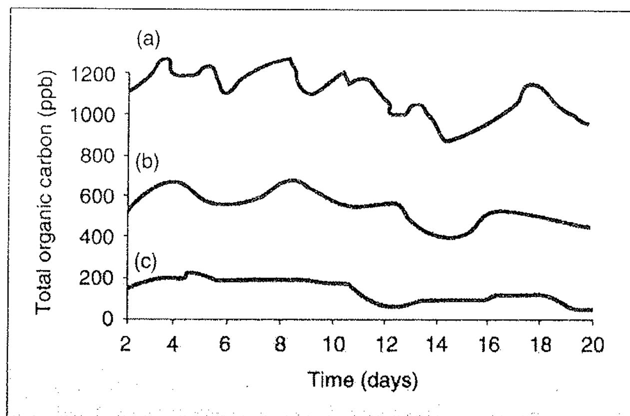

Figure 6: TOC measurements after various water pretreatment schemes using
a) deionization resin beads only
b) deionization beads and granulated activated carbon
c) reverse osmosis and deionization

tion was significant, it was above the 500 ppb proposed specification limit. GAC reduction efficiency is diminished over a short period of time and may require frequent backflushing and steam regeneration. Diminished GAC beds will cause leakage of bacteria and TOC over time.

The lower set of TOC readings shows the value of combining reverse osmosis (RO) and DI. The values were consistently reduced below 200 ppb, with the system approaching 50 ppb.

RO membranes have a typical molecular cutoff range of 300-400 daltons. TOC can range in molecular weight from <100 to >1 million daltons. TOC in organic chains can be removed effectively with RO. Although RO is not 100% efficient, all RO membranes will reduce TOC, some with greater efficacy than others.

Downstream components can add TOC to a water system. Pump seals, valves, plastic components, resin beads, and resin-composed vessels are examples of water system components made from organic material that can elute TOC into a water system. In extremely low TOC waters, elution of TOC from the water system's components can be the greatest contamination source. The elastomers used in a high purity water system can be minimized if careful consideration to materials is designed in the water system.

Ozonation and 185 nm UV lights can be excellent TOC reduction methods. First used in France in 1897, ozonation is commonly used in European drinking water as the main sanitizing agent. Ozon produces free-radical hydroxyls, which oxidize the TOC to organic acids and CO_2. Compatibility of elastomers, resins, and piping is extremely important because ozone is a very agressive compound. A 185 nm UV lamp cleaves a water molecule, yielding the free radicals H• and HO•. The hydroxyls oxidize the TOC to organic acids and CO_2. Once the TOC has been partially or completely oxidized, it can be removed from the water by ion-exchange resins and degasification. Figure 7 demonstrates the reduction of TOC from >100 ppb to <10 ppb. Installation of a 185 nm UV lamp system on a multipass polishing loop can help maintain low TOC levels.

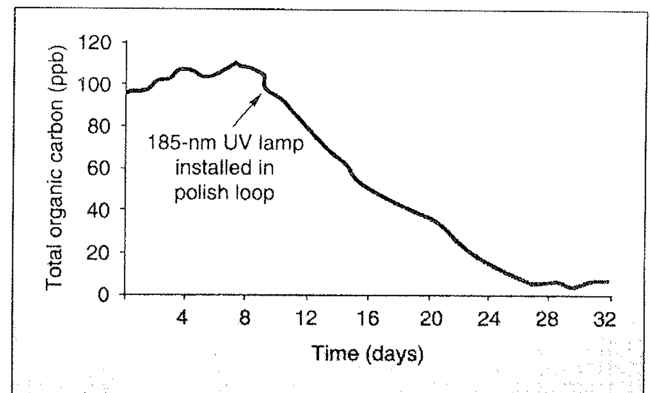

Figure 7: TOC reduction using multipass 185 nm UV lamp

In the pharmaceutical industry, most WFI water systems are composed of stainless steel. The use of stainless steel piping will retard the elution of TOC. However, many of the seals, gaskets, and diaphragm valves can contribute to the overall TOC condition. WFI systems that use distillation to deliver microprobe-free and endotoxin-reduced waters often carry over TOC, especially volatilized organics, into the production water.

It has been shown that high-pressure and high-temperature systems can produce organic acids as byproducts of complex organics. High organic loading can result in the development of acidic species levels that corrode stainless steel piping, turbines, and condensation units.

TOC analyzers offer greater data compilation and interpretation than just the replacement of the oxidizable substances test. TOC, resistivity, temperature, and a profile of the organics can readily help the facility's engineer, pharmaceutical engineer, and QC or QA personnel determine the exact operating state of a water system. The delivery of consistent and stable WFI or USP water to the production facility is crucial to the repeatability and quality of the product. In many cases, the water is blamed as a major contributing factor in the loss of a product or a batch. Specific water parameters need to be identified and isolated as cintributing or noncontributing factors to the loss of product or batch. On-line measurements of TOC, resistivity, and temperature and profiling of the organics can help in determining the causes of product or batch failure.

Well designed water systems offer the best hedge against TOC upsets. Many components exist in USP PW and WFI systems. Almost exclusively, distillation units are used for WFI. After decades of usage in pharmaceutical industry, distillation units have shown durability and efficacy in microbial reduction, endotoxin reduction, and maintaining high-quality water production.

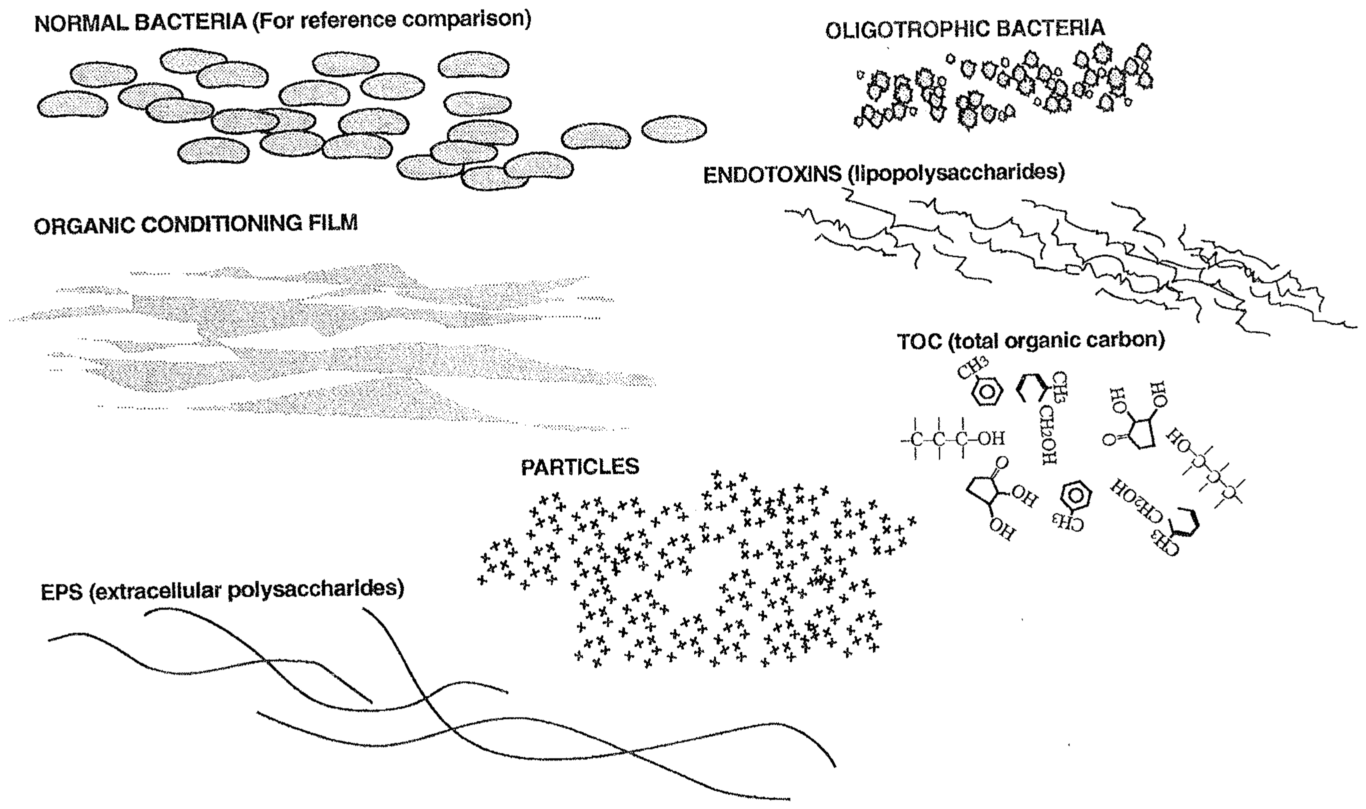

Figure 8: Micro-components of a Low Nutrient Water Environment

2.6 Relationship among TOC, bacterial cells, and endotoxins, /4 /

Although the increasingly efficient high purity water (HPW) systems being installed in the pharmaceutical industry produce a product with less and less contaminants present, closer examination shows the presence of numerous materials asssociated with living and dynamic biofilms.

The purification process does reduce the inorganic and organic constituents normally found in water to extremely low levels. For example, oxidizable carbon which serves as nutrient source for bacteria is often reduced to less than 100 ppb concentration. To cope with this low nutrient environment, the bacteria, which normally enter the system through a number of means, generally from the feed water, assume a starved or oligotrophic character. They typically become smaller, their metabolism changes and they can, under certain conditions, become stressed both in appearance and physiology.

The gram negative bacteria produce endotoxins or lipopolysaccharides as their cell membranes break down. These oligotrophic bacteria also produce extracellular polysaccharides which form a glycocalyx and organic conditioning film or biofilm. This glycocalyx can easily capture particles which become part of the biofilm.

Biofilms in high purity water systems are formed through a complex and not so sequential, dynamic sequence that begins with organic compounds loosely binding to pipe walls, bacteria attaching themselves to these walls in search of nutrients that the organics provide, cell adaptation to an oligotrophic form to survive in the hostile low-nutrient environment, and finally the forming of the lipopolysaccharide glycocalyx. Particles are also trapped and the biofilm becomes a living environment that allows the bacteria to survive.

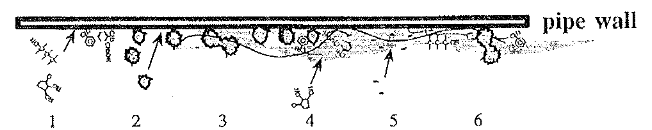

Figure 9: Theoretical development of biofilms:
1) Organic compounds including nutrients chemically bond to the surface material (organic conditioning film)
2) Planctonic bacteria seeking mutrients attach to the pipe walls
3) Bacteria form biofilms with EPS glycocalyx
4) More nutrients are captured
5) Particles are also captured
6) Biofilm becomes a living environment

Table 6: Summary table of effect of TOC changes on total cells, viable cells and endotoxins
Epi = total bacteria count by epifluoroscence microscopy,
CFU = ColonyForming Unit of viable oligotrophic bacteria,
LAL = bacterial endotoxin concentration by LAL method

Elapsed time (days)	Site	Δ TOC ppb	Δ Epi %	Δ CFU %	Δ Ebdotoxin by LAL %
77.2-77.7	RO Prod	2.2	63	/	300
80-81	RO Prod	4	4300	/	/
77-77.7	2nd MB	2.5	62	/	200
80-80.6	2ns MB	3	330	185	400
78.4-79	970POD	2	/	138	5000
78-79	Skid 2 Ain	4	367	/	1800
77.6-78.6	UV out	3.5	271	/	636
80-80.4	UV out	4	223	/	/
80.4-81.4	UV out	4	/	/	83
81-81.6	UV out	3	123	183	200
78.2	UF out	0.4	235	/	667
80-80.6	UF out	0.3	2400	/	267
81-81.6	UF out	0.6	2720	/	310

The increase in total cells and endotoxins, which are associated with the lipopolysaccharide cell membrane structure of gram negative bacteria, as a function of small increases in TOC levels is based on the theory that includes the formation of biofilms in any water system that is not sterilized regularly.

The biofilm includes living bacteria, dead cells, a glycocalyx of extracellular polysaccharides, cell fragments, endotoxins, and particles. The biofilm is a dynamic entity, even in this hostile starved environment. "Pieces" of biofilm shed from the cell wall and planctonic (free floating in the water stream) bacteria find their way into the biofilm to seek nutrients and a more comfortable environment. The hypothesis even suggests that breakdown materials from dead and fragmented cells can serve as food for other living cells. Reproduction is very slow.

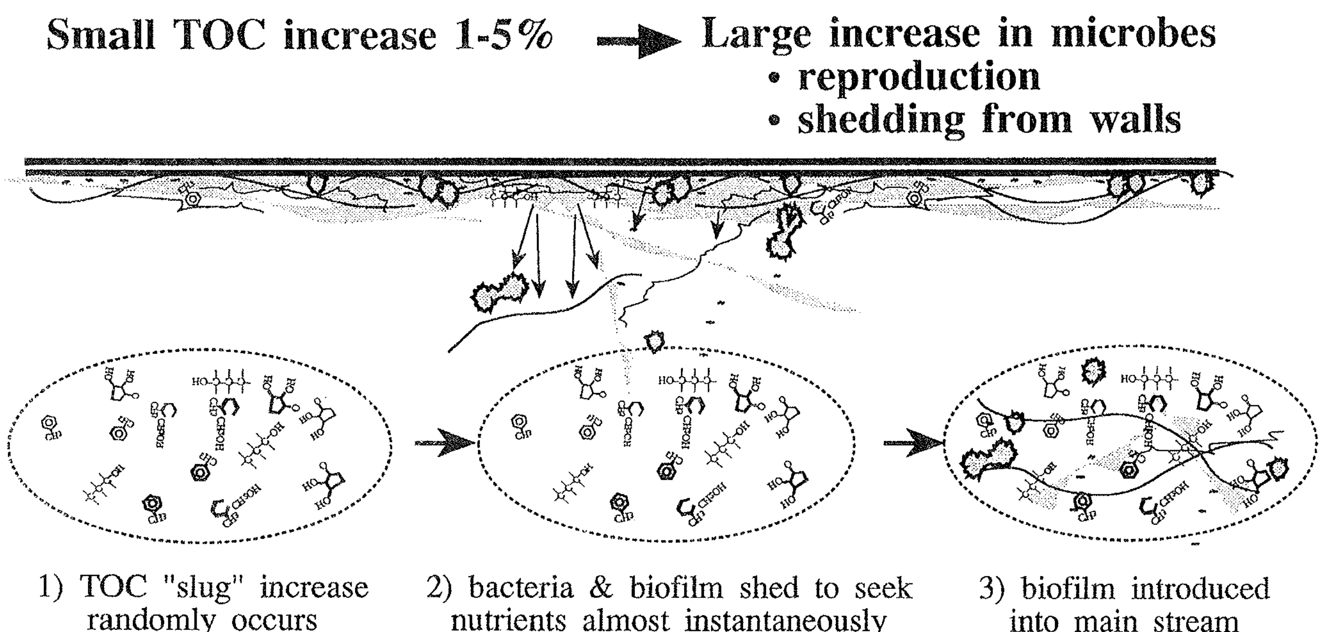

Figure 10: interpretation of data in table 6: small TOC increase of 1-5% lead to large increase in microbes

When a small increase in TOC occurs, the fragile equilibrium of biofilm and sessile (attached to the surface) cells and what occurs in the free flowing stream is upset. The sessile cells sense the increased nutrient in the flowing water and shed from the surface to seek this extra food. Since relatively large sections of the biofilm can shed under these conditions, they break down, in the turbulence and release dead cells, viable cells, endotoxins, and extraneous extracellular material. As a result, the increase of total cells and endotoxins in the flowing water is quite dramatic.

The summary table 6 shows how small increase in TOC values within the water system are rapidly followed by increase in the total cell count, viable cells, and endotoxin levels. Inconclusive results were omitted for clarity.

2.7 Conclusion

The new USP TOC and conductivity methods each require their own calibration procedure to verify the accuracy and correct operation of the chosen instrument. How frequent these calibration procedures need to be performed is not specified, but is dependent on the manufacturing application and degree of use. On-line instrumentation offers significant advantages over laboratory testing, but requires special handling when performing the USP test methods. Whether the instrument is operated on-line or in the laboratory, the instrument manufacturer should provide complete installation and operation guidelines as well as complete standard operation procedures (SOP's) to ensure that the instrument complies with all the USP requirements.

Contemporary UPW and PW systems are both complex and dynamic, yet are required to consistently produce very high purity product water. The concentrations of bacteria, metabolites like endotoxin, and particulate contaminants present in high purity waters must be adequately measured and regulated for process to remain within control limits. However, current stages rely upon off-line analyses which are inherently retrospective and thereby unsuited to feedback control in real time.

The high purity water industry has not yet developed instantaneous measurements of biofilm levels to determine its response to changing system parameters. Nor have analytical methods been developed, for real time on-line measurements of water phase bacteria or endotoxin concentrations in these systems.

Endotoxin measurements reported are approximately three logs more sensitive than conventional methods that do not employ concentration by ultrafiltration. This modification makes LAL method suitable for endotoxin measurements in high purity water systems for trending purposes.

Continuous TOC measurements at multiple system points may offer a gateway measurement to predict bacterial, endotoxin and particle variations. Transient elevations in TOC, observed to occur in high performance high purity systems, even when of modest magnitude, may produce significant variations in bacteria and endotoxin concentrations. Aggressive control of TOC may be required to consistently control bacterial and endotoxin quality of high purity water systems.

3.0 Semiconductor Applications

3.1 Background

The quest for ultrapurity in the semiconductor fabricating (FAB) environment and in the materials which are specific to the fabricating process continues to warrant investigation. As the industry goes towards deep submicron range for volume production, contamination looms as the obstacle to maintaining acceptable yields.

Primary areas where purity is mandatory are:

- process water
- process chemicals
- process gases
- fabrication equipment
- fabrication environment

It has been well established that the purity of water used in fabrication of ICs has a direct and significant effect on the level of yield. That's why monitoring of water purity is of the upmost importance.

Water is so important because it is the media that wafers come into contact most frequently with during the process. Water is used for washing and rinsing silicon wafers after etching or cleaning operations and for making steam for oxidation of wafers. A CMOS fabrication process may have about 20 separate wafer rinse steps which means thata a single IC may require up to 600 L of high purity water for complete processing.

Besides water resistivity, bacterial count and volume particle content, TOC is one of the most important water parameters that need to be monitored. In figure 11 a typical semiconductor pure-water system is depicted and in table 7, typical TOC levels at several points in a properly functioning semiconductor pure-water system are shown.

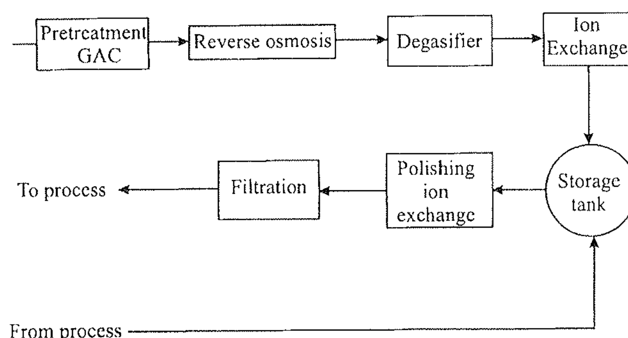

Figure 11: A typical semiconductor pure-water system

Table 7: Typical TOC levels at several points in a properly functioning semiconductor pure-water system

Measuring point	TOC in ppb	
	Mean	Range
City input water	3200	2500-6200
GAC	2950	2400-4200
Reverse osmosis unit	275	150-500
Primary ion exchange	75	<50-200
Final filter	<20	<20-150
Return line	<50	<50-225

Main sources and reasons for high TOC levels in pure water are
- raw incoming water which must be properly treated to reduce TOC levels to acceptable values
- inproperly chosen materials DI water comes into contact with (piping, fittings, filter housings, storage tanks)
- large surface areas of materials DI water comes into contact with
- inproper flow dynamics in the entire system
- high downtime of makeup and reclaim systems

This means that design and construction criteria are critical to the attainment of a state of the art DI water system. These criteria involve the piping size and layout, flow and pressure characteristics, the make up and storage capacity, and installation procedures.

The choices of construction materials are important to ensure a contamination free system. PVDF is chosen as a piping material for its ability to meet present and contemplated requirements.

Levels of less than 10 ppb TOC can be obtained through the organic removal capability of 185 nm UV irradiation.

3.2 Effects of TOC on CMOS Fabrication Processes

In table 8, typical effects of high TOC values on CMOS fabrication processes are shown.

A certain CMOS FAB reported problems in growing consistently acceptable gate oxides in the thickness range 10 - 20 nm. The nonuniformity manifested itself as areas of increased oxide thickness on individual wafers. After eliminating furnace tubes and process gas contamination as causitive factors, the wafer cleaning process was investigated. The major source of particles was found to be contaminated DI water. Analysis of the water found high levels of TOC (750 ppb range) and particles, figure 12. Wafers rinsed in such DI water showed pronounced level of hazing on wafer surface, as well as their surface appeared to be hydrofilic after prolonged DI water rinse.

Table 8: Typical TOC impact on fabrication processes

PROCESS STEP		Observed TOC impact
LAYERING	Oxidation	High particle counts
	Chemical Vapour Deposition	Uneven oxide growth
		Large CV drifts
		High leakage currents
		Low breakdown voltages
	Evaporation	Uneven deposition
	Sputtering	Poor film adhesion
		Pin-hole defects
PHOTO-MASKING	Resist	Poor film adhesion
	Exposure	Mask defects
	Etch	Pin-hole defects
DOPING	Duffusion	High leakage currents
	Ion implantation	Improper doping levels
		Carbon nucleation sites

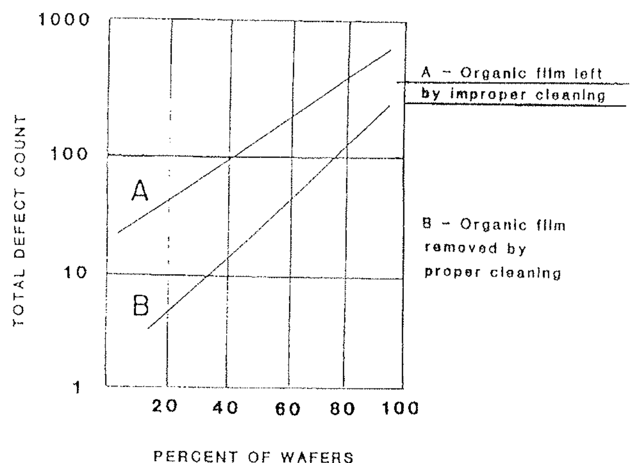

Figure 12: Defect counts by laser scatter on silicon wafers after preclean

Modification of the DI water system was innitiated. Gate oxide defect densities, threshold voltage shifts and background doping level contamination were monitored throughout the modification of the water system. Figure 13 clearly shows the level of direct TOC impact on gate oxide relative defect density. Each defect data point reflects the relative number of electrical defects per square centimeter in the gate oxide as measured by breakdown voltage test.

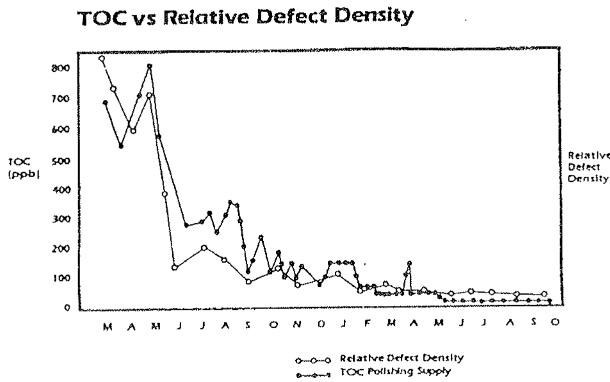

Figure 13: TOC vs relative defect density, gate oxide, 20 nm

Oxide uniformity on wafer also improved with decreased TOC values. It has been proposed that organics on the wafer's surface decomposed to form water vapour and other byproducts. The water vapour served to increase the local oxidation rate, resulting in increase in oxide thickness of as much as 6 nm.

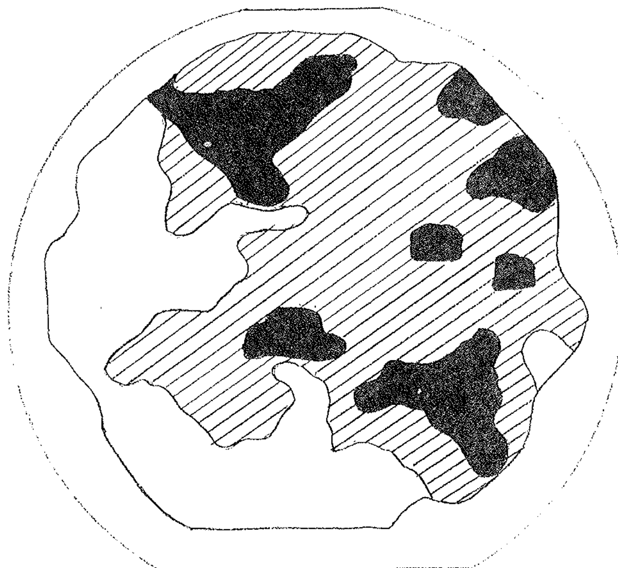

Figure 14: 100 mm wafer MAP of background concentration after gate oxidation; wafer was precleaned in TOC contaminated DI water

☐ N_D 2.5 - 4.5 E15 /cm^3

▨ N_D 4.6 - 6.5 E15 /cm^3

■ N_D 6.6 - 8.5 E15 /cm^3

Some FABs, /7/, reported large MOS transistor threshold voltage shifts and increased background wafer dopant concentrations after the wafers were exposed to TOC contaminated DI water during gate oxide preclean. In figure 14 a typical wafer MAP of average dopant concentration is presented. Wafer average concentration was measured after gate oxidation with C-V technique. Typical dopant concentration should be below 4.5E15/cm^3, while more than 50% of the wafer area shows increased phosphorous type contamination.

The above described type contamination has a disastrous effect on MOS transistor threshold voltages. In figure 15 a direct connection between PMOS transistor threshhold voltage and TOC is depicted. Clearly, allowable TOC limit for successful gate oxide preclean must be below 20 ppb.

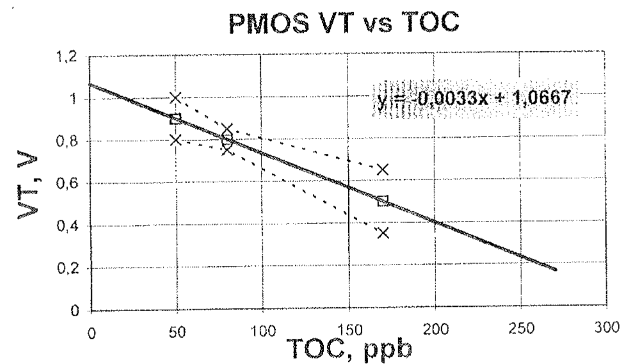

Figure 15: PMOS transistor (5 μm gate length) threshold vs TOC concentration

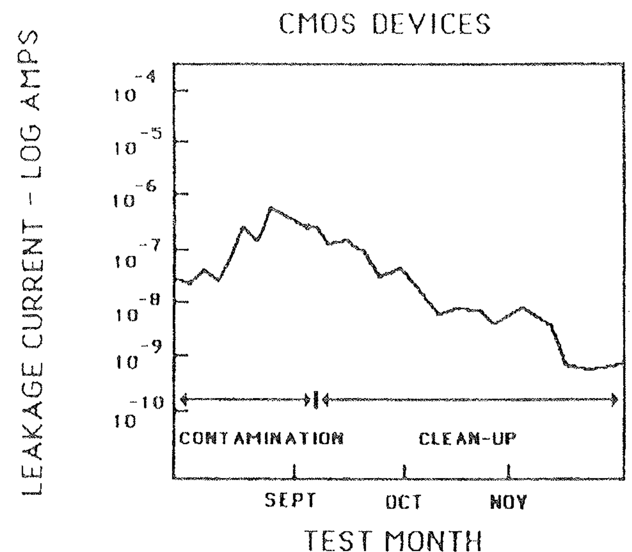

Figure 16: Effect of TOC contamination on IC leakage current: >400 ppb TOC contamination levels in water caused three orders of magnitude higher leakage currents compared to normal <50 ppb TOC levels

Further on carbon atoms as part of TOC can act as nucleation sites and attract boron, phosphorous or arsenic atoms during diffusion which alters the junction depth and hence device electrical characteristics.

Organic contaminants can carry mobile ions (e.g. Na). Once on the surface, these ions can diffuse into the wafer during high temperature steps and can migrate to an active junction and cause high leakage currents, figure 16.

For GaAs devices the group IV compounds (including C) can act as dopant species and unwanted carbon contamination can affect junction electrical parameters. In fact, TOC levels >200 ppb in pre-clean DI water have been traced to low device reliability problems.

4.0 LITERATURE

/1/ What You Should Know Before Buying A Total Organic Carbon (TOC) Analyzer for the Mesurement of Organic Impurities in Water Systems Ranging from High-Purity Water to Effluent Wastewater, Anatel Co., Boulder CO, 2nd Edition, March 1997

/2/ K. Clark, C. Flint, M. Retzik, Calibration of TOC and Conductivity Instrumentation for Meeting the Changes to the United States Pharmacopeia (USP 23) Water Monograph, Presented at Interphex '97 Philadelphia, PA

/3/ N. Cohen, Pretreatment Strategies for TOC Reduction in WFI and USP Purified Water, Pharmaceutical Technology, June 1995, pp 96-104

/4/ G. Husted, A. Rutkowski, M. Retzik, Variation in High Purity Water Bacterial and Endotoxin Concentrations in Response to Spontaneous Changes in Total Oxidizable Carbon Content, PDA Journal of Pharmaceutical Science&Technology, Vol. 50, No. 1, January - February 1996

/5/ S.J. Poirier, An Overview of Total Organic Carbon Analysis in Ultrapure-Water Applications, Microcontamination, June/July 1984

/6/ P.A. McConnelee, S.J. Poirier, R. Hanselka, The Role of Water Quality Improvements in VLSI Defect Density

/7/ Private communications

For more information on ANATEL TOC measurement systems, please, call:

Mr. Iztok Šorli
MIKROIKS d.o.o.
Dunajska 5, 1000 Ljubljana, Slovenia
tel. +386 (0)61 312 898
fax. +386 (0)61 319 170
Email: Iztok.Sorli@guest.arnes.si

PREDSTAVLJAMO PODJETJE Z NASLOVNICE
REPRESENT OF COMPANY FROM FRONT PAGE

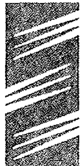

SODOBNA
ELEKTRONIKA

44. SEJEM SODOBNA ELEKTRONIKA
THE 44th MODERN ELECTRONICS FAIR

Ljubljana, 6. - 10. oktober 1997

Tradicionalna sejemska prireditev s področja elektronike bo letos potekala v času od 6. do 10.oktobra na Gospodarskem razstavišču v Ljubljani.

O pomenu sejma prepričljivo govorijo naslednji podatki. V letu 1996 se je na njem predstavilo 540 podjetij iz 29 držav, od tega več kot polovica tujih, obiskalo pa ga je okoli 34.000 obiskovalcev iz 25 držav. Poleg slovenskega trga omogoča nastop na sejmu zato vse bolj tudi poslovne stike s sosednjimi trgi srednje in jugovzhodne Evrope.

Sejem obsega predvsem programske sklope komponent, avtomatizacije z merilno elektroniko, telekomunikacij in profesionalne avdio/video opreme z radiodifuzijo.

Traditional modern electronics fair will be held this year in Ljubljana fair from October 6 till October 10.

We feel sure the following data themselves prove that this fair is very significant. In 1996, 540 companies from 29 countries introduced themselves, of which more than a half came from abroad. The fair was visited by around 34.000 visitors from 25 countries. Besides inland business contacts the participation in this fair enables also more numerous business contacts with other markets of the Central and South-western Europe.

The exhibition programmes comprise electronic components, automation with measuring electronics, telecommunications and professional audio/video equipment including broadcasting.

Čeprav je sejem v prvi vrsti namenjen strokovnjakom, pa obenem uspešno popularizira tudi novosti na področju elektronike za široko potrošnjo, zlasti s področja kabelske in satelitske televizije, HI-FI naprav in pisarniške avtomatizacije. Poleg tega obsega tudi naslednjo dejavnost: elektromaterial in inštalacije, vire električne energije, energetiko in razsvetljavo, ki sicer ne sodijo v okvir popularnega naziva sejma - ELEKTRONIKA.

Sejem bosta spremljala simpozij ISEP - Elektronika v cestnem prometu v organizaciji Elektrotehniške zveze Slovenije in strokovno posvetovanje "Inteligentne stavbe" v organizaciji Združenja za inženiring pri GZS.

Za dodatne informacije smo Vam na voljo po telefonu na številki 061/173 53 85, projektni vodja Gorazd Majcen in Irena Kogoj, korespondentka sejma SODOBNA ELEKTRONIKA.

Although the fair is above all intended for experts its role has always been significant in popular fields of electronics like cable and satellite TV, Hi-Fi appliances and office automation. The fair further comprises electromaterial and installations, electric energy sources, energetics and illuminants, which however do not belong to the frame of the famous name of the fair ELECTRONICS.

The fair will be accompanied by two symposia: "ISEP" - Electronics in (road) traffic, organized by the Electrochemical Society of Slovenia, and "Intelligent buildings", organized by the Association of the engineering with the Chamber of Economy of Slovenia.

For all further information please call Mr.Gorazd Majcen, project manager of the MODERN ELECTRONICS '97 fair, tel.+386 61 173 53 85

RAZSTAVNI PROGRAM PO DEJAVNOSTIH
EXHIBITION PROGRAMME BY ACTIVITIES

1. PROFESIONALNA ELEKTRONIKA

1.1. Krmilna in regulacijska elektronika
1.2. Avtomatizacija
1.3. Industrijska elektronika
1.4. Močnostna elektronika
1.5. Nuklearna elektronika
1.6. Medicinska elektronika
1.7. Merilna in preizkuševalna tehnika
1.8. Profesionalna avdio in video elektronika
1.9. Avtomobilska elektronika

2. TELEKOMUNIKACIJE

2.1. Naprave za komutacijo
2.2. Naprave za žični prenos informacij
2.3. Naprave za brezžični prenos informacij
2.4. Telekomunikacijski aparati in terminali
2.5. Teleinformacijske storitve
2.6. Antene za telekomunikacije

3. RADIODIFUZIJA

3.1. Oddajniki in pretvorniki
3.2. Antene in antenske naprave za difuzijo
3.3. Naprave za satelitske prenose
3.4. Kabelska distribucija signalov
3.5. Oprema za proizvodnjo radiofuzijskih programov

4. OPREMA ZA PROIZVODNJO

4.1. Oprema za proizvodnjo elektronskih naprav
4.2. Oprema za proizvodnjo sestavnih delov in funkcijskih enot
4.3. Oprema za razvojne laboratorije

1. PROFESSIONAL ELECTRONICS

1.1. Control and regulation electronics
1.2. Automation
1.3. Industrial electronics
1.4. Power electronics
1.5. Nuclear electronics
1.6. Medical electronics
1.7. Measuring and test electronics
1.8. Professional audio and video electronis
1.9. Automobile electronics

2. TELECOMMUNICATIONS

2.1. Commutation devices
2.2. Devices for wire information transmission
2.3. Devices for wireless information transmission
2.4. Telecommunication devices and terminals
2.5. Teleinformation services
2.6. Telecommunication antennas

3. RADIO BROADCASTING

3.1. Transmitters and converters
3.2. Broadcasting antennas and antenna devices
3.3. Satellite transmission devices
3.4. Cable signal distribution
3.5. Production equipment for radio broadcast programs

4. PRODUCTION EQUIPMENT

4.1. Production equipment for electronics devices
4.2. Production equipment for components and functional units
4.3. Equipment for development laboratories

5. SESTAVNI DELI, FUNKCIJSKE ENOTE IN MATERIALI

5.1. Polprevodniški sestavni deli, elektronke in integrirana vezja
5.2. Pasivni sestavni deli in enote
5.3. Funkcijske enote
5.4. Elektromehanski sestavni deli in enote

5.4.1. Stikala in pretikala
5.4.2. Spojni elementi
5.4.3. Releji
5.4.4. Sestavni deli za elektroakustiko
5.5. Sestavni deli za močnostno elektroniko
5.6. Senzorji za zajemanje fizikalnih lastnosti in veličine
5.7. Materiali za proizvodnjo sestavnih delov, enot in elektronskih naprav
5.8. Viri električne energije
5.9. Žice in kabli

6. INŽENIRING IN LITERATURA

6.1. Raziskave in razvoj
6.2. Projektiranje in inženiring
6.3. Računalniška podpora inženirskih dejavnosti (CAD, CAM, CAE ...)
6.4. Učni pripomočki
6.5. Strokovna literatura
6.6. Montaža, servis in vzdrževanje

5. COMPONENTS, FUNCTIONAL UNITS AND MATERIALS

5.1. Semi-conductor components, electron. tubes and int. circuits
5.2. Passive components and units
5.3. Functional units
5.4. Electromechanical components and units for electronics
5.4.1. Switchers and commutators
5.4.2. Connection elements
5.4.3. Relays
5.4.4. Components for electroacoustics
5.5. Components for power electronics
5.6. Sensors for gathering of physical characteristics and quantities
5.7. Materials for production of components, units and electronic devices
5.8. Electric energy sources
5.9. Wires and cables

6. ENGINEERING AND LITERATURE

6.1. Research and development
6.2. Planning and engineering
6.3. Computer support of engineering activities (CAD, CAM, CAE ...)
6.4. Teaching devices
6.5. Professional literature
6.6. Installation, servicing and maintenance

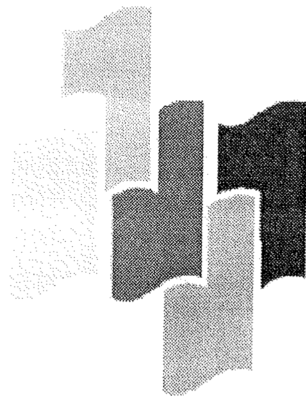

LJUBLJANSKI SEJEM

Ljubljanski sejem d.d.
Ljubljana fair Dunajska 10
1000 Ljubljana, Slovenija
tel.+386 (0)61 173 53 31
fax.+386 (0)61 173 52 32
email : Lsejem@eunet-si
http : //www.isa.tp-lj.si/Lsejem

MIDEM IN NJEGOVI ČLANI, NOVICE IZ DRUGIH SREDIN
MIDEM SOCIETY AND ITS MEMBERS, NEWS FROM OTHER INSTITUTIONS

The European Dimension in High-Tech

Siemens Dresden Semiconductor Plant

When the name of Dresden is mentioned, people first think of "the German Florence" and the "Pearl of the Baroque". Lavish architecture, painting and music made it into a European metropolis of brilliant culture. But Dresden also began very early on to develop into major commercial and engineering center. Despite the ravages of WW2, the worldwide reputation of its electrical and optical industry lived on. Today the Saxon city of Dresden is thriving again as high-technology enterprises settle here.

The Semiconductor Group of Siemens has expanded systematically over the years, creating a model, international manufacturing network. Plants in Europe, the USA and South-East Asia evidence a front-runner role worldwide that can stand up to any comparison.

When you stop moving ahead, there is danger of being overtaken. So some 700 million DM are being invested in expansion of the plants in Corbeil-Essonnes, Malacca, Regensburg and Villach. But the demand for semiconductor products is growing at such a rate that even this will not be able to satisfy the market and its potential. So further investment amounting to several billion DM is planned. Among the latest projects are a factory for logic devices in Newcastle-on-Tyne, England and an assembly plant in China.

Dresden is the focus of the ongoing investment phase. Some 2.7 billion DM are being put into a plant that sets whole new standards in European semiconductor manufacture. 16-Mbit DRAMs wlll be produced to start with. 64-Mbit DRAMs will follow and, towards the end of the decade, the first 256-Mbit DRAMs are due to be fabricated here. With manufacturing potential on this scale, the Dresden plant takes on significance that extends far beyond Saxony and Germany.

Semiconductor manufacture involves many different technical processes that have to be implemented efficiently and work highly economically. The planning team responded to this challenge with a well thougt out concept that is convincing in every respect.

The entire complex is organized symmetrically. The central facilities building forms the core, with the two

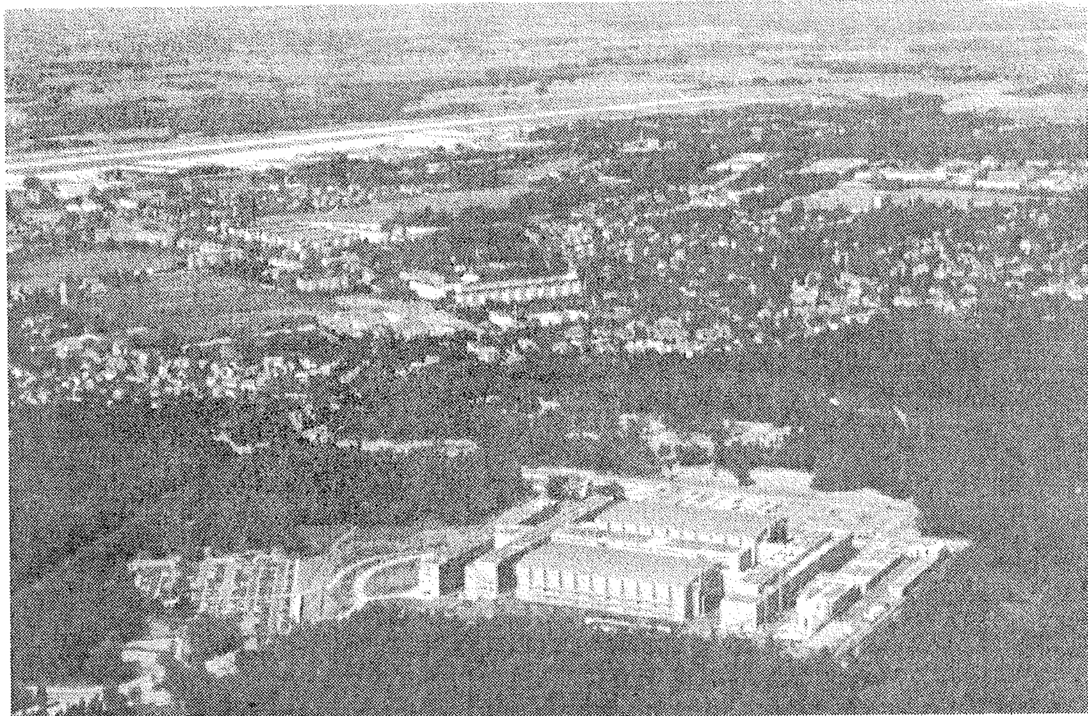

Siemens Microelectronics Center Dresden (SIMEC) aerial view (8/96)

modules, ie clean rooms with direct supply networks, arranged at the sides. In front of this production ensemble is the periphery building where the changing rooms are located for the air locks. The office building with its main entrance forms a facade facing onto Königsbrücker Strasse.

Parallel to this are the buildings for the chemical plant and technical services, setting the architectural tone for the entire rear of the complex.

The solution was aimed at creating a highly attractive work environment. Much emphasis was placed on light, air and a view of the landscape - which is even possible from the clean rooms.

The new plant will be capable of producing chip structures in quarter micron technology. This takes industrial process engineering up to the frontiers of what is currently possible. So it is understandable that only the best equipment available in the world could be used.

During the few months between RfE (Ready for Equipment) on 2 May 1995 and startup on 10 November 1995, more than 400 items of plant worth almost 1 billion DM were installed. The implantation plant came from the USA for example, wafer steppers from Japan,and wet-chemical etching and cleaning equipment from Germany. There is, of course an international team of specialists on hand at the Dresden plant to set all this technology in motion.

Dimensions of quantity equal those of quality. 10,800 m^2 of clean room call for resources and logistics of the very best. Especially when you think of the amounts of air, water and chemicals that have to bemanaged. Utmost reliability is a must. After all, the plant will be working round the clock, seven days a week in three shifts.

SIEMENS Microelectronics Center
For Public Relations
January, 3rd 1997

„Green Light" for Europe's modernst Chip-Factory in Dresden

Capital Investment of 2,7 Billions DM until 2004 -
400 additional jobs at the End of 1996!

SIEMENS Microelectronics Center in Dresden (Germany) realised a successful interim conclusion one year after the official opening: Nevertheless the planned targets were achieved in time - they were even partly exceeded. After a spectacular time of construction of only 16 months the ramp-up of production started in November 1995. The factories equipment for future Submicron-Structures in the micrometer range was calibrated in extensive characterisation runs, and the final production process could be transfered from Corbeil-Essonnes (nearby Paris in France) to Dresden.

On March 31st 1996 the first qualification lots were started; since then the 16-Megabit-Chips with structure sizes from 0.5 down to 0.4 micrometers and access times of 50 nanoseconds are produced. Two months earlier than expected - already in August 1996 - the „First Product" reached the serial qualification and with it the confirmation by the customer.

Todays production capacity is 4000 waferstarts per week and should be increased up to 7500 within the next 12 months. This means an improvement of 1900 additional wafers compared to the originally planned number of 5600. This increase will be achieved through a space-optimized arrangement of equipment and a simplified process flow. From this it is clear that the number of employees increases more than originally planned: At the end of 1996 the Chip-factory employed 1850 workers - 400 more than expected!

The number of sold devices is also higher than expected: During the past financial year 3 Mio. of 16-Megabit-Chips were produced and 2 Mio. ready assembled devices were sold.

During the present financial year a 64-Megabit-Chip production process will be transfered to Dresden which is the next Chip-generation: if a 64-Megabit-Device would be produced with conventional discrete components, at least a ground of 15 football fields would be needed to line up the components. The serial qualification is expected in Summer 1998.

Parallel to the construction in Dresden we work intensively on the developement of new processes for Memory- and Logic-Chips to save future capacity of the factory with market oriented products. A „Center of Developement and Innovation" (CDI) is continuing to develope the production equipment. Today the Innovation Center already takes care of 27 products together with suppliers of production plants and with saxon research institutions.

Historical Data

Siemens in Dresden

1892

Siemens and Halske opened their technical office at Dresden
The first power plant and street lighting was built by Siemens, Dresden

1893

The first electrical street cars drove from the city to the "Blue Miracle" bridge

Data and Facts

Fiscal Year 1995/96 - Production

Capacity	2500 WSPW	
Wafer Size	200 mm diameter (8")	
Technology	0.5 μm to 0.3 μm feature size	
Deliveries	-2 mill. Modules	
	-3 mill. 16-Mbit-chips	
Investment:	Actual 8/96	1.6 bill. DM
	Estimate FY 96/97	2.3 bill. DM

16-Mbit DRAM - Technical Data

CMOS technology
Min. feature size 0.44 µm
Cell size: 2.4 μm^2
Cell capacity: 55 fF
20.5 mill. transistors
Chip size: 79 mm^2
Supply voltage: 5.0 V/3.3 V
Access time: 50 / 60 / 70 ns
Storage capacity: 1000 DIN A4 pages
(typed single spaced)

64-Mbit DRAM - Technical Data

CMOS technology
Min. feature size 0.25 µm
Cell size: 0.6 μm^2
Cell capacity: 35 fF
70 mill. transistors
Chip size: 89 mm^2
Supply voltage: 3.3 V
Access time: 40 / 50 / 60 ns
Storage capacity: 4000 DIN A4 pages
(typed single spaced)

Data and Facts

Construction Accomplishments

Real estate	260.000 m^2
Built over area	35.000 m^2
(13 % of the area)	
Up to 3.000 workers per day	
Quantity of excavated soil	470.000 m^3
Quantity of concrete	105.000 m^3
Quantity of re-enforced stell	8.600 t
Lenght of cable strain tubes	80 km

KONFERENCE, POSVETOVANJA, SEMINARJI, POROČILA
CONFERENCES, COLLOQUYUMS, SEMINARS, REPORTS

IMAPS/NATO Advance Research Workshop and Exhibition

May 10. ÷ 13. Bled, Slovenia

V dneh od 10. do 13. maja je bila na Bledu v Grand hotelu Toplice v organizaciji IMAPS, NATO, MIDEM in Instituta "Jožef Stefan", specializirana mednarodna konferenca - delavnica z naslovom "Electronic packaging for high reliability, low cost electronics".

Od leta 1994 dalje mednarodno združenje za mikroelektroniko (prej ISHM, sedaj IMAPS) s pomočjo lokalnih organizatorjev prireja znanstvene sestanke - delavnice s področja hibridne mikroelektronske tehnologije, ki jih skoraj v celoti finančno omogoča NATO. Cilj delavnic je povezati znanstvenike in strokovnjake na omenjenem tematskem področju iz držav članic NATA in držav srednje in vzhodne Evrope. Prva delavnica je bila na Floridi (leta 1994), nato na Madžarskem (leta 1995) in lansko leto na Češkem. Na te delavnice so vabljeni vrhunski strokovnjaki teh držav z omenjenega strokovnega področja. Tudi slovenski strokovnjaki iz Odseka za keramiko na Institutu "Jožef Stefan", Ljubljana in iz firme HIPOT, Šentjernej, ki se ukvarjajo z hibridno mikroelektroniko, so že od začetka redni predavatelji na teh konferencah.

Tokratna delavnica oziroma strokovna konferenca je bila od 10. do 13. maja na Bledu v Grand hotelu Toplice. Obravnavala je področje hibridne mikroelektronike, predvsem načrtovanje in inkapsulacijo zahtevnih elektronskih vezij za vojaško elektroniko in elektroniko za široko potrošnjo. To so elektronska vezja, ki morajo zanesljivo delovati, hkrati pa morajo imeti sprejemljivo ceno. V okviru konference so udeleženci obiskali tudi Institut "Jožef Stefan" in Fakulteto za elektrotehniko v Ljubljani, ter si ogledali mesto Ljubljana.

Na konferenci je sodelovalo 35 vabljenih predavateljev, in sicer 8 iz Združenih držav Amerike, 11 iz zahodne Evrope, 12 iz centralne in vzhodne Evrope ter štirje iz Slovenije, dva s Fakultete za elektrotehniko v Ljubljani ter po eden iz Instituta "Jožef Stefan" in firme HIPOT.

Udeleženci so pohvalno ocenili okolje in organizacijo konference od priprav do izvedbe. Ravno tako so bili pozitivno presenečeni nad širino študijskega programa in nad aktivnostjo na področju mikroelektronike in polprevodniške tehnologije na Fakulteti za elektrotehniko v Ljubljani ter nad mednarodnim sodelovanjem na Institutu "Jožef Stefan".

Naslednja konferenca oz. delavnica (IMAPS/NATO Advance Research Workshop 1998) naj bi bila organizirana junija 1998 na Poljskem.

Nekaj podatkov o konferenci

Naslov:

Electronic packaging for high reliability, low cost electronics

Organizatorji:

1. NATO, International Scientific Exchange Programmes, Belgija
2. IMAPS (International Microelectronics And Packaging Society), ZDA
3. MIDEM, Strokovno društvo za mikroelektroniko, elektronske sestavne dele in materiale, Slovenija
4. Institut Jožef Stefan, Slovenija

So-direktorja konference:

1. Rao Tummala, Georgia Institute of Technology, ZDA
2. Marija Kosec, Institut Jožef Stefan, Slovenija

Organizacijski odbor:

1. W. Kinzy Jones, Florida International University, ZDA
2. Szolt Illyefalvi Vitez, Technical University of Budapest, Madžarska
3. Soeren Noerlyng, Micronsult, Danska
4. Iztok Šorli, Mikroiks, Slovenija
5. Darko Belavič, HIPOT, Slovenija

Progam je pokrival sledeča področja:

- Povezovanje golih silicijevih tabletk na substrat (Flip-chip, Ball Grid Array, ...)
- Materiali in tehnološki postopki na nivoju prve stopnje povezovanja (debeloplastna in tankoplastna tehnologija, večplastne tehnologije, ...)
- Multi-chip moduli
- Komponente in materiali za relativno cenene povezovalne tehnologije
- Ocenjevanje zanesljivosti
- Primeri zahtevnih elektronskih vezij v hibridni mikroelektronski tehnologiji

Seznam udeležencev z referati:

1. Alain Dravet, Dessault Electronique, Francija
2. C. P. Wong, Georgia Institute of Technology, ZDA
3. Darko Belavič, HIPOT, Slovenija
4. Ephraim Suhir, Bell Laboratories, Lucent Technologies, ZDA
5. Evgenij Levin, Lviv State University, Ukrajina
6. Frantisek Kolesar, Hybrid Microel, Technical University Kosice, Slovaška
7. Gabor Harsany, Technical Unversity of Budapest, Madžarska
8. Gilbert De Mey, University of Gent, Belgija
9. Giuseppe Vendramin, IBM Semea, Italija
10. Jan Vanfleteren, IMEC, Belgija
11. Janez Trontelj, Fakulteta za elektrotehniko, Slovenija
12. Josef Sikula, Technical Unversity of Brno, Češka
13. Jouko Vahakangas, VTT Electronics, Finska
14. Karel Kurzweil, BULL S.A., Francija
15. Leonard Schaper, University of Arkansas, ZDA
16. Maja Amskov, Delta, Danska
17. Marko Hrovat, Institut "Jožef Stefan", Slovenija
18. Michal Ciez, R&D Centre for Hybrid Microelectronics and Resistors, Poljska
19. N. Van Veen, Philips Electronics-CFT, Nizozemska
20. Nihal Sinnadurai, TWI, Velika Britanija
21. Paul R. Van Loan, Hewlett Packard, ZDA
22. Paul Svasta, University Politechnica of Bucharest, Romunija
23. Pavel Mach, Technical Unversity in Prague, Češka
24. Peter Sexton, Chemet Corporation, ZDA
25. Philip Garrou, Dow Chemical Company, ZDA
26. Philipp Philippow, Technical Unversity of Sofia, Bolgarija
27. Radu Mihail Ionescu, Ramelctro Ltd., Romunija
28. Rao Tummala, Georgia Institute of Technology, ZDA
29. Selim Achmatowicz, Instytut Technologi Materialow Electronicznych, Poljska
30. Seppo Leppavuori, University of Oulu, Finska
31. Slavko Amon, Fakulteta za elektrotehniko, Slovenija
32. Steve Muckett, Mozaik Technology Ventures Ltd., Velika Britanija
33. W. Kinzy Jones, Florida International University, ZDA
34. Yurij Makogon, National Technical University, Ukrajina
35. Zsolt Illyefalvi Vitez, Technical Unversity of Budapest, Madžarska

Ostali udeleženci:

1. Dubravka Ročak, Institut "Jožef Stefan", Slovenija
2. Galip Cansever, Yildiz Technical Unversity, Turčija
3. Iztok Šorli, Mikroiks, Slovenija
4. Iztok Stegel, Ministrstvo za obrambo, Slovenija
5. James Drehle, Hewlett Packard, ZDA
6. Janos Pinkola, Technical Unversity of Budapest, Madžarska
7. Marija Kosec, Institut "Jožef Stefan", Slovenija
8. Marko Pavlin, HIPOT, Slovenija
9. Richard Breck, IMAPS, ZDA
10. Soren Norlyng, Micronsult, Danska
11. Srečko Maček, Institut "Jožef Stefan", Slovenija
12. Stojan Šoba, HIPOT, Slovenija
13. Tone Sladič, Iskraemeco, Slovenija
14. Vivek Dutta, Johnson Matthey Electronics, ZDA
15. Vojan Rozman, Fakulteta za elektrotehniko, Slovenija
16. William Dennehy, William Dennehy Ltd., Velika Britanija
17. Yoshinobu Homma, Namics Corporation, Japonska

Darko Belavič
HIPOT, Šentjernej
c/o Institut "Jožef Stefan"
Jamova 39, 1001 Ljubljana

11th European Microelectronics Conference

14-16 maj, Venezia, Italia

Enajsta evropska konferenca o mikroelektroniki je bila od 14. do 16. maja v Palazzo del Cinema v Lido di Venezia. Evropske konference o mikroelektroniki so dvoletne in naslednja bo leta 1999 v Harrogate, Angliја pod novim nazivom 12th European Microelectronics and Packaging Conference.

Konferenca vse bolj postaja po tematiki širša in nima več poseben poudarek na hibridni debeloplastni mikroelektroniki. Delo konference je potekalo v dveh paralelnih sekcijah. Poleg tega pa so bili še posebej seminarji, predstavitve firm in razstava. Na konferenci je bilo približno 450 udeležencev iz 26 držav. Največ je bilo Nemcev, Francozov, Italijanov, Američanov in Angležev. Na razstavi je bilo prisotnih 154 firm iz Evrope in Amerike.

Predstavljeno je bilo 66 referatov in 38 posterjev iz področja mikroelektronike; vsi prispevki so objavljeni v zborniku.

Delo je potekalo v sekcijah: površinska montaža komponent, senzorji, materiali za mikrovalovna vezja, povezovanje in zaščita vezij, povezovanje silicijevih tabletk z bondiranjem, "flip chip" ali TAB povezovanje, debeloplastni materiali, toplotna obdelava vezij, spajkanje, pasivne komponente, polimerni materiali in multi chip moduli.

V poročilu bom opisala vsebino nekaterih zanimivejših predavanj s področja uporabe polimernih materialov pri izdelavi hibridnih vezij in multi chip modulov, novih materialov za izdelavo hibridnih vezij, ter vpliva teh materialov na zanesljivost vezij.

Pri površinski montaži komponent se veliko ukvarjajo z uporabo polimernih lepil kot zamenjavo za spajko. Strokovnjaki Ameriške firme Toranaga Tech so razvili novi polimerni material ORMET in ga uporabili za povezovanje različnih komponent na tiskanem vezju na substrat FR-4 (steklo/epoksi). Prevodna lepila imajo prednost pred spajko, ker je potrebna nižja temperatura sušenja materiala, lahko se povezujejo komponente z manjšimi razmiki med priključki, ni potrebno čiščenje z organskimi topili. Zanesljivost spoja med komponento in prevodno blazinico so preverjali z meritvami električne upornosti stika pred in po preizkusih temperaturnih šokov od - 55°C do 125°C. V primerjavi s spajko rezultati kažejo boljši mehanski in električni stik med priključki komponente in prevodno blazinico.

V referatu avtorjev iz Tehnološke Univerze v Warszavi so proučevali povezovanje komponent s spajkanjem spajk brez Pb, ki je lahko nevaren za okolico in človeka in so za to uporabili flukse "brez ostankov", ki jih po spajkanju ni potrebno čistiti. Preizkusili so različne spajke sestave SbBiAg, SbBiCu in SnAgCuSb z uporabo različnih "no residue" fluksov. Preizkuse so načrtovali s pomočjo Taguchi metode in rezultate analizirali s postopkom ANOVA. Na osnovi rezultatov analize so ugotovili, da ne glede na tip spajke, največ na dobro spajkljivost vplivajo: tip fluksa, pogoji predgrevanja pred spajkanjem in priprava površine.

Pri izdelavi večplastnih vezij zelo velike gostote prevodnih linij (60 μm linija /40 μm razmik), so avtorji iz Francoske firme SAT razvili postopek izdelave majhnih odprtin v dielektriku s pomočjo laserskega žarka. S tem postopkom so uspeli izdelati luknje dimenzij 40-80 μm v dielektriku debeline 35 ali 70 μm. Večplastna vezja so izdelali s posebnim postopkom sitotiska, da bi dosegli čim ožje prevodne linije. (<120 μm). Za tiskanje prevodne paste skozi luknje v dielektriku so uporabili kovinsko šablono ne pa sito šablone. Za lasersko luknjanje v dielektriku so razvili lastni laserski sistem SAT, uporabili so laserski žarek valovne dolžine 10.6 μm in razvili specifičen optični sistem. S tem postopkom so izdelali večplastno hibridno vezje s prevodnimi linijami 80 μm širine in 80 μm razmika, diameter lukenj je bil 65-85 μm, velikost substrata 3 x 3 inch, 8 prevodnih plasti.

Strokovnjaki s Tehnične Univerze v Berlinu so razvili novi polimerni material ORMOCER za uporabo v izdelavi multičip modula (MCM). To je kompozitni material, sintetiziran s sol gel postopkom, polimerizira se na temperaturi 170°C. Uporabili so ga za izdelavo MCM-D/L vezja (mešana tehnologija tankoplastna in tiskana vezja). Material je možno s postopkom naprševanja nanesti na različne substrate: SiO_2, Al_2O_3, GaAs in organski substrat, polimerizira se na 170°C . Debelina tako narejene plasti je 5-12 μm. Za izdelavo lukenj v dielektriku so uporabili fotolitografski postopek, s pomočjo natančnega pozicioniranja mask so uspeli narediti luknje velikosti 20 μm. Končna polimerizacija vseh vzorcev je narejena v peči na 150°C, 6 ur. Za izdelavo večplastnih vezij je pred procesom metalizacije potrebno še kratko sušenje na 150°C. Na ta način so izdelali dva vezja na SiO_2 substratu in Fr-4 substratu. Adhezija na oba tipa substrata je bila dobra, električne lastnosti ORMOCERA, kot tankoplastnega dielektričnega materiala so bile v predpisanih mejah.

Japonska firma Matsushita je predstavila rezultate studija pritrjevanja LSI čipov na substrat s pomočjo SBB tehnike (stud bump bonding), ki so jo razvili sami za izdelavo MCM vezij visoke gostote. Sestava kroglice za pritrjevanje čipa na prevodne blazinice na substratu je iz Au v dveh plasteh in prevodnega lepila. Au kroglice na čipu so narejene s pomočjo bonderja za pritrjevanje zlatih žičk, potem se tako nanešene kroglice potopijo v prevodno lepilo. LSI čip se potem postavi na prevodne blazinice na substratu pod pritiskom 1g/kroglico. Polimerno lepilo se polimerizira 2 uri na 120°C. Po vizuelnem pregledu pritrjenega čipa se razmik med čipom in substratom popolni z epoksidno smolo. SBB tehniko pritrjevanja LSI čipov so uporabili za pritrjevanje na ALIHV substrate (večplastna tiskana vezja z luknjami med notranjimi plastmi). Luknje med notranjimi plastmi so naredili s pomočjo CO_2 laserja. Testni vzorec so naredili na ALIHV substratu z 9 flip čip povezanimi silicijevimi tabletkami. Velikost substrata je bila 10 x 10 cm^2, LSI čip je imel 296 blazinic z medsebojnim razmikom 125 μm. Merili so upornost povezav in izolacijsko upornost med kroglicami na čipu pred in po preizkusih zanesljivosti vezja: staranje na 125°C, 2000 ur, staranje na -55°C, 2000 ur, staranje v vlagi 85°C,

85%RV, 2000 ur ter preizkusi temperaturnih šokov od -55°C do 125°C, 2000 ciklov. Rezultati testov kažejo, da se s kombinacijo tehnike SBB pritrjevanja LSI čipov in ALIHV substratov zmanjša dimenzija vezij na 1/20 od standardnega, brez vpliva na kvaliteto elektronskega vezja.

V sekciji o debeloplastnih materialih so avtorji iz Heraeusa, Du Ponta in ESL predstvili nove materiale za izdelavo hibridnih debeloplastnih vezij. Heraeus je predstavil nove prevodne in dielektrične materiale za izdelavo ozkih prevodnih linij za uporabo v mikrovalovnih elektronskih vezij. ESL je razvil serijo debeloplastnih prevodnih, uporovnih in dielektričnih materialov brez Pb, Cd in Ni (zaščita okolja). Du Pont je predstavil debeloplastne materiale in nove tehnološke postopke za izdelavo večplastnih vezij. Nova serija debeloplastnih materialov za izdelavo večplastnih hibridnih vezij s spajkanimi komponentami na zgornji plasti je razvita na osnovi zahtev, da vezje prenese temperaturno cikliranje. Osnova nove serije je dielektrični material visoke gostote že po tiskanju dveh plasti, po žganju pa ni videti lukenj v materialu. Žge se lahko skupaj s prevodnikom in metaliziranimi luknjami, kar zmanjšuje stroške izdelave vezja.

Strokovnjaki Magneti Marellija so uporabili postopek "diffusion patterning" za izdelavo hibridnega vezja, namenjenega avtomobilski industriji. Zaradi zahteve vezja za visoko gostoto povezav in majhno dimenzijo so izbrali tehnološko rešitev v 4-plastnem vezju z ozkimi prevodnimi linijami in razmiki. Za tiskanje prevodnikov majhnih dimenzij so preizkusili različne prevodne materiale za notranje in zunanje prevodnike in za tiskanje prevodnega materiala skozi luknje za medsebojne povezave plasti. Na osnovi zelo obsežnega programa preizkusov zanesljivosti na testnih vzorcih so ugotovili, da so s tiskanjem izbranih prevodnih materialov v čistem prostoru klase 10 000 in kontrolirane temperature in vlage v prostoru, ter z luknjanjem dilektrika z "diffusion patterning" postopkom uspeli izdelati zanesljivo vezje za delovanje v motorju avtomobila.

Japonski strokovnjaki so proučevali mikrostrukturo spajkalnega stika med komponento in prevodno blazinico, če so za spajkanje uporabili spajke brez svinca. Preizkusili so veliko število spajk sestave SnAgBi, SnAgIn, SnZnBi, SnZnIn. Spajkali so v inertni atmosferi brez uporabe fluksov in na zraku z uporabo komercialnih fluksov na Cu blazinice tiskanih ploščic. Za opazovanje reakcije med spajko in prevodnim materialom so uporabili optični mikroskop in rasterski elektronski mikroskop. Ugotovili so, da med spajko in Cu blazinico nastane intermetalni spoj, ki vpliva na mehanske lastnosti spajkalnega spoja.

Avtorji Ameriške firme Arconium so v svojem referatu o spajkanju s spajkami na osnovi In proučevali reakcije intermetalnih spojin, ter kako vplivajo na mehansko jakost spajkalnega spoja. Proučevali so reakcijo med spajko in različnimi kovinami ki se uporabljajo v elektronskih vezjih, kot prevodni material: Au, Ag, Cu, Ni. Na osnovi rezultatov raziskav so ugotovili, da spajke na osnovi In kažejo pozitiven vpliv na mehanske lastnosti spoja, če komponente spajkamo na Au, Ag, medtem ko spajke na osnovi Sn imajo boljše mehanske spoje s Cu, Fe in Ni.

V referatu avtorjev iz Heraeusa so podali rezultate preizkusov zanesljivosti testnega vezja, na katerem so za povezovanje tabletk z majhnimi razdaljami med priključki ("fine pitch") uporabili anizotropno prevodno lepilo. Tabletke so pritrjevali na tiskano vezje in steklo. Anizotropna lepila so sestavljena iz polimerne matrice in električno prevodnih delcev, ki po polimerizaciji lepila prevajajo električni tok samo v z-smeri. Ta lastnost je koristna pri pritrjevanju "fine pitch" tabletk, ker je zmanjšana možnost kratkih stikov ali električnega prevajanja med priključki tabletke. Preizkusili so različna polimerna anizotropna lepila na osnovi epoksida, polnjenega z zlatimi delci povprečnega diametra 6 μm. Lepilo so nanesli na prevodne blazinice s sitotiskom ali s pomočjo dozirnika. Po pritrjevanju tabletk so merili kontaktno električno upornost po 500 ur staranja na 85°C in po 500 temperaturnih ciklih med -40°C in 85°C. Rezultati preizkusov kažejo na zanesljivo povezovanje "fine pitch" komponent z anizotropnim lepilom.

Avtorji Ameriške firme Diemat in Angleške Multicore Solders so preizkusili različna polimerna lepila z višjo toplotno prevodnostjo za uporabo v močnostnih elektronskih vezjih. Sami so razvili lepila s toplotno prevodnostjo do 60 W/mK različne sestave, od termoplast do termoset polimernega materiala. Z meritvami vpliva vsebine polnila Ag ter oblike, velikosti in volumnega deleža delcev Ag na toplotno prevodnost materiala so določili sestavo lepila z visoko toplotno prevodnostjo. Uporaba tega lepila za lepljenje močnostnih tabletk lahko zamenja postopek spajkanja polprevodniških tabletk v močnostnih vezjih.

V sekciji o multi chip modulih (MCM) so avtorji firme Siegert uporabili "green tape" tehnologijo za izdelavo večplastnega vezja s keramičnimi plastmi dielektrika v obliki zelene folije. Več plasti s tiskanimi notranjimi prevodnimi linijami in metaliziranimi luknjami med plastmi se žge skupaj pri 875°C. Na tako izdelano večplastno vezje se potem tiskajo na standarden način prevodniki in pritrdijo komponente v obliki čipa in tako se realizira vezje; multičip modul. Pokazali so različna vezja v MCM tehnologiji za uporabo v avtomobilski industriji, medicini in vojaški industriji.

Avtorji firme Thomson CF so predstavili vezje v MCM-D tehnologiji za uporabo v okolici s težkimi pogoji (vlaga, temperatura, spremembe temperature, onesnaženost). Kvaliteto vezja so ovrednotili s termomehanskimi simulacijami in pospešenimi preizkusi. Po preizkusih staranja 2000 ur na 125°C in 150°C, 2000 temperaturnih ciklov in mehanskih vibracijah so z vizualnim pregledom vezij in merjenjem sprememb električnih lastnosti vezij ugotovili, da so najbolj kritična mesta za odpoved vezja luknje v plasti dielektrika v stiku z Al_2O_3 substratom. Rezultati električnih meritev kažejo, da vezja zadovoljujejo stroge zahteve za vojaško uporabo.

Na Konferenci smo predstavili poster z naslovom Evaluation of polymeric adhesives for solder replacement in power hybrids, v katerem smo ugotavljali vpliv polimernih lepil na toplotno prevodnost pritrjenega močnostnega vezja na hladilno telo.

Dubravka Ročak
Institut Jožef Stefan
Jamova 39, Ljubljana

IN MEMORIAM

PAVLE TEPINA

Dne 1. junija 1997 je prenehalo biti srce Pavleta Tepine, našega bivšega dolgoletnega tajnika in organizatorja naših strokovnih prireditev. V našem društvu je bil aktiven vse do leta 1992 in je z njim povezan del naše zgodovine.

V vso dejavnost SSESD, predhodnika MIDEM, je bilo od leta 1967 dalje vtkano delo našega Pavleta. Pri vseh naših akcija je pravzaprav nosil levji delež izvajanja, kjer je bil vedno pripravljen, da brez negodovanja doprinese človeško možni maksimum. Vedno se je tudi izkazal kot dober tovariš in prijatelj.

Rojen je bil 27. februarja 1915 v družini živinozdravnika v Ljubljani. Leta 1933 se je vpisal na tehniško fakulteto v Ljubljani, elektrostrojni oddelek, vendar je bil že leta 1934 aretiran, obsojen in poslan v zapor političnih obsojencev v Sremsko Mitrovico. Po izpustitvi iz zapora leta 1936 je nadaljeval študij ter že v tem času pokazal svoje sposobnosti in voljo za dodatno strokovno in društveno organizacijsko delo: bil je tajnik študentskega društva elektrotehnikov in obenem pomožni asistent pri prof. Kralu na Zavodu za raziskovo materiala na Tehniški fakulteti Univerze v Ljubljani. Diplomsko nalogo je dvignil v začetku leta 1941, nato pa je bil po prihodu Italijanov ponovno aretiran ter s skupino elektrotehnikov postavljen pred italijansko vojno sodišče v Ljubljani pod obtožbo dela za OF. Ker pa vojni tožilec ni uspel dokazati delovanja obtoženih, je bil s celo skupino izpuščen. Ko so po kapitulaciji Italije tehniško fakulteto ponovno odprli, je Pavle leta 1943 diplomiral. V italijanski okupaciji je Pavle kot ilegalec vse do septembra 1943 delal v radijskem sektorju CK KP Slovenije, nato pa ga je Centralni komite poslal skupaj z Dušanom Lasičem na osvobojeno ozemlje z nalogo, da formirata pri partizanskih delavnicah v Starih žagah na Dolenjskem tudi radijsko delavnico. Naj spomnimo, da je bila ta radijska delavnica z izdelavo radijskih oddajnikov in druge opreme za partizanske enote kovačnica kadrov, ki so po osvoboditvi odigrali pionirsko vlogo pri začetkih in razvoju industrije elektrotehnike in elektronike v Sloveniji. Junija 1944 je bil Pavle poslan v oficirsko šolo glavnega štaba Narodno osvobodilne vojske in partizanskih odredov Slovenije, ki je delovala v Črnomlju na osvobojenem ozemlju. Tam je nato do osvoboditve vodil tečaje za partizanske radiomehanike. Junija 1945 je bil zaradi svojih pedagoških strokovnih izkušenj dodeljen v Tankovsko armado v Beogradu kot komandant radiotelegrafskega kursa. Od tam je bil oktobra 1947 premeščen v Zvezni sekretariat za notranje zadeve z nalogo, da tudi tam vodi radiotelegrafske tečaje. Leta 1952 so ga dodelili v Tehnični inštitut SUP-a, s čemer je pričel tam svoje petnajstletno delovanje, najprej kot vodja sektorja in zadnjih šest let kot direktor inštituta. V tem času je pričel svojo aktivnost tudi v ETAN-u (Jugoslovanskem komiteju za elektroniko, telekomunikacije, avtomatiko in nuklearno tehniko). Leta 1967 je bil predčasno upokojen ter se je vrnil v Ljubljano.

V Iskrinem zavodu za avtomatizacijo je prevzel marca 1967 od Matije Seligerja mesto vodje Laboratorija za mikroelektroniko, kmalu nato pa se je aktivno vključil tudi v SSOSD ter v jeseni 1967 prevzel od Marjana Šefa mesto tajnika. Žal je bil laboratorij za mikroelektroniko mnogo naprednejši od svojega okolja v Iskri, zato je bil leta 1969 razpuščen, Pavle pa je prevzel mesto tehničnega direktorja v tiskarni Mladinske knjige v Ljubljani. Kasneje je delal še v Iskrini Tovarni elektronskih naprav, dokler se ni tudi profesionalno vključil v delo Elektrotehniške zveze Slovenije in SSOSD ter nato MIDEM.

Ves ta čas do leta 1992, torej petindvajset let, je bil Pavle tajnik našega odbora oziroma sekcije. Vendar tega dela ni opravljal le kot tajnik temveč kot pravi aktivist mnogo širše, predvsem pa z željo, da povsod pomaga. Kot strokovnjak v elektroniki, obenem pa z velikimi izkušnjami v tiskarstvu, je poskrbel za tisk in ureditev vseh naših zbornikov, programov in drugih publikacij in to vedno pravočasno, čeprav so avtorji referatov mnogokrat zamujali. Tudi organizacija nobenega simpozija o sestavnih delih v Ljubljani in posvetovanj o mikroelektroniki širom bivše Jugoslavije ni minila brez Pavleta. Ne smemo pozabiti tudi njegovega dolgoletnega dela kot aktivista ETAN-a, saj je bil že leta član organizacijskega odbora za letne konference ETAN-a. Za svoje delovanje je bil tudi imenovan za zasluženega člana ETAN-a.

Mi vsi se zavedamo, koliko je bilo naše strokovno društveno delovanje povezano z življenjem Pavleta Tepine in koliko od tega življenja je dal skupnosti kot strokovnjak in kot človek. Posebno kot človek nam je bil Pavle vzgled požrtvovalnega in obenem vedno na pomoč pripravljenega tovariša.

Med člani društva MIDEM je Pavletu Tepini zagotovljen trajen spomin.

Milan Slokan

VESTI-NEWS

News from AMS

Single Chip CMOS Speakerphone complies with new EMC Norms

Austria Mikro Systeme has introduced the AS2520 single chip handsfree speakerphone circuit, realised in CMOS technology[1], which complies with the new EMC norms (CE) for connection to the PSTN. The device reduces the costs of a handsfree speakerphone by integrating the line interface with power extraction, 2/4 wire conversion, speech network with speaker amplifier, switching logic with all time constants and peak detectors. Together with a micro-controller with dialler and tone generator the AS2520 performs all functions needed in a fully electronic handsfree speakerphone.

The implementation of a novel voice channel control and switching circuit accommodates a violation design approach in which the "chopper effect", experienced in traditional voice switching circuits, has been practically eliminated. The usage in a noisy environment is possible since the channel control circuit is virtually independent of any background noise and the incorporated volume control with squelch increases the signal level without increasing the surrounding noise picked up by the microphone.

The AS2520 is entirely powered from the telephone line and can operate at low currents of only 5 mA, allowing parallel operation with an electronic telephone. During ringing a DC/DC converter provides a supply of 4V which allows the use of the same loudspeaker for tone ringing, eliminating the need for a piezo.

The AS2520 has a volume control using +/- keys, alternatively the AS2521 uses a potentiometer. Both devices are available in 28 pin SOIC or DIP packages. Samples and production quantities are available now. Demo and evaluation boards as well as application notes are available on request. For a free data sheet and further information please contact your local Sales Office or

Austria Mikro Systeme Corporate Communications, A-8141 Unterpremstätten, Austria,
Thesys Marketing Communications, Haarbergstrasse 61, D-99097 Erfurt, Germany,

SAMES Marketing Communications, PO Box 15888, Pretoria, Rep. of South Africa.

[1] *Note to the Editor: To our knowledge the AS2520 is the only single chip handsfree speakerphone set on the market currently available in CMOS technology. The use of CMOS decreases time-consuming EMC design efforts, saving time and development costs. This, as well as the fully integrated timing parameters usually implemented with discrete components allows for short time-to-market and increases the reliability of the system.*

News from European Semiconductor, May 1997

ASML expansion/300 mm tool

ASM Lithography has completed a new manufacturing building at its HQ in Veldhoven in The Netherlands which has increased capacity to more than 350 steppers a year, with the potential to go to 450 a year within six months. Lens maker Carl Zeiss is expanding its supply accordingly says ASML Vice President Evert Polak.

The new building houses 4800 m^2 of Class 10,000 manufacturing space, a global logistics centre and office space. It is sited a few km from ASML's existing facility which has now gained space to expand design and R&D.

Polak says that ASML is developing a 300 mm wafer stepper of completely new design and anticipates shipping production tools in 1999 at roughly 1.5 times the cost of a 200 mm tool. This is well behind the timescale of ASML's competitors. but Polak says that they will have an 'internal' stepper before the end of 1997 and they 'do not exclude external people using it'.

Compared to SEMI's projections that there will be nine pilot 300 mm lines in operation in 1998/9, Polak says that he expects that there will be 'no pilot lines worldwide in 1998, only R&D'.

ASML also has a 193 nm Program with IMEC for the development of 0.13 μm (and lower) lithography, expecting to deliver the first scanning tool to IMEC in the second half of 1998. Polak said that ASML also has contact with ASET/SELETE in Japan (who are working on the application of 193 nm down to 0.1 μm design rules) but that ASML was supported by the EU through MEDEA.

Analog shortfall

A study commissioned by the EC at the end of '96 concluded that there is a current shortage of experienced analog and mixed signal IC designers.

Results of that study are to be used in an assessment process to determine whether a new Esprit initiative is required in this area.

It is felt that the increased use of digital ICs has led to a reduction in the number of experienced analog and mixed signal designers.

A situation compounded by expansion in such key technologies as telecommunications and sensors, where analog and mixed signal devices are increasingly used and the market is estimated as growing by up to 15% yearly. Which makes it good timing for the publication of Analog / Integrated Circuits by Edwin W Greeneich published Chapman & Hall (341 pgs £ 55).

The book deals with design and analysis of modern analog circuits using integrated bipolar and field-effect transistor technologies and is considered as suitable as text for both senior level of first-year graduate students as well as a reference work for practising engineers.

Chapters cover models for integrated circuit devices BJT, JFET and MOSFETs. Basic building blocks used in a large variety of analog circuits are analysed in the second chapter.

These consist of current sources, dc level-shift stages, single- transistor gain and two- transistor gain stages and output stages.

Both bipolar and FET implementations are presented.

Chapter 3 deals with operation amplifier circuits, with the four basic op-amp circuits analysed.

Feedback amplifiers are discussed subsequently and a detailed analysis procedure for various feedback configurations is developed with numerous examples of feedback circuits are presented. Stability consideration and methods for compensation are also discussed.

The final chapter deals with translinear circuits that exploit the near linear relationship between the transconductance of a transistor and either its current or voltage.

Applications of translinear circuits include implementation of analog function and generation of trigometric functions. These are circuits that find use in communications, signal processing and control systems.

The report on analog designer shortages suggests the identification and establishment ot a limited number of analog/mixed signal design centres ot excellence in Europe.

In the event it seems likely that Professor Greeneich's publication should be found in such centre's libraries.

Director earnings a maker's lament

PE International's 'Remuneration in Europe' survey covers directors' earnings. It had no response from France and too small a sample in Belgium to risk publishing, but it still provides pay and benefits information based on the salaries of 30,300 executives working for 3,000 companies in nine European countries.

One of the most interesting aspects to PE's findings within the semiconductor industry is the respective financial awards allocated for directors' responsibilities in finance, sales and personnel.

Despite a lack of fabs in Denmark, basic salary for an MD in small organisations was around £183,300, followed by sales earnings at £96,876, finance at £89,908 and manufacturing at £78,557. No figure was given here for personnel directors.

But in larger Danish organisations where the MD pulls down a basic £179,816, the finance director earns £106,653, manufacturing gets £83,951 and personnel lag at £74.848.

BIG EARNER IS SALES

In Germany, sales directors rule supreme. A lower quartile of £59,053 to an upper quartile of £78,593 is paid in organisations employing 100-200 persons. Lower-to-upper quartile pay ranges from £69,909 to £110,725 for companies with 500-1,000 employees. While the sales director only earns around half of MD salaries, he is still rewarded anywhere from £10,000 to £30,000 better than the comparatively lowly paid personnel head.

A guide to directors' earnings

	Organisations employing 100-250 persons Median		Orgainisations employing 500-1,000 persons Median	
Country	Basic	Total	Basic	Total
GERMANY M.D.	147,199	171,515	173,252	214,503
Sales Head	73,383	82,935	83,804	95,528
Manufacturing	59,488	66,001	69,909	78,593
Finance head	59,053	65,567	66,001	73,817
Personnel head	55,580	62,093	64,698	72,514
IRELAND M.D.	66,528	81,206	99,500	107,260
Sales Head	43,659	45,655	56,052	61,657
Manufacturing	41,990	45,364	45,738	50,416
Finance head	45,010	48,437	47,503	52,701
Personnel head	43,676	44,550	42,879	45,478
NETHERLANDS M.D.	78,663	88,326	79,242	94,704
Sales Head	45,613	49,865	59,142	61,848
Manufacturing	42,327	48,705	65,713	72,284
Finance head	48,898	51,797	66,873	71,125
Personnel head	54,890	62,234	60,302	72,284
SWITZERLAND M.D.	106,667	132,267	127,467	164,800
Sales Head	79,467	96,000	86,933	108,267
Manufacturing	72,533	79,467	88,000	109,333
Finance head	75,733	84,267	85,333	101,867
Personnel head	67,200	67,200	93,867	121,600
UK M.D.	62,625	67,726	89,184	98,285
Sales Head	40,250	41,291	52,635	58,305
Manufacturing	37,000	41,332	46,750	47,948
Finance head	43,370	45,000	57,845	59,486
Personnel head	37,600	47,440	49,500	53,817

SOURCE: PE INTERNATIONAL

Sales, finance and personnel directors battle it out for best paid in the European semiconductor industry. But most are unanimous in assigning manufacture to the bottom of the heap. Small wonder that students opt to study finance, marketing or personnel skills

In Germany the financial reward ranking of sales, followed by manufacture, finance and personnel is consistent in big and small companies. Switzerland, however, shows some disparity in its best-paid option, depending on the size of the organisation. In the bigger companies, best paid after the MD is the head of personnel (from £80,000 to £150,933) followed by manufacturing, sales and finance.

Smaller companies rank sales top, finance, then inanufacture and personnel.

DIFFERENT PRIORITIES

The UK also has a distinct split in organisational attitude between small and large organisations.

Personnel are put as top dog in small companies, followed by finance with sales and manufacturing neck and neck. But in larger organisations money is all, with finance taking the king-pin role, closely followed by sales. Personnel and no-glamour manufacture tag along behind, as usual.

News from IMEC

LCI-SMARTpen™ identifies signer

The LCI-SMARTpen™ was presented at CeBit '97 in Hannover (Germany) by LCI Computer Group nv. The device is a ball-pen that includes sensors allowing authentication of people through the biometric characteristics of their signature.

The advanced micro-mechanics and microelectronics enabled the miniaturization in what looks like a normal pen. The pen generates a biometric signature, based on the dynamic characteristics of the signing on a piece of paper. The wireless connection to the computer is tamper free thanks to a built in challenge-response encryption mechanism. As the LCISMARTpen™ unequivocally authenticates a person, it can be used to make Internet transactions or bank transfers more secure. It may impact electronic commerce, corporate or private environments. This pen is also interesting for financial institutions for the control of home banking and for automation of bank transfers. The health care industry may use LCISMARTpen™ for guaranteeing privacy of medical records or for tracing prescription drugs. Industrial companies can use it for commerce over the Internet or when they consider tightening the network security.

The LCI-SMARTpen™, the result of a collaboration between IMEC and LCI Computer Group nv, is commercialized by LCI-SmartPen nv (Zaventem, Belgium), a spin-off company of both organizations.

World's largest active pixel image sensor?

The Fuga22 is a 2048x2048 active pixel image sensor: The image area measures 16x16 mm, using 7.5 μm pixels. This active pixel sensor is not only the largest of its kind, it has more than 12 million MOSFETs, and is thus probably also the largest standard CMOS circuit in the world. Prototype samples are available through IMEC's spin-off company, C-Cam Technologies.

This imager sensor is in fact an "imaging system on a chip", and is intended to be interfaced to the outside world without additional external circuitry and a digital protocol.

Just as its predecessors Fuga11, -12, -15, -18 and -19, the Fuga22 is a true random addressable image sensor. Pixel intensity information is obtained after applying the X- and Y-coordinates of the required pixel. This interface is purely digital. Any pixel can be accessed at any time, of course while respecting a minimum addressing latency. Purely random addressing, or windowing (electronic pan & tilt), or subsampling (electronic zoom), may be used to exchange frame speed specifications for image resolution or amount of data. Potential applications will be situated in industrial inspection or control, situations where a very high resolution is required, and yet a fast acquisition of parts of an image, electronics pan and zoom, etc. The 4 megapixel FUGA22 opens new application niches for more advanced inspection tasks, requiring a huge field-of view, a high electronic zoom factor, or electronic pan & tilt with a broad range.

Technical information can be found on our web pages
http://www.imec.be/fuga/datasheets.html and
htlp://www.imec.be/fuga/fuga22.html.
C-Cam Technologies, +32.16.39 83 00

IMEC licenses flash EEPROM technology to Thesys

IMEC has signed a licence agreement with Thesys Microelectronics, the German ASIC and ASSP supplier, which allows Thesys to make first industrial use of a new Flash EEPROM technology developed by IMEC.

The "High Injection MOS" (or HIMOS) technology developed and patented by IMEC offers a unique combination of low processing cost together with very high performance in terms of programming speed and power consumption. The EEPROM module can be combined with analog and high-voltage modules to provide cost-effective system solutions, a high level of reliability and secure manipulation. Target application areas are automotive and industrial electronics, security engineering and telecommunications.

The IMEC solution will be integrated into Thesys' established 0.8 μm process platform in a joint development and transfer program to be carried out by IMEC and Thesys engineers. Consideration is already being given to further scaling of the HIMOS technology for the 0.6 μm platform currently under development at Thesys. Simultaneously, IMEC is already developing a 0.35 μm HIMOS technology which is aiming at substantially higher densities for low voltage, low power embedded memory applications.

KOLEDAR PRIREDITEV 1997

SEPTEMBER

07.09.-11.09.1997
24th International symposium on Compound Semiconductors
San Diego ,CA, USA
Info.: +1 765 494 3528

08.09.-12.09.1997
Semiconductor Technology Seminar
Glasgow, Scotland
Info.: + 1 415 941 8272

10.09.- 12.09.1997
SEMI/IEEE Advanced Semiconductor Manufacturing Conference and Workshop
Cambridge, MA, USA
Info.: +1 415 964 5111

15.09.-18.09.1997
Failure&Yield Analysis Seminar
Glasgow, Scotland
Info.: +1 415 941 8272

15.09.- 18.09.1997
20th Durham Conference on X-ray Analysis
Durham, UK
Info.: +44 1223 374411

21.09.-23.09.1997
3rd International Workshop on Thermal Investigations of IC's and Microstructures
Cannes France
Info.: E-mail: Bernard.Courtois@imag.fr

21.09.-25.09.1997
Electrical Overstress/Electrostatic Discharge Symposium
Santa Clara,CA,USA
Info.: +1 315 339 6937

22.09.- 24.09.1997
SEMICON Taiwan 97
Taipei, Taiwan
Info.: +3 573 3399

22.09.- 24.09.1997
ESSDERC '97 - 27th European Solid State Device Research Conference
Stuttgart, Germany
Info.: + 49 7141 910 774

24.09.- 26.09.1997
MIDEM - 33rd International Conference on Microelectronics, Devices and Materials
Gozd Martuljek, Slovenija
Info.: +386 61 312 898

29.09.- 30.09.1997
SPIE's 1997 Symposium on Micromachining and Microfabrication
Austin, TX, USA
Info.: + 1 360 676 3290

OCTOBER

01.10.- 03.10.1997
5th Conference on Materials and Technology
Portorož, Slovenija
Info.: +386 61 1251 161

04.10.- 10.10.1997
IPC Works '97
Washington, DC, USA
Info.: +1 847 509 9700